Leibniz Universität, Hannover

Fakultät für Bauingenieurwesen und Geodäsie

Investigations on the water balance of the Upper Arkavathy catchment, India, using remote sensing products.

Master Thesis

In partial fulfilment for the degree of Master of Science in Water Resources and Environmental Management

Submitted by

Tejas Kulkarni

October 14, 2019

First Examiner: Dr. Sanaz Vajedian

Second Examiner: Prof. Dr. Mathias Gassmann

Supervisors: Dr. Sanaz Vajedian, Prof. Dr. Mathias Gassmann

Declaration

I declare that this document and the accompanying code has been composed by myself, and describes my own work, unless otherwise acknowledged in the text. It has not been accepted in any previous application for a degree. All verbatim extracts have been distinguished by quotation marks, and all sources of information have been specifically acknowledged.

Hannover, October 14, 2019

Acknowledgment

I would like to firstly thank my thesis supervisor Dr.Sanaz Vajedian of the Institute of Photogrammetry and Geodetic Sciences at the Leibniz Universitat, Hannover for her continuous support and troubleshooting. She consistently helped right from the conceptualisation of the study to writing of this thesis. I am grateful to the time she spent in writing the code for the extraction of the data and the analysis. I am much obliged to the persistence of her inputs and availability to include me beyond office hours and during break times. Her magnanimity and composure as a supervisor is something I will always look up to personally and professionally.

I would like to thank my co-supervisor Prof.Dr. Mathias Gassmann from the Department of Hydrology and Substance Balance, Universitat Kassel, for his encouragement in guiding me and providing me with valuable comments on the thesis. His passionate participation and backing in terms of time, co-ordination and funding has been valuable beyond expressible terms.

I would also like to thank the Dr.Veena Srinivasan from Asoka Trust for Research in Ecology and Environment (ATREE) without whose help, I could not have steered towards the validation of my findings. I would like to thank her students Lakshmikantha and Rashmi for their consistent support in providing data from the study area in India.

I would also like to acknowledge the support of my colleague Lukas Ditzel for his patience in listening, discussing and beneficial comments on formulating my hypothesis and also helping me in the plotting and proof reading my thesis

Additionally, I would like to thank my friends Ravi, Ankur and Isabelle for providing me with unfailing support in accommodating me into their hearts and homes and understanding me during stressed times.

Finally, I would like to express my profound gratitude to my parents for providing me with tremendous support through the years of my study and the discourse in my scientific career. This accomplishment would not have been possible without their treasured morals and care.

Author

Tejas Kulkarni

Contents

Chapter. 1 Introduction 1
1.1 Background 1
1.2 Water Budgeting 1
1.3 Remote Sensing in Hydrology 2
1.4 Research Objectives 2
1.5 RS Databases and their Applicability in Hydrological Modelling 3
1.5.1. Individual WB components 3
1.5.2. Assimilated datasets 6
1.6 Total Water Storage and GRACE 7
1.7 Spatial Characterization of LUCC 8
Chapter. 2 Study Area 9
2.1 Regional WRM Context 10
2.2 Land and Human Water Use 10
2.3 Groundwater and Hydro-Geology 12
2.4 State of Hydrological Research 13
Chapter. 3 Data and Methods 14
3.1 De-trending and De-seasonalization 14
3.2 Data Selection to highlight drivers in WB equation. 15
3.3 Quantifying Groundwater Storage Changes 16
3.3.1. TWS from GRACE Mascons 17
3.3.2. TWS from GLDAS 18
3.3.3. Observed Groundwater Levels 18
3.3.4. Observed GPS Data 18
3.4 Quantifying Vegetation Index 19
3.4.1. Image processing technique 20
3.5 Framework of Methodology 21
Chapter. 4 Results and Discussions 22
4.1 Temperature and Potential Evapotranspiration 22
4.2 Long term Rainfall Analysis 24
4.3 Groundwater Storage Variability in Upper Arkavathy through RSP's 26
4.3.1. Harmonization and Scaling of GRACE-TWS Dataset 26
4.3.2. TWS and TWSC from GLDAS-LSM 27
4.3.3. Comparison of TWSC GLDAS and TWSC GRACE 30

4.3.4. GWSC Determination 30
4.3.5. Groundwater Variability and Deseasonalized Data 32
4.3.6. Groundwater Level Trends 34
4.3.7. GWSC and Land Subsidence 34
4.4 Spatio-Temporal Analysis of Vegetation Dynamics 35
Chapter. 5 Discussions 39
5.1 Lack of Evidence of Drought 39
5.2 Characteristics of Groundwater Storage Change in UAC 39
5.3 Vegetation Phenology 41
5.4 Limitations and Way Forward 41
Chapter. 6 Conclusions 42
Publication bibliography 44

List of Appendix

Appendix. 1 – List of Landsat Data Used for NDVI Analysis

Appendix. 2 – Matlab Script for Processing of GRACE Mascons Data

Appendix. 3 – Matlab Script for Processing of GLDAS data

Appendix 4 – Matlab Script for Processing of NDVI images

Appendix 5 – Python and R scripts for time series analysis and plots.

List of Figures

Figure 1. Components and visualization of total vertically integrated water storage 8
Figure 2. Location and major features in the Arkavathy catchment 9
Figure 3. Monthly inflow and rainfall data at the TG Halli reservoir 10
Figure 4. Landuse map of Upper Arkavathy Catchment for the year 2014. 11
Figure 5. Changes in irrigation sources in the Upper Arkavathy Catchment 12
Figure 6. Conceptual model explaining the flow in fractured rock aquifer region 13
Figure 7. Overlay of Upper Arkavathy Catchment on GLDAS grided dataset. 16
Figure 8. Overlay of Arkavathy Catchment on grided GRACE Mascon dataset 17
Figure 9. Spatial Map for Observed Raingauge and Borewell data used in the study. 19
Figure 10. Pictorial representation of Scanned Line Error in Landsat-7 images. 20
Figure 11. Framework of Methodology for the study 21
Figure 12. Box plot showing variations of temperature between datasets. 22

Figure 13. Long term trend in temperature for the UAC. 23
Figure 14. Monthly Precipitation and Potential Evapotranspiration GLDAS. 23
Figure 15. Boxplot showing variations of the Precipitation Datasets. 24
Figure 16. Decomposed trend analysis for long term rainfall in mm in the UAC 25
Figure 17. Scatter Plot of GRACE solutions for UAC from GFZ, CSR and JPL centres. 26
Figure 18. Timeseries plot of GRACE derived Total Water Storage in mm 27
Figure 19. Decomposed timeseries data for TWS in mm derived from GLDAS 28
Figure 20. Yearly Average Soil Moisture and Rainfall in mm for UAC 29
Figure 21. Comparison of TWSC derived from GLDAS and GRACE for UAC 30
Figure 22. Yearly GWSC and precipitation trends in UAC 31
Figure 23. Decomposed time series for GWSC (mm) in UAC 32
Figure 24. Groundwater storage variability from GRACE-GLDAS assimilation 33
Figure 25. Interpretation of observed groundwater levels data in metres. 34
Figure 26. Groundwater Storage Change and Land Deformation through GPS data. 35
Figure 27. Spatial Depiction of Yearly Variation in NDVI 36
Figure 28. Timeseries of NDVI, Precipitation and Rootzone Soil Moisture for UAC. 38

List of Tables

Table 1. Satellites and Sensor for Water Budget Components. 5
Table 2. Output variables from Hydrologic Land Surface data and services at NASA 6
Table 3. Decadal Average Annual Rainfall in mm for UAC 25
Table 4. Yearly and Monthly rainfall patterns in UAC 29

List of Appendix

Appendix 1 – List of Landsat images used to derive NDVI

Appendix 2 – Matlab Code for extracting data from GRACE

Appendix 3 – Matlab Code for extracting data from GLDAS

Appendix 4 – Matlab Code for extracting NDVI from Landsat data

Abbreviations

AET – Actual Evapotranspiration

ANN – Artificial Neural Network

BBMP – Bangalore Bruhat Mahanagara Palike

BWSSB = Bangalore Water Supply and Sewerage Board

CWS – Canopy Water Storage

DEM – Digital Elevation Model

ET – Evapotranspiration

GRACE – Gravity Recovery and Climate Experiment

GIS – Geographical Information Systems

GLDAS – Global Land Data Assimilation System

GW – Ground Water

GWSC – Ground Water Storage Change

IMD – Indian Meteorological Department

ISRO – Indian Space Research Organization

LWE - Liquid Water Equivalent – Output given by GRACE solutions

LSM – Land Surface Models

LUCC – Land Use Cover Change

MSL – Mean Sea Level

NASA – National Aeronautics and Space Administration

NDVI – Normalized Differentiated Vegetation Index

P – Precipitation

PET – Potential Evapotranspiration

R – Runoff (Surface Discharge)

RS - Remote Sensing

RSP – Remote Sensing Products

S – Storage

SDG – Sustainable Development Goals

SW – Surface Water

SM – Soil Moisture

SMC – Soil Moisture Change

T – Time

TWSC – Terrestrial Water Storage Change (Given by GLDAS)

TWS – Total Water Storage (Monthly anomalies given by GRACE months)

UAC – Upper Arkavathy Catchment

WRM – Water Resource Management

WB – Water Balance

Chapter. 1 Introduction

1.1 Background

The Sustainable Development Goal (SDG) number six set by United Nations aims at ensuring safe and clean - water and sanitation in countries affected by water scarcity, drought and desertification by the year 2030. On the contrary, socio-hydrological theories are often associated with complications of regional water flow conditions and human applications in practice depending on socio-economic and politico-legal-cultural conditions, especially in low income, high population countries (Rodriguez-Iturbe, 2000). Blöschl et al. (2019) describes in their paper "twenty three unsolved problems in hydrology" - the lack of a holistic understanding of eco-system sciences and societal needs, to predict the response and evolution of hydrologic systems under changing conditions. Wagener et al. (2010) recognized that a paradigm shift in managing this resource towards a sustainable regime would require the hydrologic community to enhance cross integration of disciplines. Hence, Sivapalan et al. (2014) calls for interfaces in communicating with the society about the uncertainties, synergies and trade-offs in the water-environment-energy-food-health nexus across goals and sectors. In this context, the demonstration of computed scenarios of water management enables 'behaviour changers' (researchers, funders, policymakers, implementers & water end users) to decide on resource allocation and water rights regimes.

1.2 Water Budgeting

A water budget from a regional water resource management (WRM) perspective, provides an estimate of the balance and helps in controlling and managing the water system. The basin level water budget can be assumed with no lateral groundwater flow across a basin with the following equation

$$P = ET + SM + R + Baseflow +- TWS \quad (1)$$

Where,

P = Precipitation; R = Surface Runoff discharge or Streamflow (Usually measured quantity);

ET = Evapotranspiration; SM = Soil moisture; TWS = Change in Terrestrial water storage including interception (canopy water storage), SM and shallow and deep groundwater storage, snows and glaciers etc.

Or rearranged as,

$$R = P - ET - \Delta S/\Delta T \quad (2)$$

Where, $\Delta S/\Delta T$ (mm/t) representing the total terrestrial water storage change (TWSC) including SM, Baseflow and TWS. While discharge and precipitation can be accurately measured, the estimation of the other parameters in the WB equation at a catchment scale remain a challenge (Chen et al., 2019; Blöschl et al., 2019). The calibration and scaling techniques in the estimation of direct ET and SM require exhaustive data on plant physiology, irrigation management, and various hydro-geological inputs at a plot scale (Blöschl et al., 2019).

1.3 Remote Sensing in Hydrology

Remote sensing (RS) is the science of obtaining critical information without physical contact to the target investigation. Their ability in providing reliable information on climate-water-vegetation cycle dynamics has significantly improved in the 21st century (Schmugge et al., 2002). The capabilities of space-borne RS measurements have been effective in a number of hydrologic studies such as drought assessment, evapotranspiration estimation, flood forecasting, runoff estimation for the Indian River basins (Banerjee and Kumar, 2014; Mondal et al., 2016). Remotely sensed data in hydrological applications enables understanding surface features (delineation), detailed interpretation and classification (land use/vegetation types) and estimation of hydrologic state variables in the Water Balance (WB) components. RS based data products (RSPs) are effective research tools in the application of water management and in some cases are more favorable than field measurements for various reasons. Firstly, they provide for global coverage compared to ground studies which are confined to small pilot areas and non-uniform point measurements. Secondly, in areas with human interferences to water cycle, they are more objective, in the sense of over-ruling public opinions. Thirdly, the availability of web based tools which provide free near-real time data collected in a systematic way allows for easy analysis of time-series data and visualization of spatially representative subsets through Geographic Information Systems (GIS). However, Jha and Chowdary (2007) noted that the calibration of RS data products for hydrologists requires transformation and merger of multichannel, multi temporal and more sophisticated models with adequate field data.

An observation-modelling framework has been used by several studies at a regional scale to differentiate between water scarcity (human induced) and drought (natural causes) by comparing a simulated naturalized (undisturbed) hydrological system to a real (interfered) situation (Ferreira et al., 2019; Cui et al., 2019). However, since it require intensive data on hydro-meteorological state variables and computed fluxes for both the periods of without and with human influences, RSPs perform poorly in data scarce regions (Sun et al., 2019). Nevertheless, RSPs can be combined with Land Use Cover Change (LUCC) models to provide insightful hints and proximate drivers in basin level monitoring and management (Gandhi et al., 2015). Studies note that this ability for the fusion of quantitative with non-quantitative data, with other hydrological data (land-use, socio-economic etc.) opens up the traditional black box approach and extrapolate process based modelling methods (Wagener et al., 2010; Srinivasan et al., 2016).

This research investigates the potential of the latest RSPs in combination with ground observations compiled by ongoing projects and literature to investigate on the human influences in river basin management in a water-stressed, data-sparse arid catchment in Southern India.

1.4 Research Objectives

The goal of this research aims to reinvigorate on the long term hydrological processes and the human drivers of change in the Upper Arkavathy watershed.

The objectives are

- To assess the socio-hydrological dynamics of the Upper Arkavathy catchment through the use of remotely sensed hydrological applications.

1.5 RS Databases and their Applicability in Hydrological Modelling

RS products are available for most of the constituent variables with varying spatial and temporal resolution, coverage and accuracy and are discussed in detail in table 1.

1.5.1. Individual WB components

Terrain Data: Digital Elevation Models (DEMs) are raster formatted topographic data from satellites like Shuttle Radar Topographic Mission (SRTM) used in delineating river basins based on topography, providing datasets on stream networks, watershed basin boundaries drainage directions, flow accumulations etc. The Indian Space Research Organization (ISRO) provides validated DEM datasets through their CartoSAT programme.

Precipitation data is derived from microwave radiometric observations aggregated from the Tropical Rainfall Measuring Mission (TRMM), Global Precipitation Monitoring (GPM) products and other multi-satellite algorithms from national and international satellites. The TRMM Multi-Satellite Precipitation Analysis (TMPA) is further extended to match with the Intergrated Multi-satellitE Retrievals for GPM (IMERG) used widely in many applications. Ground observations of precipitation is collected through automatically operated or tipping bucket rain gauges which represent point observations. It is noted that uncertainty in assessment also arises here due to distortion of wind field, installation and operational errors and spatial smoothing. Radar weather stations as a substitute provide better spatial resolution. Mishra and Rafiq, (2019) and Sinha et al. (2019) indicated a poor performance of RS based rainfall data of Indian monsoon. This is primarily attributed to the fact that India is a topographically complex region.

Evapotranspiration (ET) is the sum of water transferred from the surface by evaporation from soil, water and all other surfaces to vapour form and transpiration from plants. ET depends upon the radiation at the surface, land and air temperatures, humidity, winds, soil type, vegetation cover. The significance of ET in drought monitoring is especially magnified. Potential evapotranspiration is derived from number of parameters of which temperature and solar radiation are primary through methods used by the Food and Agricultural Organization (FAO) (Chen et al., 2019). On the other hand, Actual Evapotranspiration on field scale is estimated through the use of Lysimeters and Eddy Covarince towers. ET can be spectrally measured through sensors in the visible, near infrared (IR), middle IR, and thermal IR. Several RS based ET products are available from the MODerate Resolution Imaging Spectroradiometer (MODIS), Mapping and EvapoTranspiration at high Resolution with Internalized Calibration (METRIC), Multi-satellite ET from the Atmosphere-Land EXchange Inverse (ALEXI). Shwetha and Nagesh Kumar, (2018) showed high coefficient of determination values of r^2 of 0.84 of satellite based reference crop ET from the MODIS against the FAO calculated observations from automated weather stations for the Cauvery basin.

Soil Moisture is the measure of water content in the soil. Insitu measurement of soil moisture is done using Frequency Domain Reflectometer (FDR), Time Domain Reflectometer (TDR), Neutron moisture gauges, Soil resistivity or Galvanic cells. In remote sensing, this parameter

is derived from the L-Band spectral measurement of the microwave radar. Soil moisture Active Passive (SMAP) data from Synthetic Aperture Radar from the Sentinel-1 provides a spatial resolution of 36km and 9 km and a temporal resolution of 3 days for a temporal coverage from March 2015. Prior to this, the Advanced Microwave Scanning Radiometer-Earth Observing System (AMSR-E) has obtained and combined extensive ground truth information with hydrological models to provide reliable soil moisture data from 2002. Pangaluru et al. (2019) estimated the r^2 of RS derived soil moisture as the primary variable with secondary variables precipitation, surface air temperature, total cloud count and total water storage (TWS), to 0.65, −0.72, 0.71, and 0.62 respectively, for the Indian subcontinent. The study also indicated a small negative trend for the period of 2002-2017 in southern India. Further, Feng, (2016) indicated that the vegetation change accounts to up to 40.21% in the regional soil moisture drying.

Streamflow is generally derived through gauged data at streams or reservoirs. This is a crucial component required to validate hydrological research. Gauged data provides for discharge fluxes and hence can be used to reduce the errors estimates in the other components. Satellite altimetry through the Jason 1, 2, and 3 missions provide for reservoir height data exclusively for 315 bigger reservoirs in the world currently. Moreover, runoff in streams is generally determined through a gauged measurement.

Baseflow is the contribution of drainage from soil and ground water to the streamflow. It cannot be directly observed by satellites and is calculated as the redundant of equation (1).

Balancing errors arise due to the temporal and spatial variation depending upon the satellite data used for water budgeting. The upscaling of ET and SM from field data is highly subjected to errors due to variation and hence these components need to be carefully considered while using RS products. Hence, data should be selected accordingly depending upon the research requirements and it must be made sure that all datasets are in a common spatial and temporal resolution.

Table 1. Satellites and sensor for water budget components. (http://arset.gfsc.nasa.gov)

Water Budget Component	Satellites	Coverage	Spatial resolution	Temporal Resolution	Sensors	Spectral Measurements	Data Source
Precipitation	TRMM/GPM/ TMPA	12/1997 - present	0.25 x 0.25 degree	3 hours	Microwave Radiometer and RADAR, TMI, PR, GMI, DPR	TMI: 10–85 Ghz GMI: 10–183 GHz	http://giovanni.gfsc.nasa.gov/giovanni http://pmm.nasa.gov/data-access
	IMERG	2/27/2014 – present	0.1 x 0.1 degree	30 minutes			
Evapotranspiration	MODIS/ Terra & Aqua	2010 – present	500m	8 days	MODIS	Visible. Near IR, Middle IR	MODIS - http://lpdaac.usgs.gov/node/1191 MOD16 A2 - http://earthdata.nasa.gov
	LANDSAT - METRIC	2011 – present	30m	16 days	TM, ETM, OLI	Visible. Near IR, Middle IR, Thermal IR	http://arset.gfsc.nasa.gov/sites/default/files/water/ET-SMAP
Soil Moisture	SMAP	March 2015 – present	36km , 9km	3 days	L band radiometer		http://smap.jpl.nasa.gov
Groundwater (TWS)	GRACE & GRACE-FO	March 2002 – 2019	0.5 x 0.5 degree	250 gravity profiles per day	Microwave radar	K - Band	https://podaac-tools.jpl.nasa.gov/drive/files/allData/grace/L3/land_mass/RL06
Terrain Data	SRTM, (NASA) CartoSAT (ISRO)	2004 - present 2005 - present	30 m 30 m		Microwave based sensory Optical based sensory		https://earthexplorer.usgs.gov/ https://bhuvan-app3.nrsc.gov.in/data/download/index.php
Vegetation dynamics	LANDSAT 4-5/7-8	1982- present	30 m	15 days approx.	TM/ETM 8 bands	0.45 micro m - 0.90 micro m	https://earthexplorer.usgs.gov/

TMI: TRMM Microwave Imager DPR: Dual-frequency Precipitation Radar SRTM: Shuttle radar topography mission

PR: Precipitation Radar TM: Thematic Mapper

GMI: GPM Microwave Imager ETM: Enhanced Thematic Mapper OLI: Operational Land Imager

1.5.2. Assimilated datasets

Historically, the individual datasets along with the measurement of each of these components have been used, though they have proven to be cumbersome in their integration to quantify water balances consistently and precisely. Cui et al. (2019) note the shift in data acquisition for single constituent variables (precipitation, evapotranspiration, soil moisture, etc.) to a more comprehensive approach in producing self-verified data sets for integrated research of watershed processes and interactions. Emerging advances in Data Assimilation (DA) systems from RS products provide continuous hydro-climatic data in gridded datasets and have proved their performances in many parts of the world (Müller, 2017). Land Surface Models (LSMs) integrate physical, chemical and biological components. They couple RS measurements in adjustments to in situ observations and distributed hydrological models through Artificial Neural Networks (ANN), which are effective self-learning algorithms, to provide efficient information on water budget components (Rodell et al., 2004). The aim of this approach is to account for optimal merging of inaccurate model simulations, uncertain observations and forcing data. NASAs Earth Observing System (EOS) and other satellite platforms have been instrumental for processing, archiving RS and model data and grants open source hydrological LSM output variables as shown in table 2 (https://disc.gsfc.nasa.gov/data-access). The NASA Goddard Earth Sciences Data and Information Services Center (GES DISC) provides for varied robust hydrological LSM products like the Global Land Data Assimilation System (GLDAS including the assimilation of newer satellite data like TRMM, SMAP and MODIS (Pokhrel et al., 2016).

Although there have been considerable improvements to the assimilated forcing data models, Qi et al. (2018) note that these are applicable only to the parameters of precipitation and temperature. Contrarily, Nayak et al. (2019) states these LSMs have lower uncertainties in the estimation of ET and SM than other satellite products in long term studies, however perform poorly in highly interfered catchments.

Table 2. Output variables from Hydrologic Land Surface data and services at NASA GES DISC. (Rui et al., 2019)

Type		Variable	Unit
Meteorological Forcing		Wind Speed	M
		Total Precipitation rate	$Kg/m^2/s$
		Near surface air temperature	K
		Near specific humidity	Kg/kg
		Surface pressure	Pa
		Downward short-wave radiation	W/m^2
		Downward long-wave radiation	W/m^2
Land Surface Model (LSM) Output	Energy Balance	Net short-wave radiation flux	W
		Net long-wave radiation flux	W/m^2
		Latent heat flux	W/m^2
		Sensible heat flux	W/m^2
		Ground heat flux	W/m^2
	Water Balance	Rain rate	$Kg/ m^2/s$
		Snow rate	$Kg/ m^2/s$
		Evaporation	$Kg/ m^2/s$
		Transpiration	$Kg/ m^2/s$
		Evapotranspiration	$Kg/ m^2/s$
		Surface runoff	$Kg/ m^2/s$
		Baseflow runoff	$Kg/ m^2/s$

		Snow melt	Kg/ m^2/s
	State	Surface temperature	K
		Albedo	~
		Snow depth water equivalent	Kg/ m^2
		Soil moisture	Kg/ m^2
		Soil temperature	K
	Others	Stream flow	M^3/s
		Flooded fraction	~
		Flooded area	m^2
		Irrigated water rate	Kg/ m^2/s
		Terrestrial water storage	Mm
		Groundwater storage	mm

1.6 Total Water Storage and GRACE

TWS consists of groundwater, soil moisture, surface water, and snow/ice equivalent. The Gravity Recovery and Climate Experiment (GRACE) and the follow-on satellite missions is composed of twin satellites operating at a K-band microwave ranging providing spatial and temporal information on the total mass changes on the earth system. The post processing applied to these monthly anomalies give the water compartment on land surfaces, which are useful in hydrological studies. Be that as it may, deriving solutions from gravity mass variations requires complex combinations of astrophysical and earth system sciences. These have been developed at three centres – (i) the Centre for Space Research (CSR) in Austin, Texas, United States, (ii) the GeoForschungs Zentrum (GFZ) in Potsdam, Germany, and (iii) the Jet Propulsion Laboratory (JPL) in Pasadena, California, United States. Alongside, GRACE also provides for monthly TWS anomalies through the mascon (mass concentration blocks) solutions with improvised information on earth surface processes (Rowlands et al., 2010). Sakumura et al. (2014) state that the differences between the three solutions for the water equivalent height for land data are very minimal and suggests that the simple arithmetic mean of the three would be the most effective solution.

GRACE solutions have no vertical resolution i.e. they quantify TWS anomalies in terms vertically integrated equivalent water heights (EWH) or Liquid Water Equivalent (LWE) of both shallow and deeper aquifers as shown in figure 1.

Satellite derived storage estimates have correlated well with groundwater models which are rather data intensive (Landerer and Swenson, 2012). Besides, GRACE LWE has also been applicable in calibrating evapotranspiration, soil moisture and runoff estimations (Frappart and Ramillien, 2018).

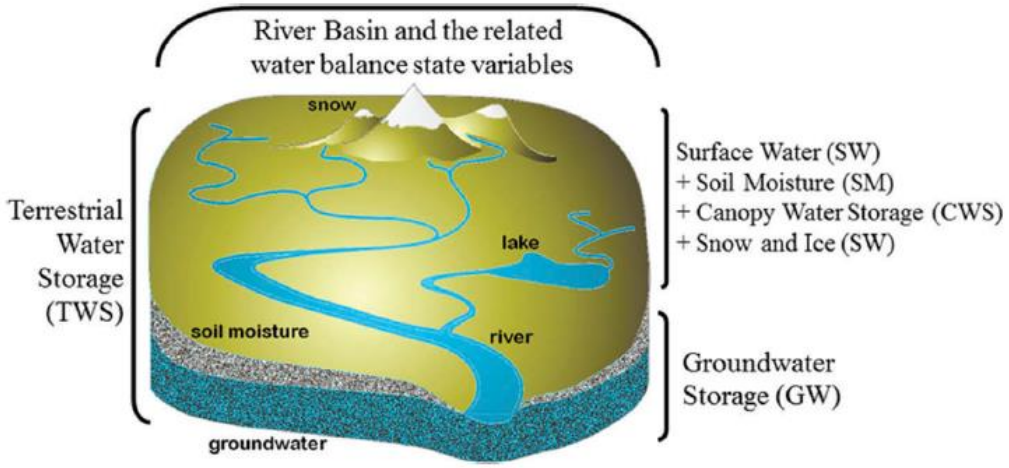

Figure 1. Components of total vertically integrated water storage and visualization of the TWS determination concept. (Ouma et al., 2015)

However, GRACE's spatial resolution and relatively short span of data coverage may not be appropriate for smaller basin studies. Chen, (2018) pointed out on the challenges to simulate ET and recharge dynamics under human induced systems of reservoir regulation in the Songhua river basin in North East China using RSPs. The effect of the three gorges dam on TWS using GRACE and LSMs has been well documented in the study of Huang et.al, (2015) on the Yangtze River basin in China.

An alternative approach to quantitatively map GW depletion is through the RS derived ground displacement data. This is mainly based on Earths surface's elastic and porous response to ground mass variations in the aquifer. Several studies indicate a good correlation between ground subsidence and groundwater depletion (Vissa et al., 2019; Hao et al., 2019). Castellazzi et al. (2016) notes that this approach can enhance the fractured aquifer understanding without the requirement of intensive lithological data.

1.7 Spatial Characterization of LUCC

Similar to hydro-climatic DA, RS products are highly instrumental in land use planning and has been providing information on the physical characteristics of land (Woodcock et al., 1983). Dynamic Global Vegetation Models (DGVM) have been developed to simulate transient dynamics between vegetation and climate. Index stacking using spectral indices is the most common method for assessing landscape features, vegetation and water layers through satellite data (LANDSAT imagery). Vegetation is a good immediate indicator for water stress and Normalized Difference Vegetation Index (NDVI) is the measure of the vegetation which is active in photosynthesis. The comparison of absorption through photosynthetically active radiation and reflection and other hydrological parameters helps assess the characteristics of vegetation phenology and agricultural practices in a region. Atmospheric and vegetation interaction is also processed through products developed for vegetation canopy like Gross Primary Productivity (GPP), Vegetation Continuous Cover (VCC), Leaf Area indices (LAI), (Feng 2016). Verbesselt et al. (2010) introduced new techniques on monitoring seasonal

drought vegetation conditions through satellite images using other indices including the Normalized Difference Water Index (NDWI).

Several studies have also explored the inter-linkages between human induced vegetation phenology and GW storage. McCandless (2014) noted that the inter-annual change in moisture dependence of vegetation has a good correlation with the combination of GRACE TWS and NDVI indices for drought identification in Texas. Hao et al. (2019), indicated decreased streamflow is a result of extended growing seasons fed by groundwater and decreased wet season were the primary reason for basin water loss in China.

Chapter. 2 Study Area

This research focuses on the Arkavathy River, which is a sub-basin of the larger east flowing Cauvery River in Southern India (see figure.1). The 3314 km^2 catchment overlaps with the city municipality's (Bangalore Bruhat Mahanagara Palike (BBMP)) boundaries and receives an average annual rainfall of 830mm. The Arkavathy was the major source for water supply to Bangalore city from 1937 to 1980s. But it is to be noted that post-1990s, reservoirs on the Arkavathy hardly provide any of the stipulated $1.5x10^5$ m^3/day to the city. The rate of drying up of the river has been alarming.

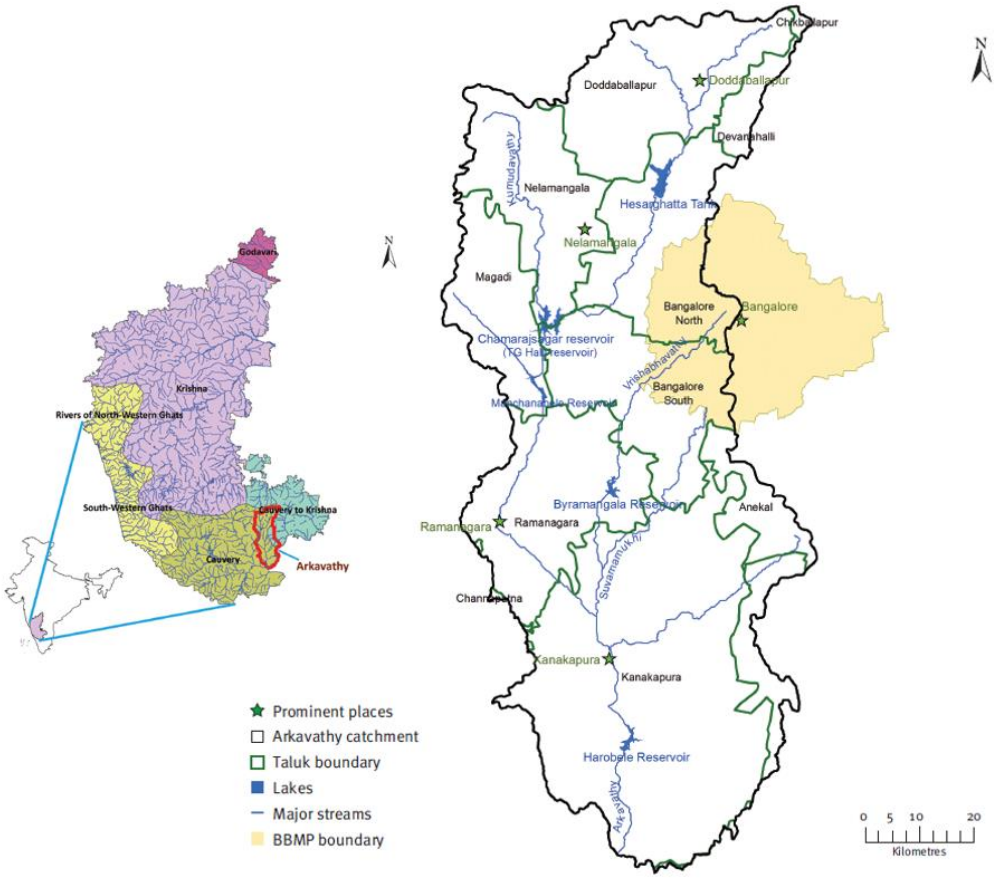

Figure 2. Location and major features in the Arkavathy catchment. (Lele et al., 2013)

2.1 Regional WRM Context

Parallely, the Bangalore Water Supply and Sewerage Board (BWSSB) noted that the city's water imports from other reservoirs on the Cauvery River increased from 1.85x103 m^3/day in 1974 to 1.35x10^6 m^3/day in 2017. This is primarily sourced through the Krishna Raja Sagara (KRS) dam located 145kms away, noted to have considerable pipeline and evaporation loses (Poyil et al., 2016). However, water diversions from the Cauvery to the city drastically affect the water budgeting closure, which assumes no inter-basin transfers. Basically, there would be considerable uncertainty in accounting for the return flows (waste water from the city) in the lower Arkavathy catchment directed through the Vrishbhavathy River (catchment area, 561km^2.). Moreover, the catchment is conveniently divided into the upper and lower part at the Chamrajsagar or Tippagondahalli (TG Halli) reservoir, built in 1935 on the confluence of the Kumudavathy and Arkavathy Rivers. The stream gauge data, in an otherwise data sparse area, shows a decrease of 96% in inflow from 3.85x10^5 m^3/day during pre-1975 to 1.5x10^4 m^3/day in 2013 (see figure.3). The upper catchment covers an area of 1447 km^2 (89%- rural ; 11%- urban) and contains another reservoir called the Hessarghatta tank which has completely dried up as well. Hence, it is obvious to apply water accounting techniques to develop socio-hydrological theories only on the Upper Arkavathy Catchment (UAC) and avoid the uncertainty of the inter basin transferred return flows in the lower catchment.

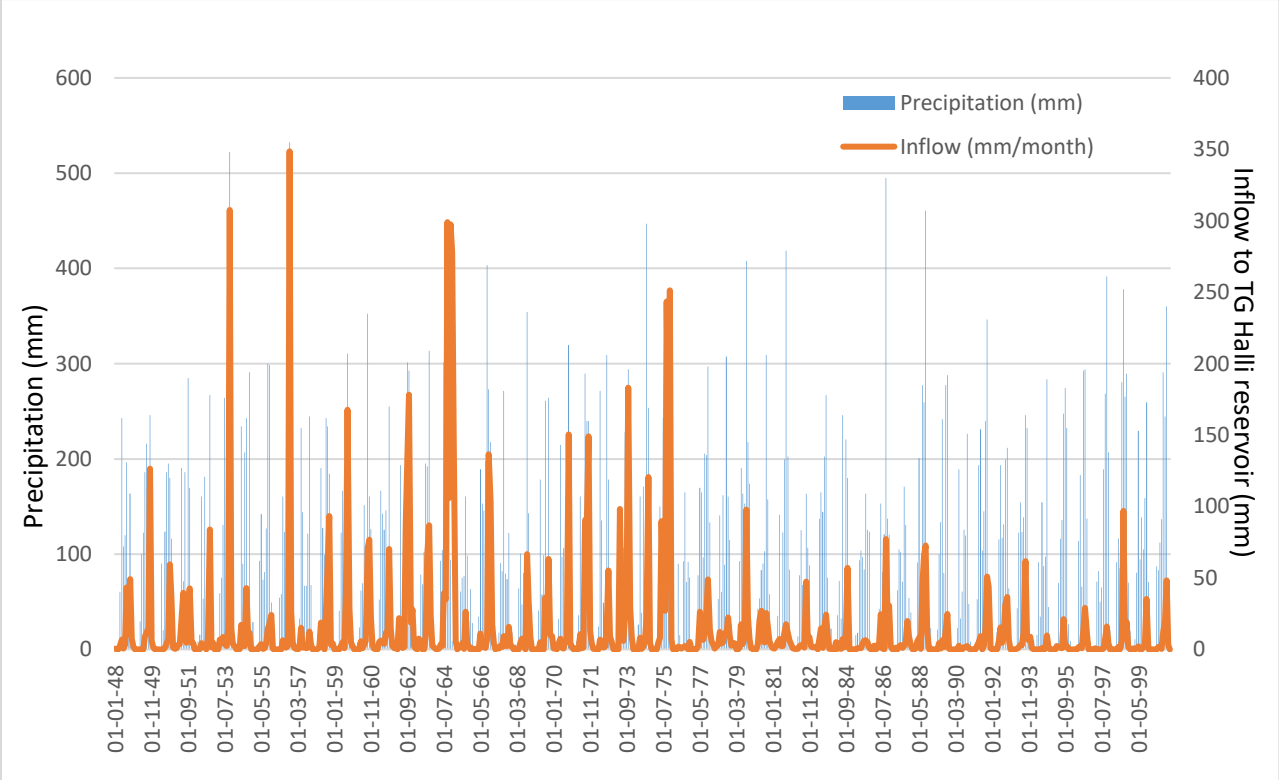

Figure 3. Monthly inflow and rainfall data at the TG Halli catchment in the upper Arkavathy.

2.2 Land and Human Water Use

Land use cover changes reported an urbanization rate of 2.3 km^2 per year in the pre-2002 period and 3.8 km^2 since 2002 in the UAC (Lele and Sowmyashree, 2016). Penny et al., (2018) noted

that the area under eucalyptus plantations increased from 11 km^2 in 1973 to 104 km^2 in 2001 as they required less maintenance and no irrigation. Rural watershed development programmes constructed over 277 check dams or obstructions to promote capture of streamflow and increase aquifer recharge. They could also act as sediment retaining structures. Figure.4 depicts the land use cover in the catchment for the year 2014.

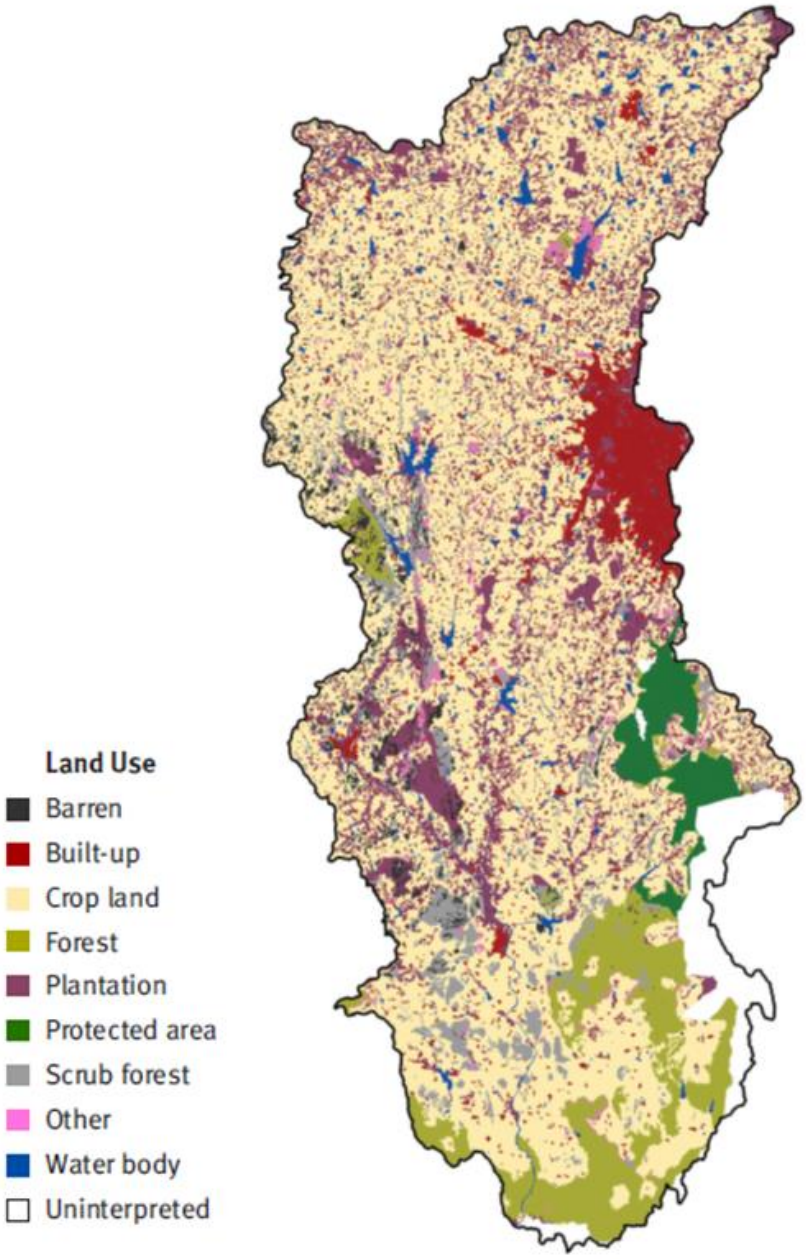

Figure 4. Landuse map of Upper Arkavathy Catchment for the year 2014. (Lele et al., 2013)

The rural watershed supports both rain fed and irrigated agriculture which is mostly supplied by groundwater and has undergone important land use cover changes. Irrigation schemes changed from tank system to groundwater fed drip irrigation systems (Thomas et al., 2015).

The shift towards groundwater usage coincides with the drying up of the surface water bodies (see figure.5). This has also had consequences on the farmers in the Arkavathy catchment area, who either have to decide to abandon their land or drill for deeper groundwater (Ballukraya and Srinivasan, 2019).

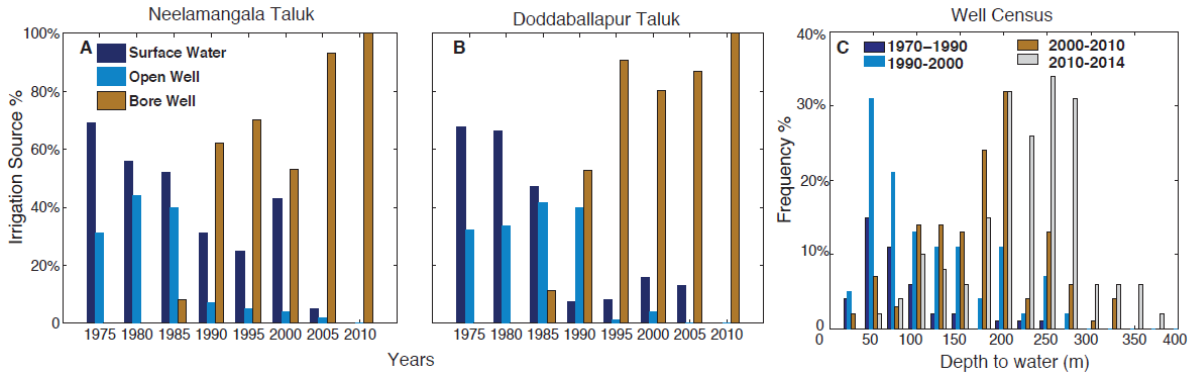

Figure 5. Changes in irrigation sources in the Upper Arkavathy Catchment (Srinivasan et. Al 2018)

Patil et al. (2019) explain that the problem of crop choices and farmers responses in the catchment is two-fold. Firstly, with the rapid urbanization of the city, the farmers have the opportunities to diversify their income outside agriculture, hence they adopt the described "Go deep or quit" strategy. Secondly, due to the lack of incentives and regulatory mechanisms in conserving water, both smaller (poorer) and larger (well off) farmers both have the tendency to adopt water intensive crops (Bierkens et al., 2019). The cumulative effects due to this intensive GW extraction has not only led to the drying up of the water bodies but has also created an inequitable and unsustainable dominion among the farmers livelihoods (Lele et al., 2018).

2.3 Groundwater and Hydro-Geology

The geology is predominated by migmatites, granodiorites and intrusive granites which generally do not carry potential fractures beyond 280 m depth (Ballukraya and Srinivasan, 2019). However, since the unconfined and part of the semi-confined aquifers have gone dry, boreholes are being drilled at deeper depths even down to 400 m (Sekhar et al., 2018). Furthermore, the observed levels in the wells are highly heterogeneous in space and time and the interpretation of the fractured gneissic complex that underlie the area remains a challenge (Kulkarni and Shankar, 2014). There is a powerful rhetoric in achieving groundwater sustainability by banning the digging of private borewells and encourage citizens to depend on monitored community borewells (Kulkarni et al., 2015). In opposition, Srinivasan and Lele (2017) indicated to completely reject the concepts of sustainable yield or achieving "non-diminishing groundwater levels. They rather pointed out that there are hardly any other alternatives for the rural-urban transects water supply.

A camera inspection of 83 wells in the study area led Ballukraya and Srinivasan (2019) to hypothesize on the fracture and groundwater movement in these highly stressed aquifers. They suggest as shown in figure 6 – the natural state for hydrogeological conditions and the conditions for the severely exploited systems in UAC. Basically they reported a high density of fractures close to the ground surface which is mainly attributed to high spatial density of the drilling activities which we refer to as the surficial aquifer. Due to this high density of borewells,

they suggest that there is high downward movement through the borewells shafts which has led to the formation of a dewatered zone above the saturated zone (sub-surficial aquifer).

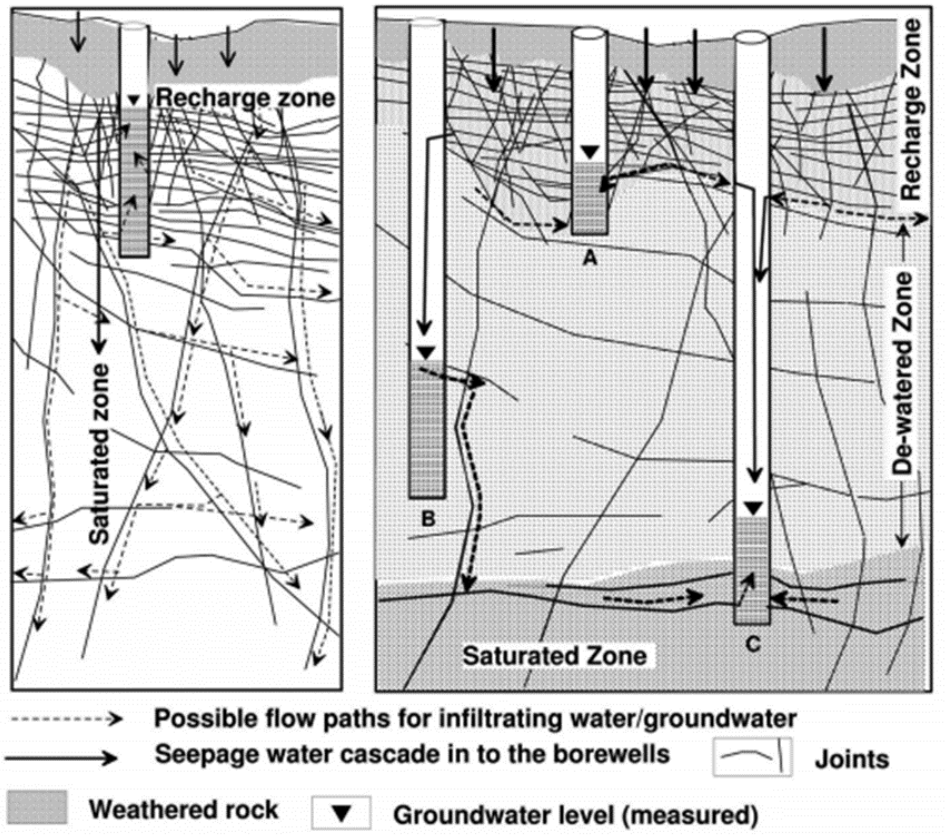

Figure 6. Conceptual model explaining the flow in fractured rock aquifer region. (a) Normal hydrogeological condition. (b) Conditions in severely exploited system. Note the flow of water from shallower borewell through an exposed joint near water level (Ballukraya and Srinivasan, 2019)

2.4 State of Hydrological Research

The drivers to explain the drying of the river derived from stake holder and scientific perceptions were identified as (i) Declining rainfall, (ii) Increasing potential ET due to climate change (iii) Declining baseflow due to groundwater overexploitation (iv) Increasing actual ET due to expansion of water-intensive plantations, (v) Million puddle theory – check dams acting as recharge structures or evaporation ponds obstructing structures to overland flow in the river. In the absence of data, Srinivasan et al. (2017) developed a scale model particularly aimed to determine if the perceived hydrological drivers have changed and if so, the magnitude of these changes are adequate to explain the consistent decline of flow in the Arkavathy river. The daily rainfall data recorded from four rain gauges in the catchment showed no significant statistical trend in rainfall and increasing average temperatures were within the stipulated climate change literature. Hence, they inferred that the natural climatic drivers were not responsible for the loss of inflow in TG Halli. It was observed that the baseflow started declining in the early 80s and

there was no baseflow contribution after 1992 (see figure 3). In absence of long term groundwater data, the months of inflow into the reservoir with no rainfall were investigated. A recession analysis showed that the mean relationship between aquifer storage and discharge was in line with the Dupuit-Bossinesq theory (Srinivasan et al., 2017). On comparison to previous studies by Indian Space Research Organization (ISRO) which stated that a minimum of 20 mm of rainfall is required to generate surface runoff in Arkavathy stream, Srinivasan et al., (2015) catchment model did not show any statistical significance in such threshold values. Furthermore, Penny (2017) isotope study of the rainwater and discharge indicated that most of the waters signals matched the new rain water indicating overland flow generation. Although several studies have documented the high ET of Eucalyptus plantations, Srinivasan et al. (2017) suggest that post 2002 even though there was an increase in their area and changes in irrigation schemes, ET began to drop, despite increasing population and domestic water needs. Moreover, Penny et al. (2018) measurements of soil moisture under the plantations failed to explain the drying up of the deeper aquifers. Additionally, Penny (2017) measured the hydraulic conductivity of dried tank beds (unaltered) at the land surface using a Tension infiltrometer and Disk Permeameter and concluded that they do not act infiltration or recharge structures. It was observed that other irrigated crops had higher correlation to the drying up of the tanks than Eucalyptus (Penny, 2017).

Theoretically, the check dams should have increased soil moisture and therefore ET and GWS as well. However, Penny et al. (2018) estimated hydraulic conductivity is similar to that of the catchment, and further stated the overland flow captured by the check dams mostly continued as overflow or evaporation, and recharge did not take up much of the water balance fraction. Although farmers in the vicinity of the check dams would favour the use, the efficiency to mitigate GW recharge at a catchment scale was found to be negligible (Kulkarni et al., 2015). Lele et al. (2018) argue that on a policy perspective, quantifiable surface water was being converted to “invisible” GW which was pumped out leading to unsustainable distribution of the resource. Nevertheless, these studies acknowledge that process based reconstruction of the saturated hydraulic conductivity and the storm dynamics and timing cannot not clearly associate with each other due to the high hydro-geologic heterogeneity in the aquifer (Srinivasan et al., 2017; Penny, 2017).

Comprehensively, these studies indicated that the human influence in altering the hydrological cycle was implicit in the drying up of the Arkavathy River. Hence, a constructive way for further research is to dwell into the scientific assessment of this understanding these through RS based datasets.

Chapter. 3 Data and Methods

This study approaches the understanding of this socio-hydrological system through the application of multiple criterion to detect drought and scarcity through the use of remote sensing products. The framework of the methodology is given in figure 11.

3.1 De-trending and De-seasonalization

Any hydrological time series data generally require decomposition to account for the trend and seasonal components. These factors can overstate or underestimate the actual patterns in a time

series and often need to be split into the base level, trend and seasonality. There are several methods to decompose the time series which has been detailed by Verbesselt et al., (2010). The decomposition was done using classical seasonal decomposition by moving averages package in Python "statsmodels.tsa.seasonal.seasonal_decompose" (Hirsch and Slack, 1984). The multiplicative seasonal component is chosen for hydrological data as suggested by Mondal et al., (2018). The procedure for smoothening of trends is adopted by the application of LOESS - Locally weighted polynomial regression method uses the weighted least squares giving weightage points based on the basis of the distance from the response being estimated (Cleveland and Devlin, 1988). The LOESS model was applied to the curves through the package in Python (Cappellari et al., 2013). The seasonal Mann-Kendall test is used to ascertain non-parametric trend tests for seasonal data (Hirsch and Slack, 1984). The application of the Mann Kendall test for the time series data was done with the package in Python (Hirsch and Slack, 1984). A significance level of 95% with the null hypothesis (there is no trend) was used as a threshold for this study. This test checks the trend from one month in a year to another and the overall trend. A tau value which indicates the variance is calculated for each season and then averaged for the overall trend. The seasonal and annual fluctuation are further examined with a linear regression to other parameters to indicate and infer the significance in each data time series.

3.2 Data Selection to highlight drivers in WB equation.

Two different satellite datasets were checked against each other - The globally accepted GLDAS version 2.1 and the more locally used India Water Portal (IWP) meteorological data which uses the Tyndal Centre for Climate Change dataset. Both datasets provides hydro-climatic data at a spatial resolution of 25 km x 25 km grid (0.25 degree) and one degree with a temporal resolution of monthly scales from 1948-2018. They were checked against the Indian Meteorological Department (IMD) rain gauge data at Nelmangala (Wien, 2019; Skaskevych, 2014). The GLDASv2.1 showed a better regression to the rain gauge than the IWP with r^2=0.89>0.73 for long term rainfall. The GLDAS also showed higher regression to observed data of average temperature as compared to IWP with r^2=0.97>0.96. Hence, GLDAS was selected as the baseline LSM for this study. GLDAS-2.0 provides daily, monthly data product and the GLDAS v.2.1 additionally provides a 3-hourly dataset. The monthly product was considered sufficient temporal resolution for this study.

The output of GLDAS models are forced with the results of four land surface models: the Variable Infiltration Capacity (VIC) model, Community Land Model (CLM), NOAH (National centres and Oregon state university Airforce and Hydrology lab) and Mosaic. However, products forced with the VIC and the CLM are yet to be published. The GLDAS NOAH v2.1 (giovanni.gsfc.nasa.gov/) is forced with the Global Meteorological Forcing Dataset from Princeton University containing 33 variables with errors given and corresponding to Rodell et al. (2004). The overlay of the Upper Arkavathy Catchment is shown in figure 7.

An areally averaged time series was generated in Matlab for the parameters of total precipitation rate, PET, average temperature, Canopy Water Storage (CWS), soil moisture (SM), Surface Water (SW) and Root Zone Soil Moisture (RZSM). The data for these parameters were downloaded as NetCDF files from the NASA Giovanni website for the study area and time period. The time series was extracted based on the area overlapped on a grid and the grid value from these NetCDF files. The parameters were converted from their individual units as shown

in Table 2 by multiplying the values with the catchment area, time conversion to months and density of water to obtain them in mm/month scale. The fully reproducible code is available in the Appendix.

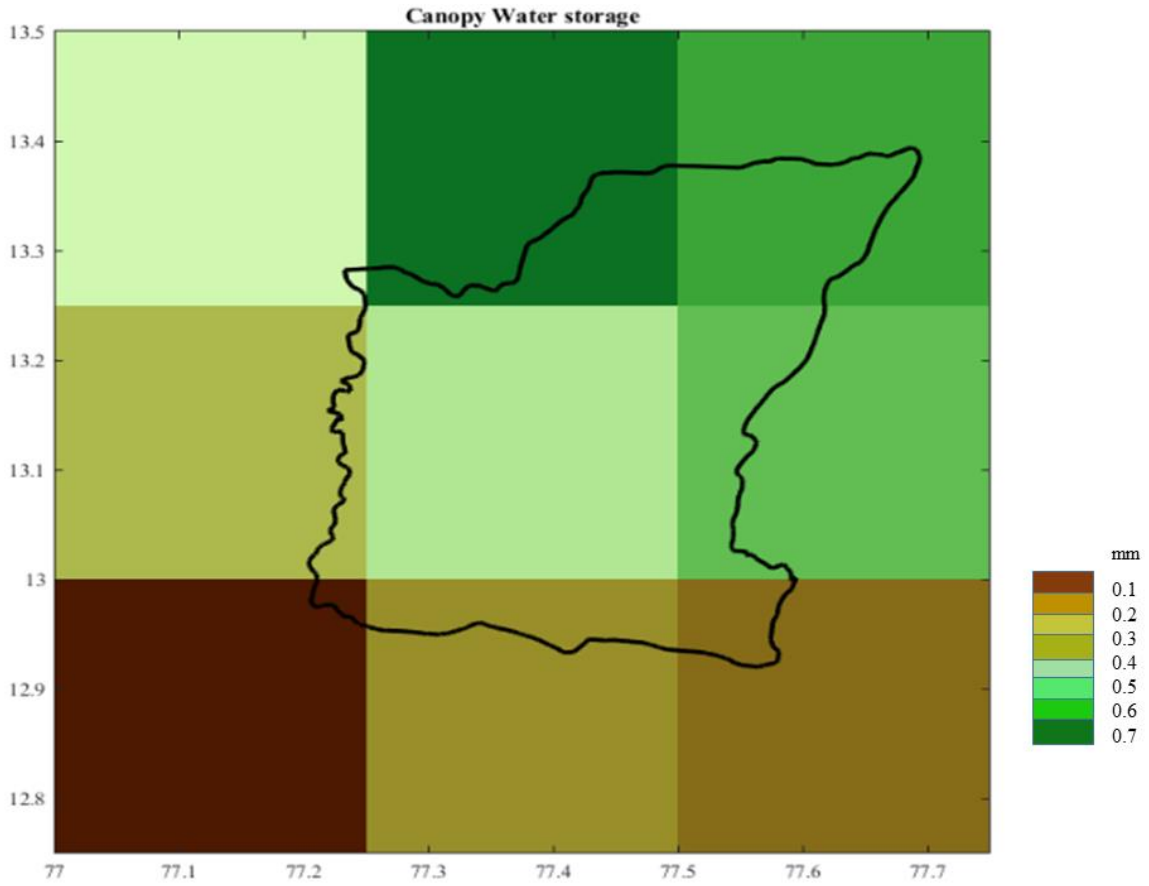

Figure 7. Overlay of Upper Arkavathy Catchment on GLDAS gridded dataset.

3.3 Quantifying Groundwater Storage Changes

Mukherjee and Ramachandran (2018) found that the relationships between the TWS in predicting GW levels in India is more significant through GRACE TWS calculations rather than through the GLDAS water components, which do not capture unmodelled anthropogenic processes. This is primarily due to the reason that GRACE lumps the shallow and deeper GW together as a single quantity. In other words, the mismatch of LSM's TWS signals are attributed to the lack of representation of human interventions which disrupt the empirical solutions for complex dynamic processes dependent on ET estimation, rainfall intensities and saturated hydraulic conductivity of the soil. However, Sun et al. (2019) demonstrated the correction of the GW component in GLDAS through an ANN model to match GRACE data for the Indian subcontinent. Several studies have also investigated on the applications of GRACE data with in-situ and/or modelled simulations to assess GW depletion. Assimilation of GRACE observations with GLDAS provides the ability to disaggregate the TWS components and their fluxes (Wu et al., 2019). This approach is used to quantify groundwater storage change (GWSC) in this study and further assessed with the groundwater levels and land deformations in the area.

3.3.1. TWS from GRACE Mascons

For this study, the latest Release 6 -level 3 monthly mascon TWSA product (RL-06) released by the JPL, CSR, GFZ was downloaded from the Physical Oceanography Distribute Active Archive Center (PODAAC) (https://podaac-tools.jpl.nasa.gov/drive/files/allData/grace/L3/land_mass/RL06). McCullough et. al (2019) note that the RL 06 products are more accurate than the previously released RL-05 mascons in terms of application of the implementation of time correlation between the previously released GRACE and first time release of the GRACE-FO and indicates that all the solutions for all the other months have also been slightly re-estimated from previous solutions.

The Net CDF files for land mass water equivalent solutions were downloaded from all the three centres. The processing of the Mascon solutions was done in Matlab and the code is enclosed in the appendix. The liquid water equivalent is computed for the center of the upper grid which almost covers the entire upper Arkavathy catchment (see figure 8).The liquid water equivalent is given in cm for given time periods where the satellite has recorded. A time series was generated with the average of all three solutions products (GFZ, CSR, and JPL) and converted to mm scale. It must be noted that the satellite does not have an equidistant temporal coverage. Moreover, there are missing days due to instrument issues in the generation of the nominal month and data are now readily available. These missing data were filled up through linear interpolation according to Landerer and Swenson (2012).

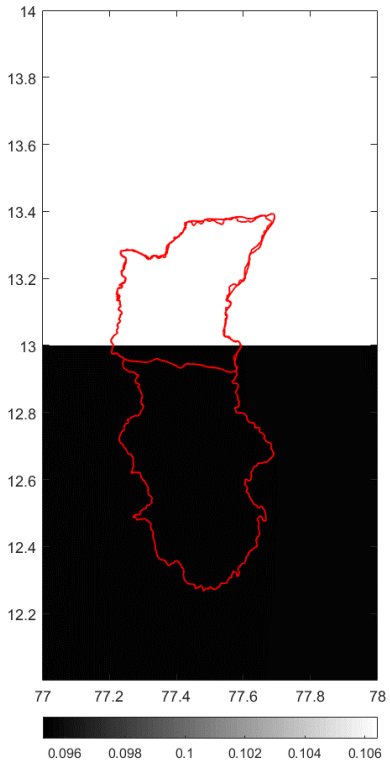

Figure 8. Overlay of Arkavathy Catchment on grided GRACE Mascon dataset

The components of the water balance equation are re-arranged in form of the equation below to equalize the inflow and outflow fluxes in the system.

$$\Delta TWS_{GRACE} = \Delta GWS + \Delta SM + \Delta SWE + \Delta SW + \Delta CWS \quad (4)$$

$$\Delta GWS = \Delta TWS_{GRACE} - (\Delta SM + \Delta SW + \Delta CWS) \quad (5)$$

3.3.2. TWS from GLDAS

The procedure for extracting the time series data has already been explained in 3.2. Unlike GRACE data, GLDAS provides consistent monthly data starting from the first of every month. Since GW is not modelled directly by the GLDAS model, TWS is the sum of soil moisture, surface runoff and snow water equivalent. As the study area is in the tropical latitudes with no snowfall, snow water equivalent does not become an important factor to consider. It is also important to note that SW is considered as the intersection of static water table and the land surface according the GLDAS, hence SW can be considered as an extension of the groundwater particularly because we are only dealing with low or no flows.

$$\Delta TWS_{GLDAS} = \Delta SM + \Delta SW + \Delta CWS \quad (6)$$

$$\Delta GWS = \Delta TWS_{GRACE} - (\Delta TWS_{GLDAS}) \quad (7)$$

The NOAH LSM incorporates total volumetric soil moisture and volumetric liquid soil moisture, soil temperature in four soil layers (0–10 cm, 10–40 cm, 40–100 cm, and 100–200 cm), for a soil depth of 2m to compute near surface soil moisture.

3.3.3. Observed Groundwater Levels

The Ground water levels in borewells and piezometer levels was compiled by the Central Groundwater Board (CGWB) as district wise monthly data in the Arkavathy catchment (http://cgwb.gov.in/GW-data-access.html). There were 20 wells within the catchment which had long term available data from 2000-2017 which were used in this study.

3.3.4. Observed GPS Data

To understand the change in land deformation and relate to the change in groundwater storage, GPS data becomes crucial to validate our findings. The Magnet GPS network by the Nevada Geodetic Laboratory provided for long term GPS data. Since there was no data available directly in the catchment, the measurements at the Indian Institute of Sciences (IISc) (2002-2019) station located closed to the catchment is utilized for this study (Blewitt et al., 2018).

The spatial description of the data points used in the study are shown in the figure 9.

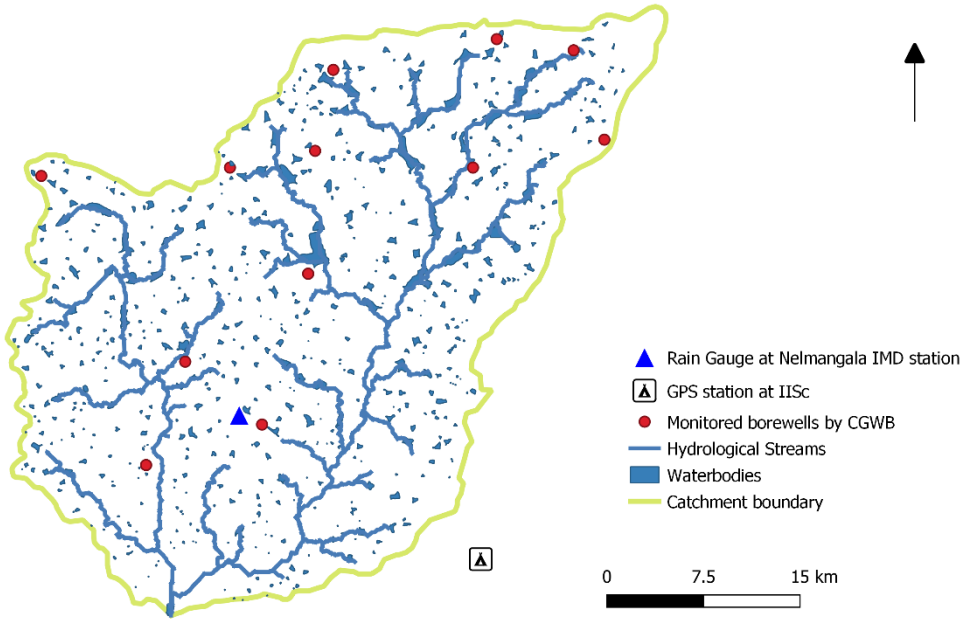

Figure 9. Spatial map for observed rain gauge and borewell data used in the study.

3.4 Quantifying Vegetation Index

To detangle the human influences, it becomes important to identify the influence of agricultural practices on the catchment. The vegetation dynamics in the catchment are modelling using the NDVI index to highlight any change in long term and seasonal changes in greenness in the area. It is a unit less quantity varying between +1 and -1 and is calculated using the below equation. Basically, the comparison of the visible light and the near infrared light reflected from the plant helps assess the type and state of vegetation. Healthy and dense vegetation absorb higher visible light and reflect higher NIR light as compared to unhealthy or scarce vegetation (Feng 2016). Similarly water bodies have low radiation and higher absorbability of visible IR ranges.

For this, a combination of LandSAT data Collection 1 images was used from 1988-2018. The LANDSAT level-2 imagery were downloaded from the Earth Explorer USGS (https://earthexplorer.usgs.gov/) website. The level two products for Landsat 4-5 TM, Landsat 7 ETM+ and Landsat 8 OLI/TIRS have 7 bands along with global surface reflectance, temperature and cloud cover bands. NDVI is calculated using the following formula from the Near Infrared (NIR) and the Red (Red) bands.

$$NDVI = (NIR - Red) / (NIR + Red) \quad (8)$$

$$\text{In Landsat 4-7, } NDVI = (\text{Band 4} - \text{Band 3}) / (\text{Band 4} + \text{Band 3}). \quad (9)$$

$$\text{In Landsat 8, } NDVI = (\text{Band 5} - \text{Band 4}) / (\text{Band 5} + \text{Band 4}). \quad (10)$$

It is important to bear in mind that several studies have noted a systematic error in the computation of NDVI due to variations in atmospheric and cloud cover, changes in illumination and observation angles and calibration errors (Xie et al., 2016; Gandhi et al., 2015; Blöschl et al., 2019). Hence, this study adopted a technique to generate precise NDVI by minimizing the errors. This methodology is further explained in the paragraph below.

It is also noteworthy that since NDVI does not distinguish between vegetation types, a trend (negative or positive) would not necessarily mean permanent modifications in the land forms. Mishra and Rafiq (2019) suggested that vegetation growth could have a strong relationship with the root zone soil moisture in the land, a state variable output of GLDAS.

3.4.1. Image processing technique

An algorithm was developed to generate cloud free, radiometrically logical Landsat composites with a flexible set of rules for pixel selection. A total of 272 images were used. Firstly, the near infrared, red and the cloud cover bands for all the available images were scrutinized. The atmospheric correction of the images included for consideration of the pixels with cloud cover less than 10%. The NDVI is calculated using the above formula. Thereafter, only the pixels within the range of 0.15 to 0.7 was stipulated to provide more consistent phenological values.

Further, images collected by the Landsat 7 ETM+ after May 31, 2003 have an error due to the failure of the Scan Line Corrector (SLC) as seen in figure 10.

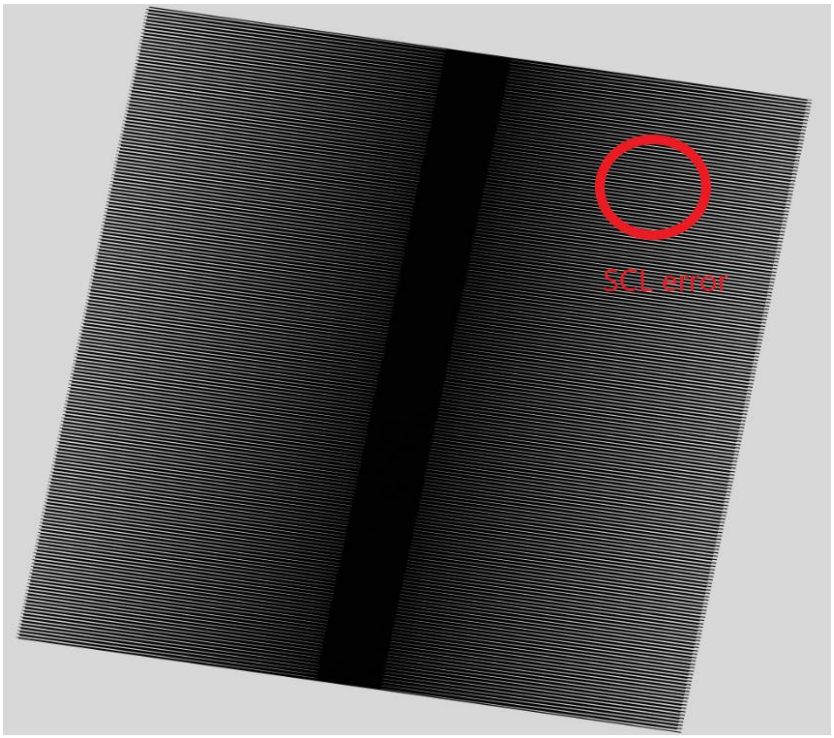

Figure 10. Pictorial representation of Scanned Line Error in Landsat-7 images.

To account for this, the pixels with the SCL error were omitted. The mean and standard deviations for the UAC area were calculated and a time series was generated.

The list of the satellite images processed for this study is enclosed in Annexure 1. Images have been selected to depict the inter-annual (seasonal) and long-term temporal variability in the results.

3.5 Framework of Methodology

The methodological framework are devised to highlight the drivers of change discussed in the literature for the Upper Arkavathy Catchment using discussed data products (figure 11).

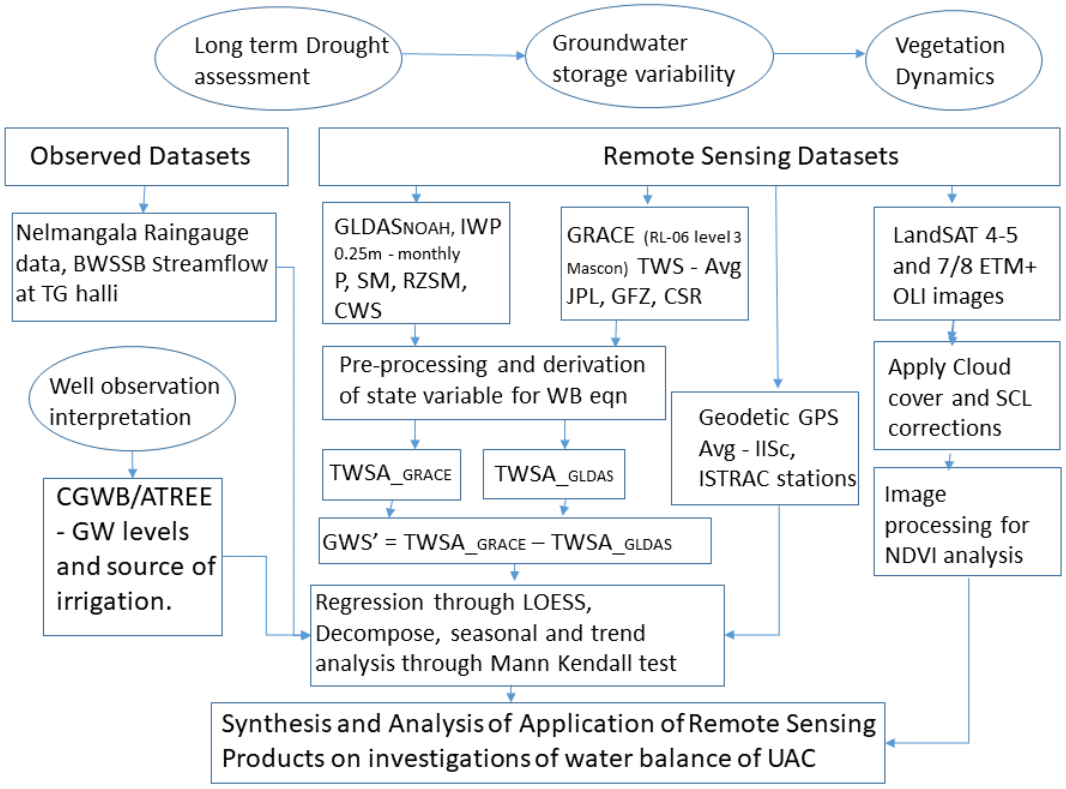

Figure 11. Framework of Methodology for the study

Chapter. 4 Results and Discussions

4.1 Temperature and Potential Evapotranspiration

The average temperature derived from GLDAS showed a good correlation of r^2=0.97 to the observed data. The boxplot show in figure 12 shows the variations in monthly temperature between the GLDAS and the observed datasets. GLDAS seems to have overestimated the temperature values for the winter months and underestimated values for the summer and monsoon seasons.

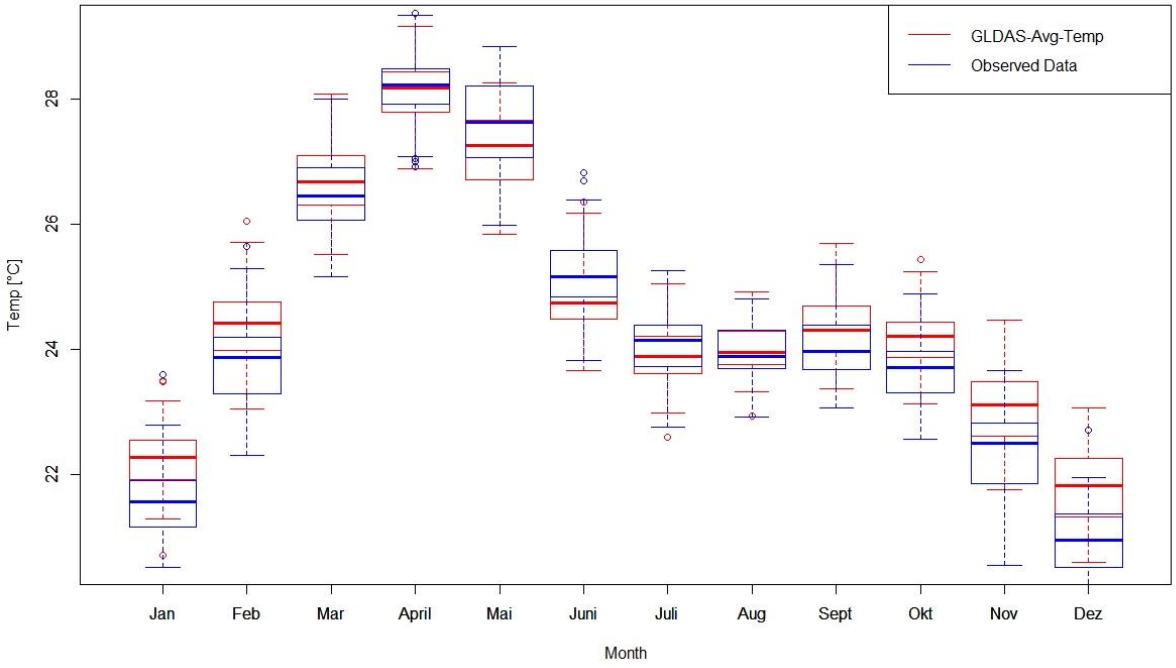

Figure 12. Box plot showing variations of temperature between the GLDAS and the observed datasets.

Figure 13 shows the trend analysis of the temperature for the area. The seasonal Mann Kendall test showed a tau = 0.475, 2-sided pvalue =< 2.22×10^{-16}. Although there is an increasing trend in the temperature Srinivasan et al. (2015) suggest that this is well within the stipulated climate change literature for the area.

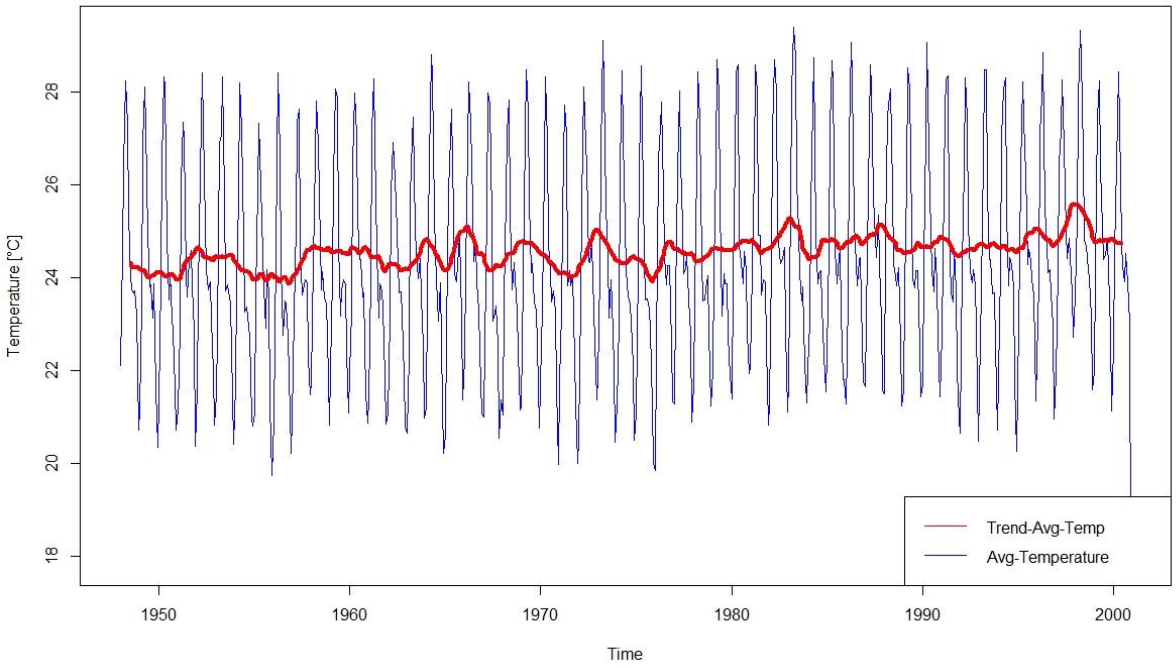

Figure 13. Long term trend in temperature for the UAC.

In term of quantifying potential evapotranspiration, figure 14 shows that PET is significantly lower than P and hence cannot suffice the condition for drought. The LSM couples the Penman Monteith PET calculation as compared to more fundamental Hargreaves equation used by Srinivasan et al. (2015) and hence is an admissible comparison.

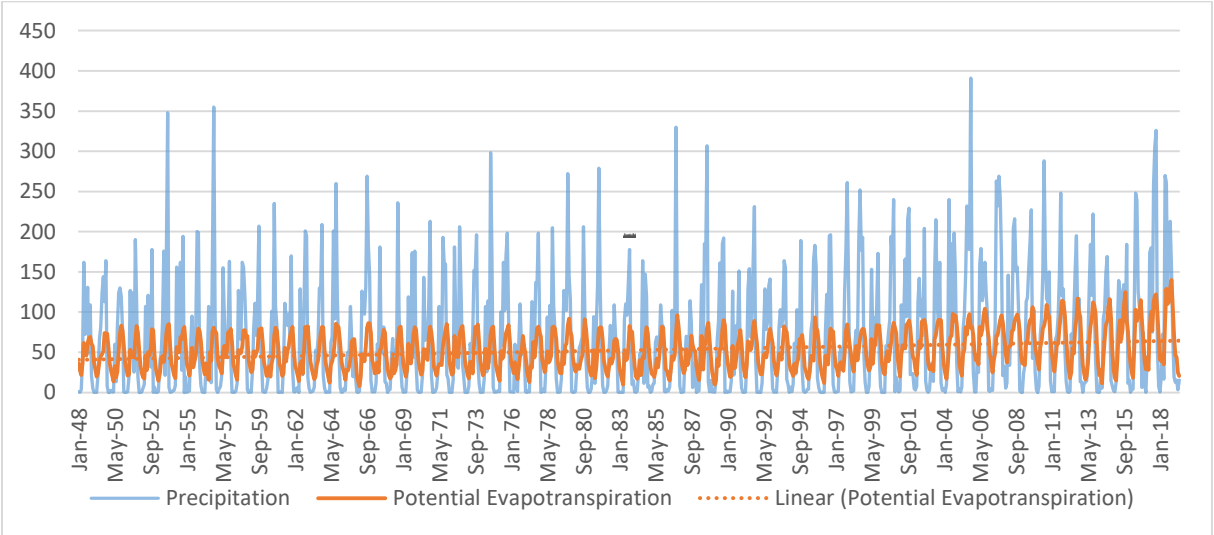

Figure 14. Monthly Precipitation and Potential Evapotranspiration in mm given by GLDAS.

Hence, long term rainfall data becomes a crucial parameter to differentiate drought and from scarcity dynamics in such semi-arid regions with intensive human impact (Mondal et al., 2018).

4.2 Long term Rainfall Analysis

The box plot in the figure 15 shows the monthly statistical variation of precipitation of the GLDAS and observed precipitation at Nelmangala Rain gauge (1948-2000). Although, a high r^2 of 0.87 is observed for the whole dataset, it can be observed that there are high monthly variations particularly during the monsoon months. Rainfall is concentrated over the months June to November, over two spells - the Southwest Monsoon (June to September) the shorter NE rains which are between October to November, while the dry season is between December to May. Highest average monthly rainfall was seen in September with an average of 158mm. The months of July, August and October had the highest variances. For the months of July and October, GLDAS seems to have an overestimated median value and August shows an underestimation (see figure 15).

Hence, trend analysis on this data is conducted to verify the purpose of understanding long term rainfall variability.

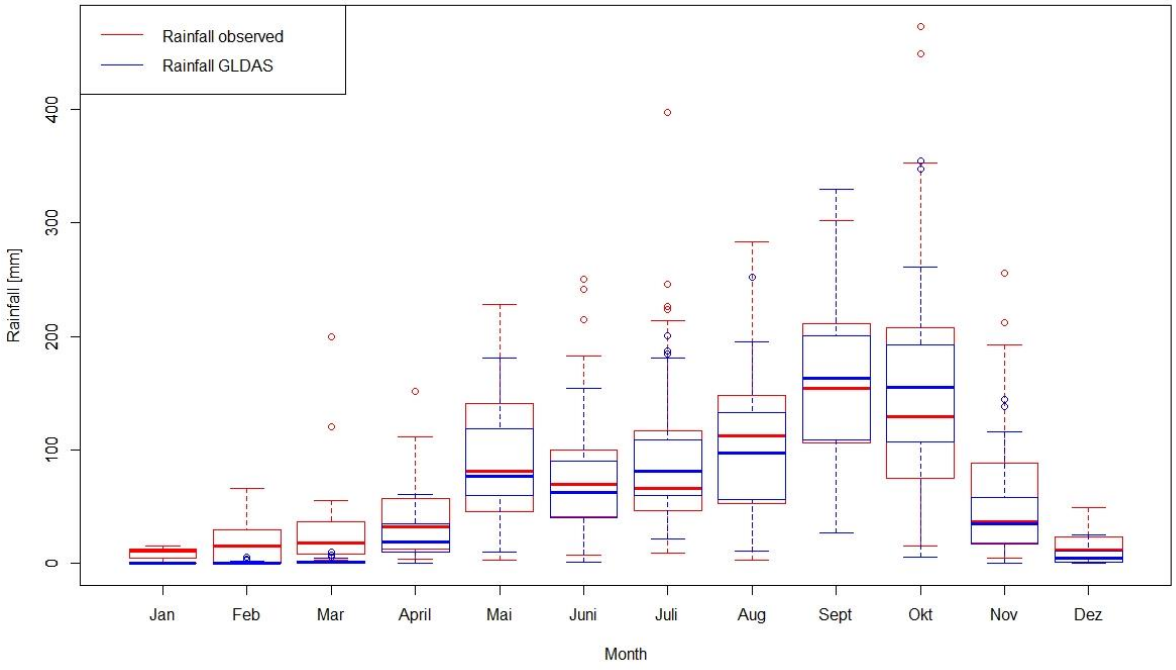

Figure 15. Boxplot showing variations of the Precipitation Dataset given by GLDAS and Observed Rain gauge in mm.

The decomposition and trend analysis through the seasonal Mann Kendal test did show significant trends with the GLDAS precipitation data as seen in figure 16. The Trend in this figure is derived from the LOESS smoothening and the multiplicative signals of the random and trend would give us the observed data. The seasonal component explains the time at which there is a change in slope of the trend. The seasonal Mann-Kendall test indicated minimal monotonic trend (tau value = 0.0897 close to 0, 2-sided pvalue =0.00116) which does not indicate any significant seasonal trend either. Although there is a significant trend, the amplitude of change in rainfall is not strong enough to explain declining flows in the Arkavathy River.

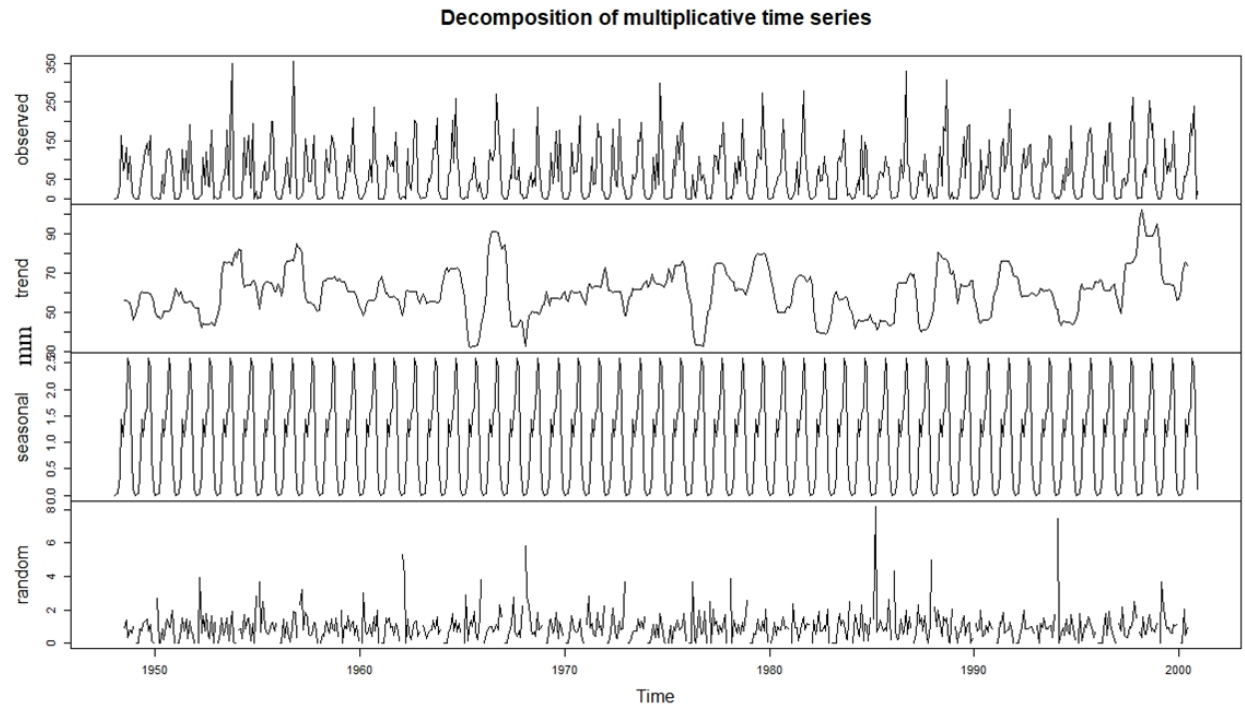

Figure 16. Decomposed trend analysis for long term rainfall in mm in the UAC (1948-2000)

Table 3 shows the average annual values of decadal rainfall. The analysis of decadal precipitation helped to assess that the different periods in the catchment. The area received high rainfall during the decade of 1990-2000 with an average of 769.5mm annually and had a relatively low rainfall decade 1980-1990 with 667.7 mm annually. The data is used till 2000 to depict the drought analysis. It is also important to bear in mind that the two decades after 2000 have reported an increase of 23% and 16% increase as compared to the 860mm which is the average of a 119 year dataset (1901-2019) from IMD for the study area.

Table 3. Decadal Average Annual Rainfall in mm for UAC (1950-2019)

Rainfall Decade	Average Yearly rainfall in mm
1950 – 1960	739.2
1960 – 1970	695.5
1970 – 1980	763.7
1980 – 1990	667.7
1990 – 2000	769.5
2000 – 2010	1063.1
2010 – 2019	990.7

The results are analogous to Srinivasan et al. (2015) findings, that there is indeed a lack of evidence in the natural drivers even through the use RS data explaining the decline of flow in the Arkavathy River.

4.3 Groundwater Storage Variability in Upper Arkavathy through RSP's

4.3.1. Harmonization and Scaling of GRACE-TWS Dataset

The data had to be harmonized from the Net CDF file formats to form one cohesive set, considering that the study area is less than the recommended 200,000 km^2 for GRACE applications (Landerer and Swenson, 2012). Since 95% of the study area was in one pixel of the Mascon data, the values for centre of the gridded box was used for the determination of LWE for the UAC as suggested by (Miro and Famiglietti, 2018). The newly processed RL-06 GRACE TWS data from GFZ, CSR and JPL were compared to each other to see the anomalies. These are attributed to the fact that the processing centres have different strategies to provide solutions from mass variations. The comparison of the three solutions through a scatter plot (figure 17) shows high correlation values between all the three centres. Moreover, the average of the three solutions was chosen as the optimal use of GRACE Mascon data as suggested by Sakumura et al,. (2014). The average of the three solutions for our catchment definitely shows a slight declining trend as seen in figure 18.

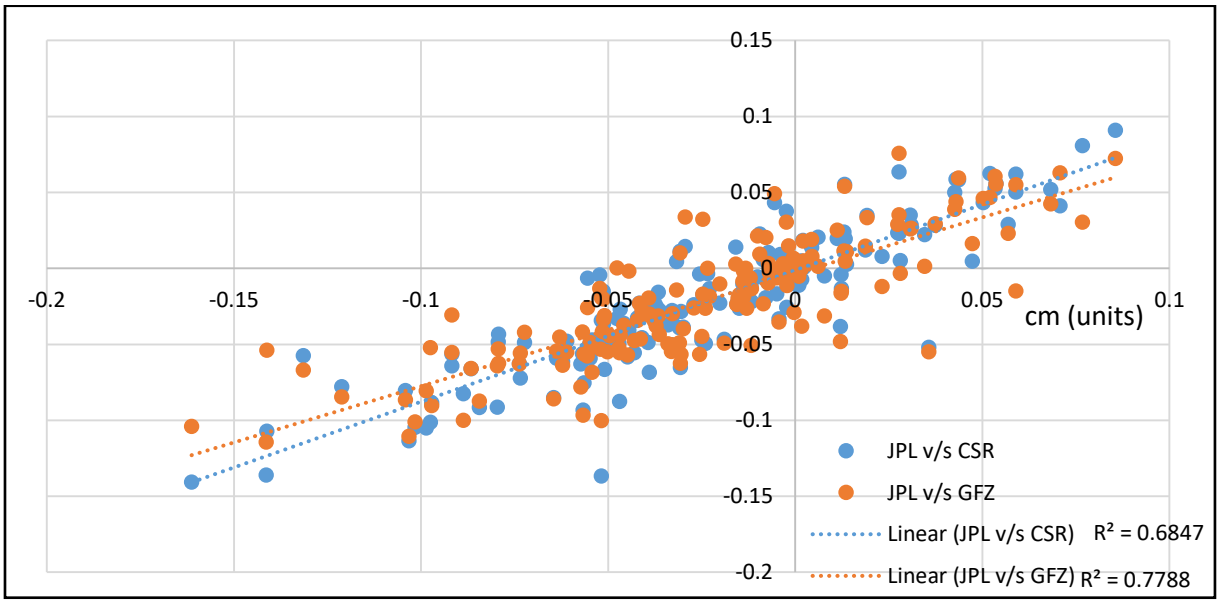

Figure 17. Scatter Plot of GRACE solutions for UAC from GFZ, CSR and JPL centres.

The seasonal Mann Kendal test has the following parameters for the trend at a 95% significance level is as follows (trend='decreasing', h=True, p=5.296x10^{-5}, z=-4.042, Tau=-0.240, s=-244.0, var_s=3613.99, slope=-1.607). The values of p close to 0.0001 shows a weak monotonic trend, however Tau<0 shows that there is a significant seasonal trend in the time series for GRACE data. A net decrease in the basin storage of the 0.7Mm^3 is calculated for the catchment in entire time period. Similar to the case of long term rainfall, although the Mann-Kendall test shows a significant trend, the magnitude of change shown by GRACE to affect catchment water balance is very minimal. A linear trend indicates shows a decline of -0.5mm for 15 years which can practically be considered relatively flat.

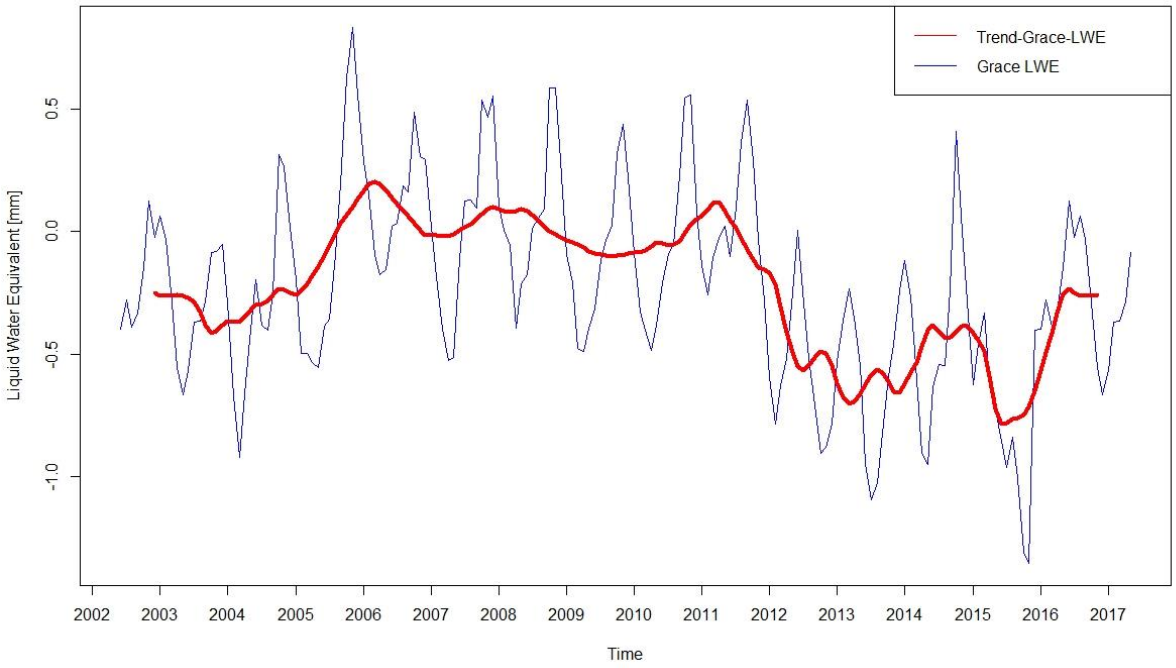

Figure 18. Time series plot of GRACE derived Total Water Storage in mm (2002-2017)

4.3.2. TWS and TWSC from GLDAS-LSM

The monthly TWS is obtained by summing the Soil moisture and Canopy water storage variables as explained in the methodology. Similar to the generation of precipitation time series, data from the GLDAS were areally averaged over the catchment and a cohesive TWS time series is generated as seen in figure 19. We noted that values of soil moisture are much higher than CWS in the order of magnitude 10^{2} and 10^{-4} respectively. Hence are the dominant factor in the TWS of the top 2m. This is because canopy cover is directly proportional to the transpiration and density of plants which is primarily seasonal. On the contrary, soil moisture may have a more random signal as depends on soil type, topography and local climate. A linear regression line predominantly indicates a decreasing trend of 60mm for the entire time period of 2002-2017. This translates to about a net decrease of 8.628 Mm^{3} in the basin storage. As expected, the highest gains between May to December and highest reduction in TWS is experienced in the dry months of January to May. The downward curve of the cycle indicates removal of water through transpiration, evaporation, streamflow discharge and infiltration to deeper groundwater.

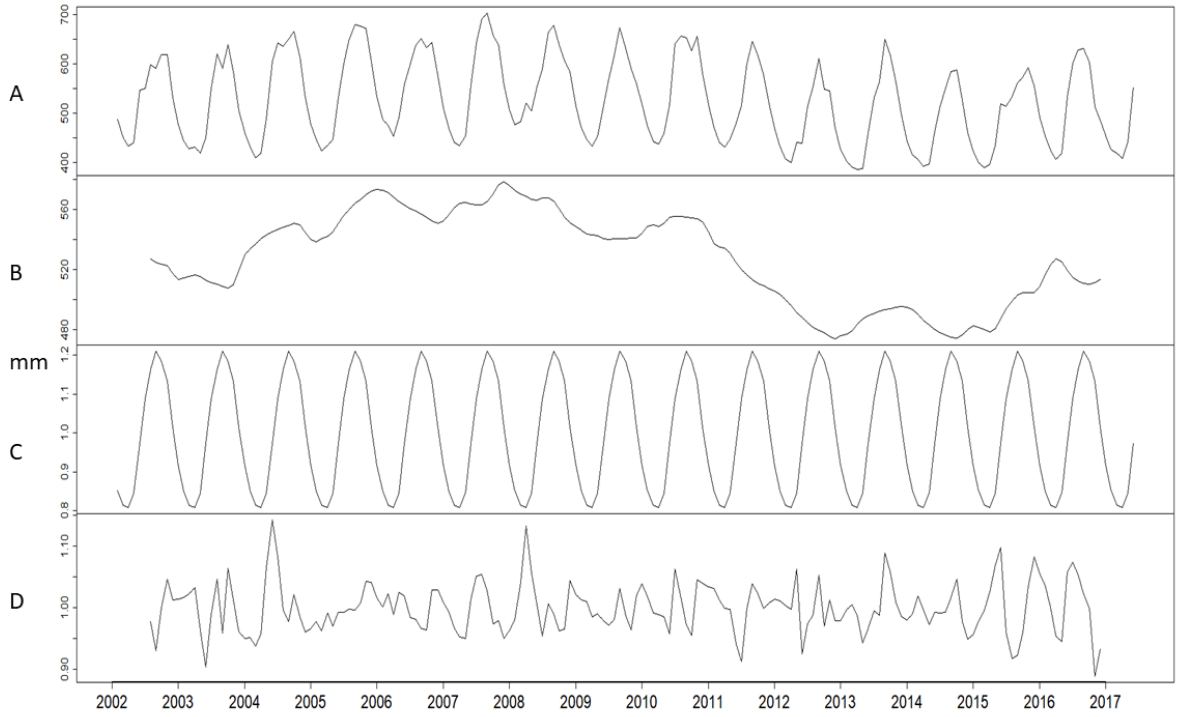

Figure 19. Decomposed timeseries data for TWS in mm derived from GLDAS for the UAC (2002-2017). A:Observed ; B:Trend ; C: Seasonal ; D: Residual

The seasonal Mann-Kendal test also showed a decreasing trend with the follow parameters (trend='decreasing', h=True, $p=7.603x10^{-10}$, z=-6.153, Tau=-0.330, s=-471.0, var_s=5835, slope=-4.08). The p-value ($<<10^{-4}$) shows the rejection of the null hypothesis suggesting a significant trend in the time series when monthly seasonality is taken into account. The low z and tau values indicate that there has been a change in the mean in the time series. The figure predominantly indicates a decreasing trend of 60mm for the entire time period of 2002-2017. This translates to about a net decrease of 8.628 Mm^3 in the basin storage. The general decline is at the rate of –5.3mm/year was considered for further analysis. This decreasing trend is a clear indication of an aridification processes which can be attributed to change in land cover through water intensive agriculture and urbanization.

TWSC is derived from subtracting the monthly values from the mean monthly values of TWS (Ouma et al. 2015). A linear decline has a rate of decline of -3.6mm/year when fitted with a linear trend line. The TWS and TWSC derived from GLDAS relates mutually with the precipitation data. It is an indication that soil moisture is primarily dependent on rainfall. In terms of the monthly averages, no long term trends is observed except for the month of January which shows a declining trend of -34.54mm for the entire period. But for the other months, seasonality is primarily dependent on the uneven distribution of rainfall in the time period. Therefore, yearly trends are shown as storage change as a more reliable representation of TWSC in the catchment (see figure.17). Anyhow, seasonal and daily variations of the rainfall and intensities also drastically affect the soil moisture. The steep decline post 2010 in TWSC from GLDAS is similar to the phenomenon seen in GRACE during the same period.

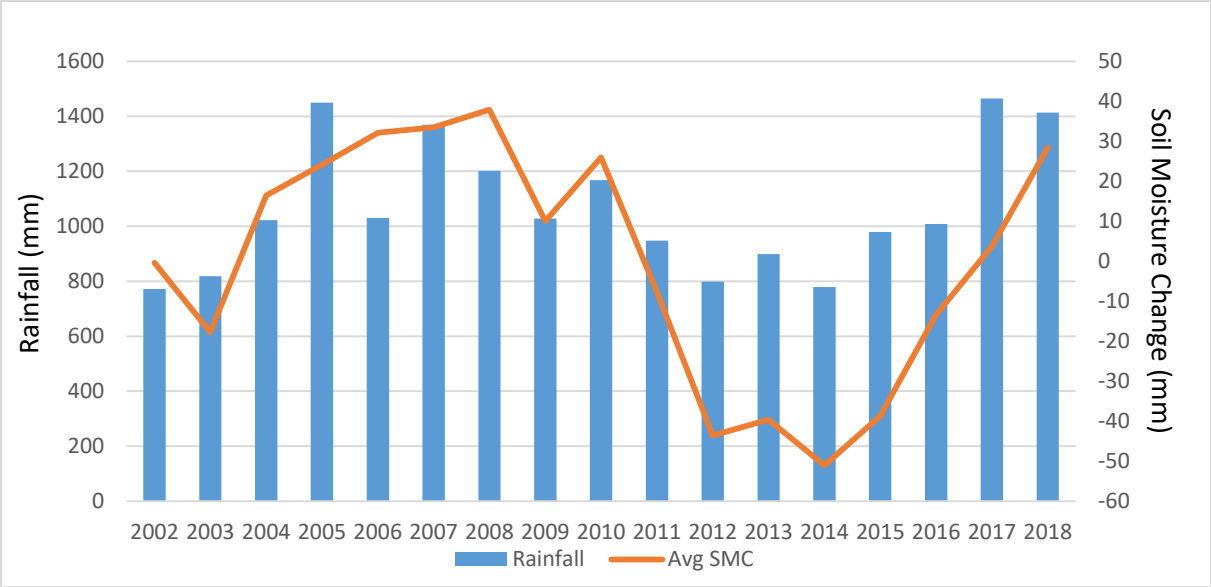

Figure 20. Yearly average Soil Moisture and Rainfall in mm for UAC from GLDAS (2002-2017)

The seasonal MK test shows a high seasonality variation for the TWSC with the following parameters "trend='decreasing', h=True, p=1.3232x10^{-9}, z=-6.0645, Tau=-0.333, s=-440.0, var_s=5240.0, slope=-4.0664". The high slope definitely indicates a high monotonic trend and high variance S values depict a high variation for the monthly values. The low z and tau values indicate a hypothesis that there is indeed a change in distribution and average of this time series.

Table 4 depicts the yearly and monthly rainfall patterns for the reference period of the groundwater storage variability.

Table 4. Yearly and Monthly rainfall patterns in UAC (2002-2018)

Month	Avg Rainfall
Jan	3.23
Feb	3.50
Mar	25.74
Apr	39.70
May	115.24
Jun	149.49
Jul	168.33
Aug	170.15
Sep	160.49
Oct	153.28
Nov	63.65
Dec	15.12

Year	Rainfall
2002	772.4
2003	818.0
2004	1022.9
2005	1450.1
2006	1030.1
2007	1369.8
2008	1201.3
2009	1028.1
2010	1168.2
2011	948.1
2012	799.2
2013	899.4
2014	778.7
2015	979.1
2016	1008.2
2017	1464.5
2018	1413.3

4.3.3. Comparison of TWSC GLDAS and TWSC GRACE

Both the GLDAS TWSC and TWSC given by GRACE have a downward linear trend. There seems to be a temporal delay of the TWSC for GLDAS w.r.t. rainfall, which can be justified by the fact that during the dry months, there is dry conditions and at the onset of the rains in June, soil and biomass is relatively dry and needs water and time to bring the TWS up to the expected mean value. On the other hand, during the wet spell the TWSC of the GRACE seems to decrease only in the end of November. But the seasonal cycles of GLDAS TWSC has high variability even across time scales. This could only indicate the changing soil moisture conditions even during the wet season and hence needs to be investigated further.

However, despite the difference in amplitude, the TWSC estimates of both the datasets agree quite well with each other. The difference in amplitude is due to the fact that the components of GLDAS TWSC showed clearer indication of decrease of storage in the surficial aquifer in terms of amplitude when compared to GRACE. In order to further explain this difference, a comparison of the TWSC from GRACE is plotted with Soil moisture as shown in figure 21. A simple regression between the GRACE derived and GLDAS TWSC gives an r^2 of 0.29 which is within the acceptable range of 0.2-0.5 as noted by Rowlands et al. (2010).

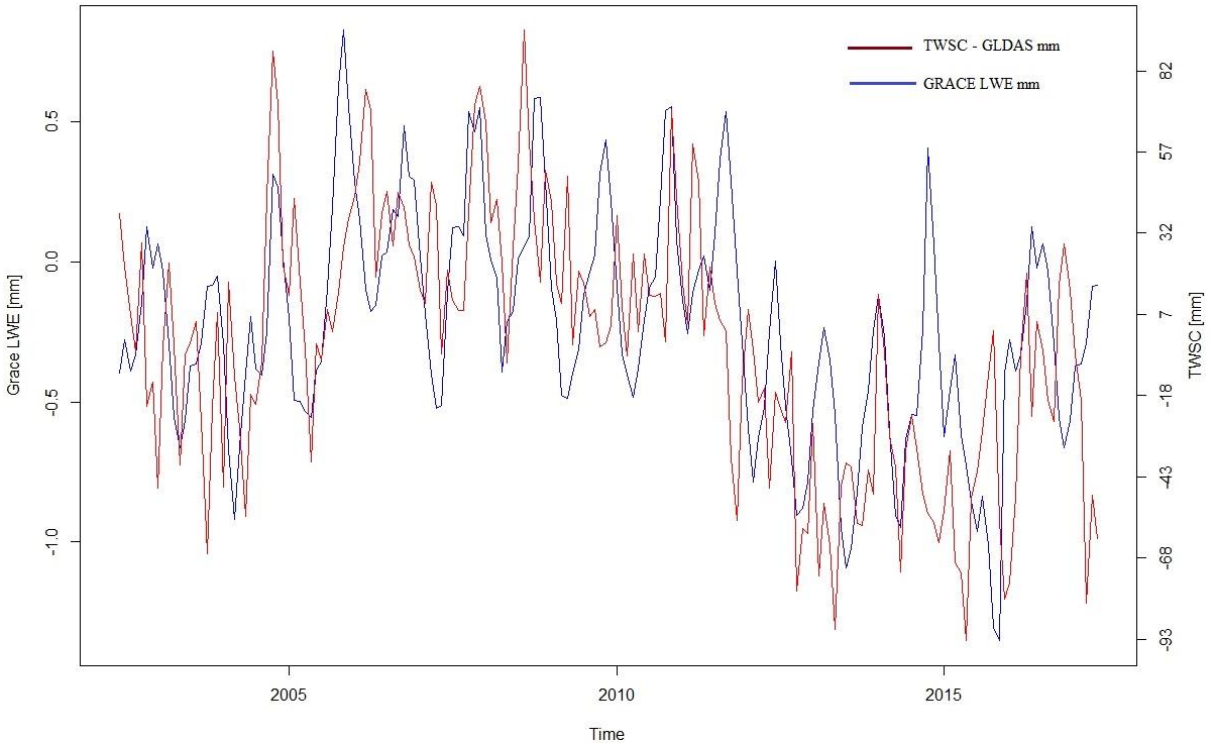

Figure 21. Comparison of TWSC derived from GLDAS and GRACE for UAC (2002-2017)

4.3.4. GWSC Determination

The groundwater storage change is redundant from equation 6 and is a function of the TWS from GRACE and the state variables from GLDAS. It represents the column of water below

the first two meters from the ground surface. It must be noted that the time series data obtained from the GRACE and GLDAS have different time scales. Hence, it becomes important to acknowledge the errors developed in the system due to the linear time-averaging of the two timescales. The GWSC obtained from the subtracting the time averaged GRACE and GLDAS TWSC. A yearly trend of the GWSC w.r.t rainfall is shown in figure 22. A linear trend line indicates an overall increase in GWSC in the catchment for the time period 2002-2017. The increasing trend is in order of the magnitude of +47mm/year.

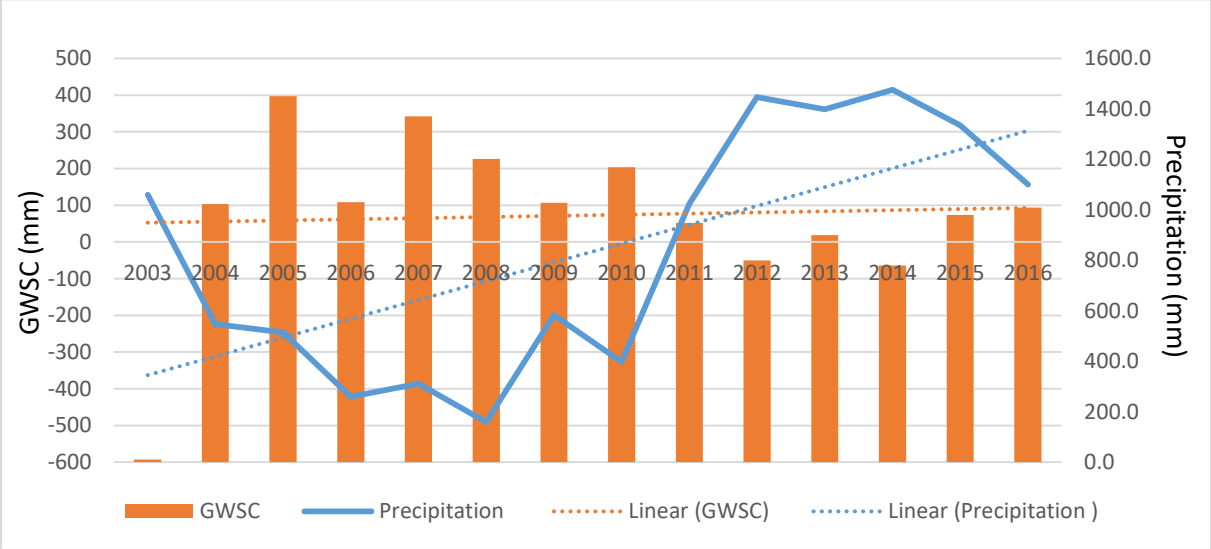

Figure 22. Yearly GWSC and precipitation trends in UAC

However, there is high variability in decadal and seasonal scales in the time frame. The years 2002-2010 recorded a decrease in GW storage and the latter 7 years recorded an increase. The trend is further decomposed to check for seasonal variation in figure 23 which also shows two outliers highlighted in the de-seasonalized data in 2004 and 2012 which arise due to linear interpolation of the missing GRACE months.

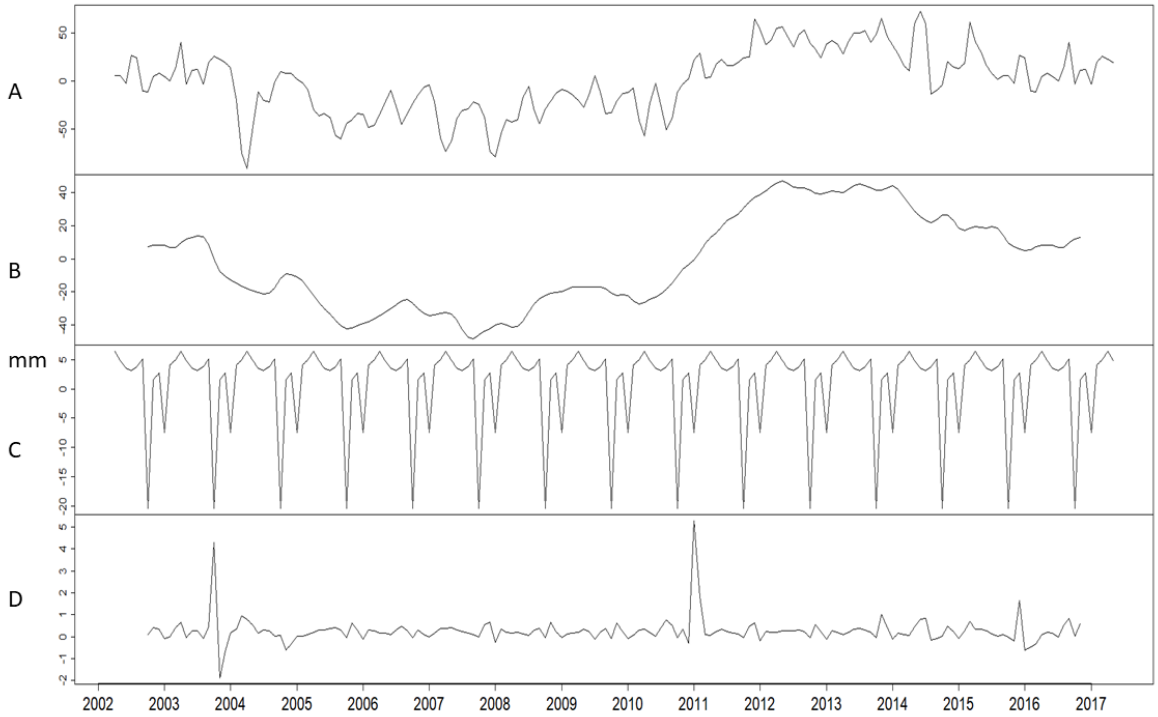

Figure 23. Decomposed time series for GWSC (mm) in UAC (2002-2017) A: Observed ; B:Trend ; C: Seasonal ; D: Residual

4.3.5. Groundwater Variability and Deseasonalized Data

Figure 24 is an interpretation of the groundwater storage variability with the TWS derived from GLDAS and the TWS from GRACE along with precipitation. There seems to be groundwater abstraction before the year 2009 and a recharge period after 2009. The GWSC tends to decrease even though there are higher rainfall years during this period. The years of 2003-2009 received higher rainfall (1131.2mm/year) but the GWSC still showed a declining trend. Only at the end of 2009 there is a rising curve in the GWSC despite comparatively lower rainfall (940.1mm/year- 2010-2016). This observed lag in the rising slope can be justified as the state variable in the surface water must change in order to impact the GWSC. As already discussed in the comparative results, it can be suggested that unsaturated storage changes due soil moisture are high compared to the TWSC from GRACE. This implies land use change and needs to be explained with anthropogenically induced vegetation or irrigation dynamics. Hence, it is deduced that there is ambiguity in relating the results of GWSC to precipitation.

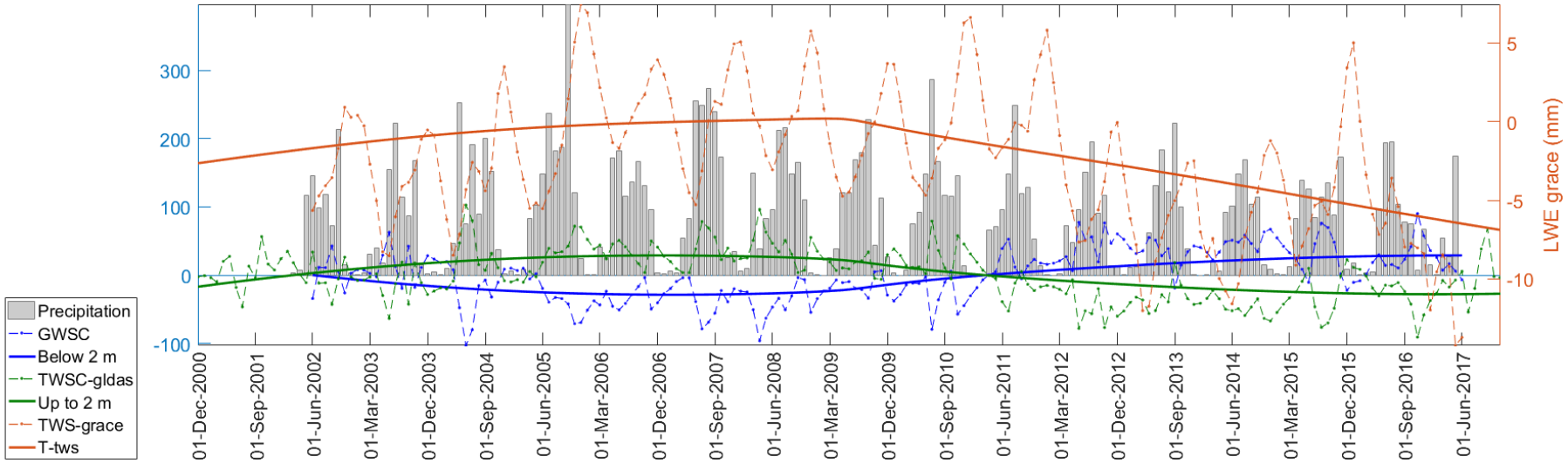

Figure 24. Groundwater storage variability for UAC derived from GRACE-GLDAS assimilation.

GWSC – Groundwater Storage Change predicted by the Assimilation of GRACE and GLDAS

(Below 2m) – Trend line for GWSC using LOESS smoothening Curve

TWSC-gldas – Terrestrial Water Storage Change predicted by GLDAS. This is the change in the top two metres of the surficial aquifer.

Up to 2m – Trend line for TWSC-gldas using LOESS smoothening Curve

TWS – GRACE – Total Water Storage variations given by GRACE

T – tws – Trend line for TWS given by GRACE using LOESS smoothening

4.3.6. Groundwater Level Trends

Variations of water levels in the borewells indicate the changes in the groundwater storage changes. The long term monthly variation in the insitu groundwater well data (figure 25) also show a declining trend in the magnitude of -153mm/year. No major seasonal variation could be detected with these data. Noticeably, the GWSC derived from satellite data is quite anomalous to the observed levels. However, Ballukraya and Srinivasan (2019) also question the validity of the CGWB data and their investigations suggest groundwater level variations of upto 200m. It also becomes important to account that the variability in characteristics of these borewells extraction in terms of pumping capacity, well depth, pumping hours etc. have not been considered due to the absence of data.

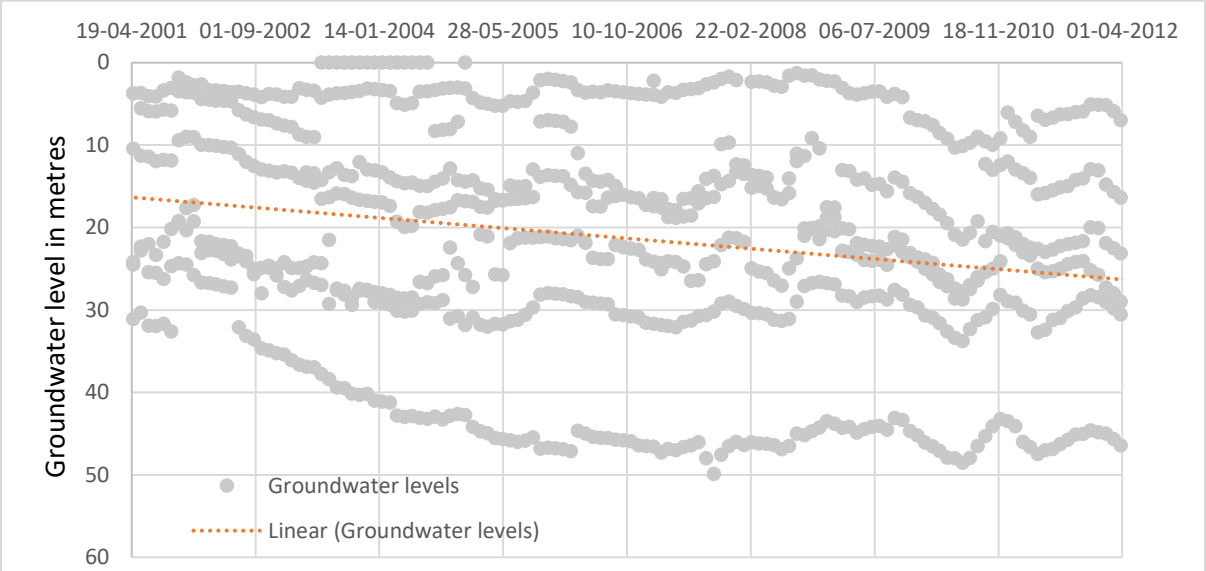

Figure 25. Interpretation of observed groundwater levels data in metres.

4.3.7. GWSC and Land Subsidence

Figure 26 shows the variation of land deformation and groundwater storage change for the catchment. Ground uplift and subsidence in response to the effects of groundwater storage change is clearly evident in this time series data. The GPS data corroborates well with the GWSC. This implies that the deduced GWSC is reliable. The peak to peak amplitude of the GPS and GWSC annual variation is about 3mm and 6mm respectively. Both the time series showed a seasonal variation. Groundwater storage change exhibited higher variation to the continuous GPS data by two or three times in terms of actual displacement. The similarity of the drop in the curves upto 2009 and a gradual increase after 2009 confirms that seasonal vertical displacements are mainly cause by groundwater mass loading variations. Srinivasan et al., (2015) used porosity estimates of 20% for the unconfined sediments, and 1% for the fractured rock to estimate the order of magnitude of the groundwater. With such estimates, a depth porosity model can be approximated for a coefficient of volume change corresponding to the specific storage. These results imply that seasonal vertical displacements could be useful to

reflect groundwater pumping for irrigation activities in the dry months and needs to be examined further.

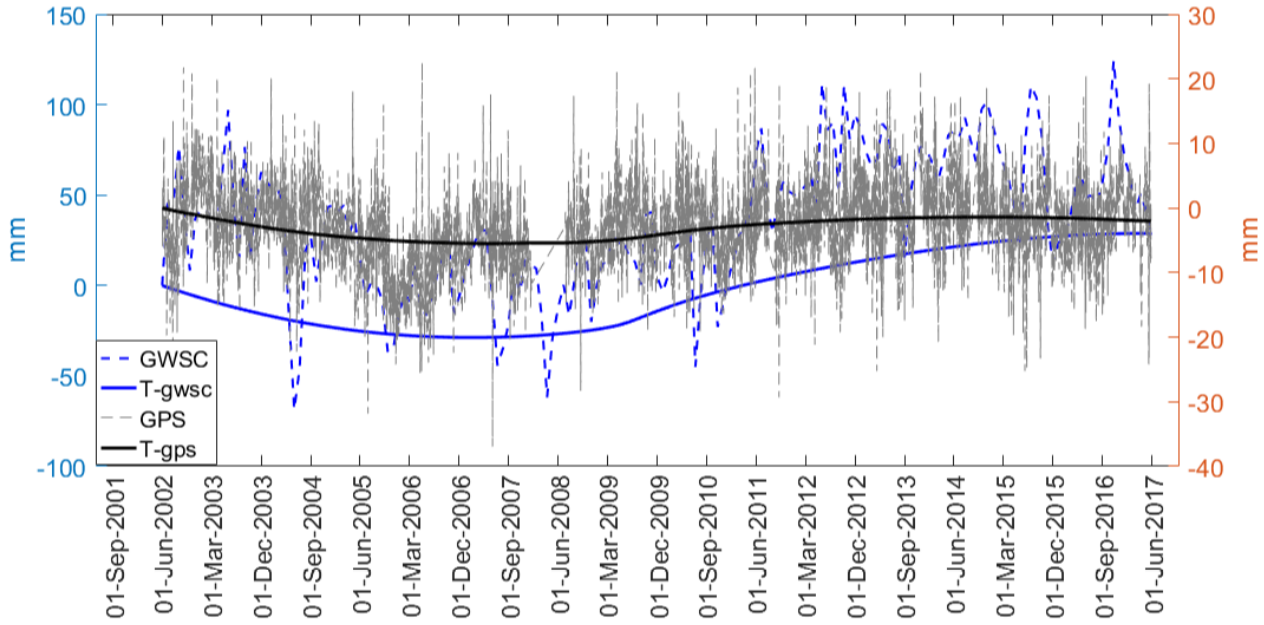

Figure 26. Groundwater Storage Change and Land Deformation through GPS data.

4.4 Spatio-Temporal Analysis of Vegetation Dynamics

The NDVI is used to understand the vegetation density and growth rate, relationship between spectral variability. Images are selected to depict the inter-annual (seasonal) and long-term temporal variability of these indices in the catchment shown in the figure 27. The maximum NDVI variability was observed during the year 2014-2015. The year 2014-2015 received relatively average rainfall of 860 and 970mm and hence are apt to depict for spatial patterns.

Figure 27 shows the spatial distribution of NDVI over the Upper Arkavathy Catchment.

- Blue indicates low NDVI values which means Barren land
- Red indicates Smaller Shrub Growth
- Green indicates Thicker Green Cover

Gradual changes in the vegetation cover can be seen across the year. The summer months of April and May which are before the monsoon record the lowest NDVI. The monsoon months of June-July-August-September have high cloud cover and hence these images are neglected. There is a steady increase of NDVI in the months of October and November which indicate the growth of shrubs in the area. The NDVI reaches a maximum value in December and gently starts declining in the dry month starting from January.

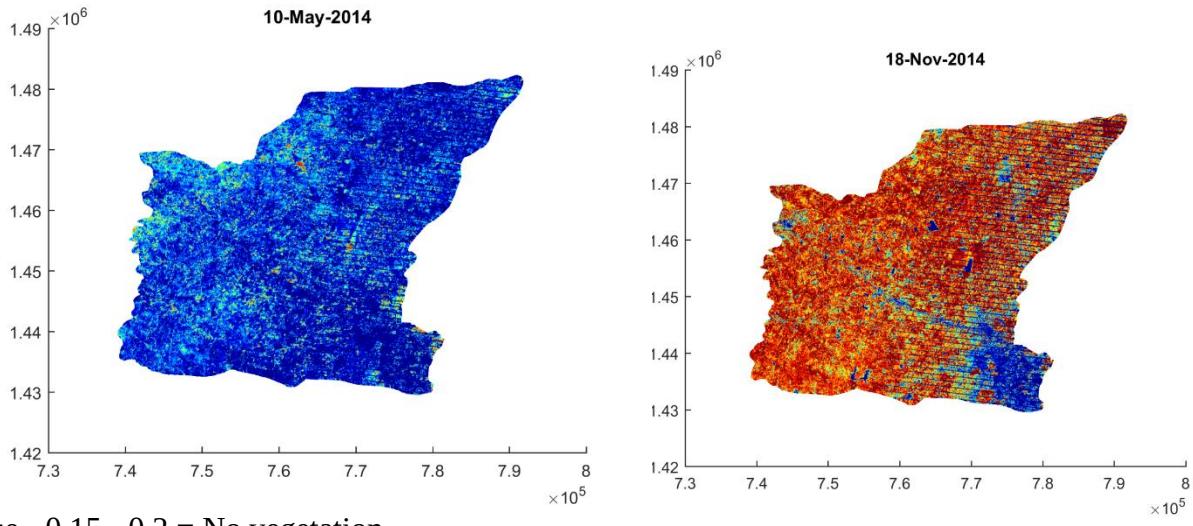

Blue - 0.15 - 0.2 = No vegetation

Red - 0.2 – 0.35 = Growing of Shrubs

Green – 0.35-0.7 = Green Cover

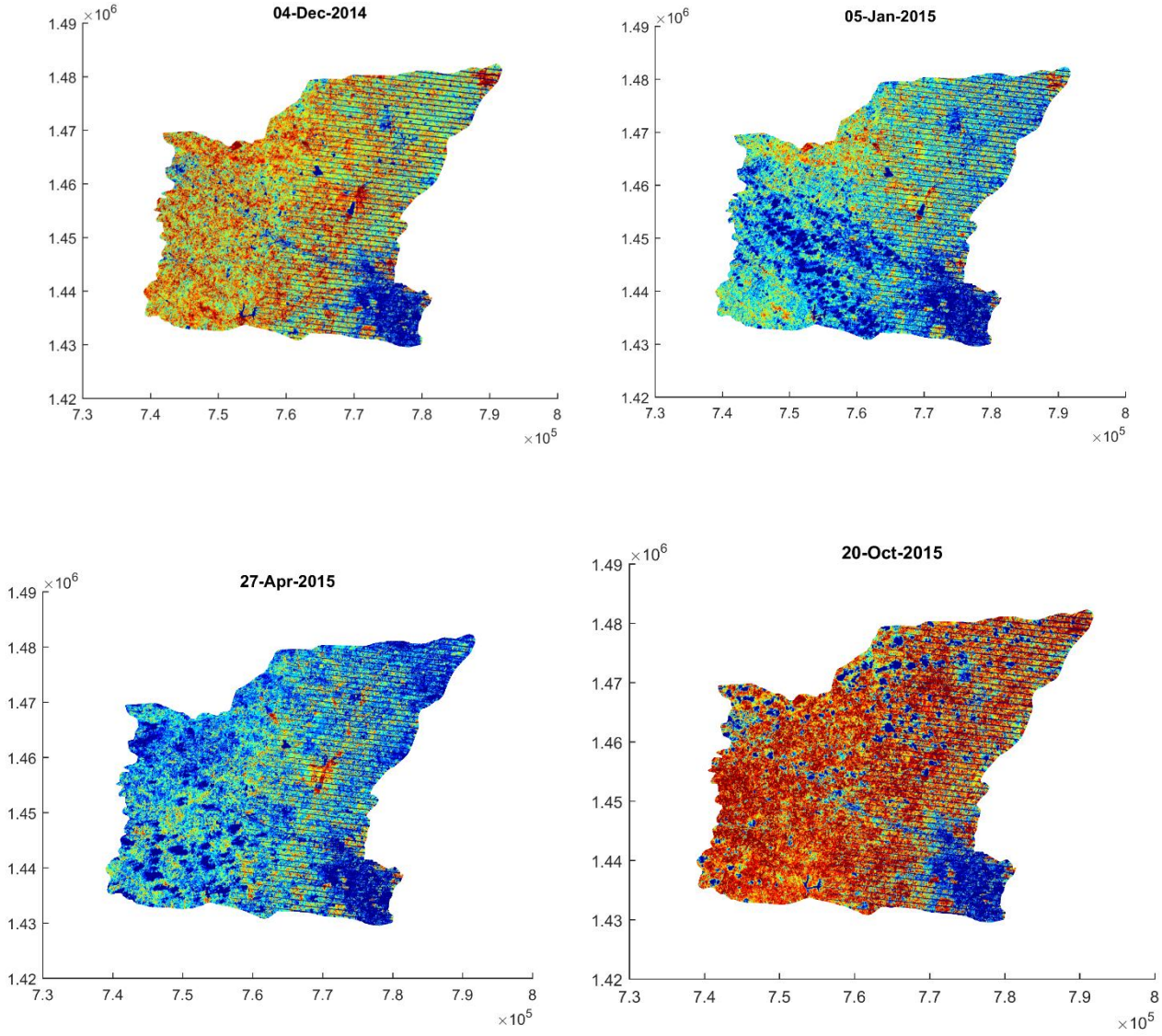

Figure 27. Spatial Depiction of Yearly Variation in NDVI

Considering the increasing trend in ET, land use change through vegetation indices becomes a good indicator to assess the change in water balance. In order to further explain the relationships of vegetation, the index is compared to the parameters from GLDAS, mainly root zone soil moisture and precipitation. Root zone soil moisture varies with vegetation root depth which is function of land use types. The change in the greenness index is plotted through the NDVI and is checked for its seasonal correlation with RZSM which the static input for the top 1.5m of the soil.

Theoretically, higher positive NDVI indices (>0.4) would mean pixels with thicker vegetation (dense forests) and lower positive NDVI (0.2 to 0.4) indicates shrubs and grassland. Values around 0 (-0.1 to 0.1) indicate barren land, rock and sand. Negative values primarily corresponds to water.

The vegetation dynamics in the catchment corresponds well to the rainfall patterns. The higher NDVI indices are visible during the months of September and October after the monsoon season indicating higher green cover. The NDVI is the lowest right before the monsoon in April-May which is the dry season. This seasonality also shows by the delayed response of plant growth as compared to rainfall. There are two main cropping seasons in India namely the Kharif – which starts with the onset of the monsoon and ends in November, and the Rabi- grown in the winter and harvested before the start of the summer in March. However, the results show an increase in NDVI only after the wet season. This is blamed on the lack of availability of accurate data due to the temporal resolution and the cloud disturbances of the imagery does not allow for a continuous representation, unlike for rainfall data. More importantly, the long term increasing trend seen in the figure 28 is a likely indication of irrigated agriculture in the catchment. The NDVI values for the period after 2013 observe higher values than the previous years. The RZSM corresponds well to the rainfall patterns and shows a similar trend to that of total SM.

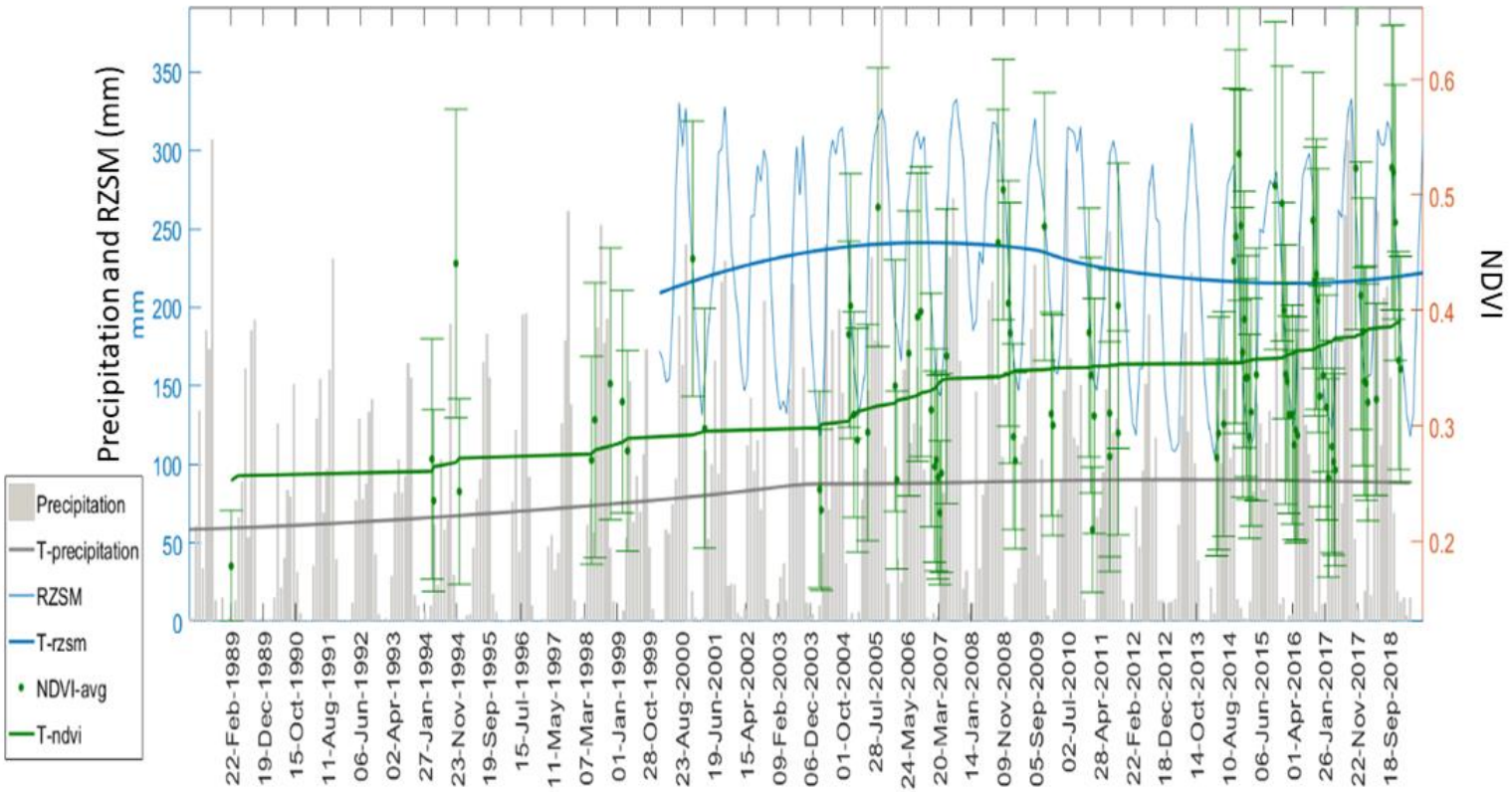

Figure 28. Time series of NDVI, Precipitation and Root Zone Soil Moisture for UAC.

T – Precipitation, rzsm, NDVI: Trend for the precipitation, root zone soil moisture and NDVI through LOESS smoothened curve

Chapter. 5 Discussions

5.1 Lack of Evidence of Drought

The study addresses each of the hypothesis used to explain the drying up of Arkavathy by (Srinivasan et al. 2015) through different approaches with the use of RS data. The parameters of precipitation and temperature have matched up well with long term observed data. However, it is acknowledged that only one rain gauge cannot rightly represent the variability of the rainfall in the whole catchment. The study recognizes this improper estimation of error of the GLDAS precipitation dataset. RS based rainfall were plotted for areally averaged values from 9 grid values and need to henceforth be graded against more than this one rain gauge. Although this might not be an equitable approach for the whole catchment, no compelling trends in rainfall or temperature were observed anyhow. The fluxes in the natural state of the system do not show any convincing tendencies of PET>P to have a meaningful explanation to the decline of the inflow to TG halli, purely due to climatic factors. Thus, it is concluded that there is indeed a lack of evidence of climatic driven drought for the upper Arkavathy catchment.

5.2 Characteristics of Groundwater Storage Change in UAC

Since there is no satellite data available to assess GW for the period before 2002, it becomes equivocal to assess these trends compared to long term studies. It is important to stress that only GRACE's TWS signals showed only a -0.35mm/year trend which is almost relatively flat and does not corroborate to the over-extraction paradigms seen in figure.3. Hence, an assessment to reflect on the methodological approach on the assimilation of GRACE and GLDAS and to show the characteristics of the shallow and deep groundwater changes was conducted. The results of this assimilation predicted a decline of -5.3mm/year (2002-2017) as compared to -33.8mm/year (1934-1970) given by Srinivasan et al., (2015) in the surficial aquifer. Furthermore, the results recorded an increase of +47mm/year (2002-2017) in the sub-surficial as compared to a decrease of -657.6mm/year (1934-1970) given by Srinivasan et al., (2015). Hence, the GWSC from the assimilation is concluded as merely a mathematical deduction which follows a converse trend to the GLDAS curve.

Essentially, satellite data still underestimated GWSC when compared to the representative well observations which showed a decrease of -153mm/year. The study considered the possibility that this irregularity can be attributed to the higher decadal rainfall of 1168mm for (2002-2017) annually as compared to 720mm (1934-1970). Other plausible factors influencing this divergence could be increasing rainfall leading to higher recharge or the adoption of artificial (human induced) aquifer recharge techniques (Vissa et al., 2019). Hence we assessed the findings to other studies in the surrounding catchments. Nair and Indu (2018) estimated much higher negative trends in the larger Krishna Basin in the Deccan plateau, north of the Cauvery basin to a decline of -340 mm/ year with the same methodology of using GRACE and GLDAS TWSC. Chinnasamy et al. (2018) also showed the same trait (-70 mm/year) of GW depletion in Tamil Nadu, south of the Arkavathy basin attributed the depletion to irrigated agriculture. These figures seem more realistic than the +41.4mm/year predicted in our catchment. However, it is important to note that these studies used the assimilation of groundwater authority provided well data to predict these results. The GRACE TWS with the assimilation of this data predicted

a depletion rate in Delhi of -750mm/year as compared to -170mm/year with just GRACE data (Girotto et al., 2017). Ignoring the aquifer structure, storage and discharge or recharge, which are generally modelled through empirical equations which are highly dependent on assumptions, a simple addition of the trend in GW data leads us to a declining trend of -106.6mm/year for UAC. To exacerbate this discrepancy, Ballukraya and Srinivasan (2019) and Bhanja et al. (2018) have completely dismissed the dependability of governmental groundwater data in the severely exploited hard rock aquifers of South India. The unreliability is primarily attributed to the operational errors in collecting, recording and representing of the well data in the present ground water monitoring programmes. The CGWB monitoring wells are generally older shallow defunct wells, where water level stabilizes in the upper recharge zone, however, deeper private wells beyond the dewatered zone show deeper water levels (Hora et al. 2019). They point out that only deeper functioning borewells with a condition of having yielding fractures below the static water level can provide correct estimates of the regional groundwater table. Ballukraya and Srinivasan (2019) concluded that the movement and stabilization of static water levels in borewells have no distinctive pattern across depth or spatial clustering.

The decreasing surficial aquifer storage re-iterates that there is no infiltration or saturation excess which is why there is no visible stream flows in the Arkavathy. On the other hand, the increase in GWSC could suggest that there could a high rate of infiltration between the surficial aquifer and the deeper aquifer with the presence of an aquitard like layer in between. This prevents the groundwater discharge into the stream channel but allows for deeper aquifer recharge. One of the hypothesis could be that the pressure potential in the deeper aquifer is very low due to high density of borewells and high pumping activity which accelerates the seepage. This is compatible to Ballukraya and Srinivasan (2019) findings, which suggests that fractures at shallow depths directly recharge waters through the borewell shafts which leads to a dewatered zone between the surficial aquifer and the saturated zone. The camera inspection of 100 borewells in a sub-watershed of UAC determined a high fracture density close to the ground surface and a small frequency peak at a depth of 75-85m. They argue that the high density of borewells allows vertical movement of water, reducing the flow along the already low permeable pores in hard rock and preventing any recharge in the intermediate zone. Although this may be the case, GWSC signals show decreasing trends even during high precipitation months and a time delay for the increase. At the same time, the corresponding validation from the "incorrect" data of observation wells also adds to the uncertainty in error estimations. Nevertheless, this could still not explain the increasing depth of borewells and the irrigation sources of well census shown in figure 3. Hence on these basis the reliability of GRACE-GLDAS-GWL assimilation was also rejected.

On the other hand, the reliable correlation of groundwater storage and land subsidence trends indicate the response of aquifer systems to natural or anthropogenic factors. There were clear indications of land subsidence and uplift with the ability to detect groundwater storage variations, however these can only be restricted to the surficial aquifer.

To sum up, the principal constraint of this methodology to quantify GW abstraction lies in the following reasons.

1. The primary reason is that GRACE TWS does not seem to include groundwater extraction in deeper aquifers used for irrigation and this has been well documented (Girotto et al., 2017; Banerjee and Kumar, 2014; Frappart and Ramillien, 2018).

2. Moreover, the spatial scale of GRACE does not provide enough reliability in TWS estimates for this small catchment (1432 km^2). Each grid size covers 2500km^2 and the general recommended area is 200,000km^2. Although some studies report that GRACE data is also useful in smaller catchments and some have applied techniques to downscale GRACE, it is surely not applicable to this study area (Ouma et al., 2015; Miro and Famiglietti, 2018).
3. The dissection of the aquifer systems into surficial and subsurface parts purely on the basis of GLDAS is questionable, besides the actual inaccuracy in SM data (Pangaluru et al., 2019; Nair and Indu, 2016). Moreover, the state variable values of GLDAS do not consider anthropogenic processes of irrigation and intensive agriculture and drastically undermines actual ET in disturbed catchments (Vissa et al., 2019).
4. The assimilation of GRACE and GLDAS only assigns inclusion of only the shallow storage fluxes in the surficial aquifer and modelling of deeper aquifer is neglected (Sun et al., 2019; Wu et al., 2019). Moreover, the modelling of the continuous irrigation return flows is an important parameter is not captured in these assimilations (Nair and Indu, 2018).
5. The complexity in the interpretation of GW well data is erroneous and not representative of the hard rock aquifers of South India (Ballukraya and Srinivasan, 2019).

As we see, there seems to be a huge ambiguity in the estimation of groundwater storage anomalies through both RS based products and in-situ groundwater level data. This is consistent to the finding of Hora et al., (2019) and Girotto et al., (2017) who argue that neither satellite data nor GW well data cannot rightly be representations of the on ground reality in highly stressed fractured aquifers. The study concludes that satellite data needs better spatial resolution and consolidation of other socio-hydrological metrics to measure groundwater stress.

5.3 Vegetation Phenology

At a regional scale, the NDVI signatures showed high potential to classify and capture the range of phenological variability. The land surface phenology derived from the NDVI processed images broadly associated the seasonal developmental stages in the plant life cycles associated to the landscape. A change in irrigated area was noted if the NDVI value of an irrigated pixel in any of the previous years is less than the maximum NDVI value of that pixel for the whole time period. As observed, there has been a long term increase in NDVI and therefore irrigated area over the time series. This is especially noticeable for the Kharif season (with peak values during December-January) when compared to the Rabi season. However, the highest uncertainty in NDVI occurs in the monsoon due to the cloud coverage which also happens to the start of the cropping season in the region. Hence, spectral matching techniques through the use of other indices and higher resolution satellite data like the MODIS are essential in monitoring, planning and managing agriculture at a basin level. Furthermore, the integration of ground survey in conjunction with other methods for calculating irrigated area and accuracy assessments would help identify water stress due to rainfall variability, water management, irrigation and agro-economics for the area.

5.4 Limitations and Way Forward

Bhanja et al. (2018) applied an ANN to downscale the GRACE data by incorporating NDVI, GWSA and GW levels monitored wells (n>15000) and found a correlation of $r > 0.6$ in naturally

vegetation covered areas in India. Such conclusiveness cannot be established in this study primarily due to the anthropogenic influence in the catchment. However, such a downscaling approach with through an assimilation and uncertainty estimations of the continuously being generated better satellite and field data should be the foreword course of this study. Hence, we first discuss on the drawbacks and foreword in approaches in the water budgeting and then briefly discuss on an outlook of sustainable strategies for the catchment.

The lack of observed hydro-meteorological data particularly in terms of validation of WB components viz. precipitation through rain gauge, soil moisture sensor data from available field data and ET measurements are missing and need to be incorporated. Secondly, incorporation of social, land use and agricultural and irrigation data can significantly improve estimates. The downscaling of assimilations can improve the simulation of ground water at finer spatial resolutions. The way forward would be to incorporate the latest High Resolution Land Data Assimilation System (HRLDAS) with the assimilation of SMAP/SMERGE and MODIS-ET and NDVI products customized for the Indian region with a 3 hour resolution to further improve accuracy (Gu et al., 2019; Nair and Indu, 2016). Finally, the Landsat data used to quantify vegetation along with farmer surveys and irrigation statistics can highlight the agronomic inquiry in terms of understanding fluxes at a field scale. In regard to the de-seasonalization methodologies and statistical analysis, the study acknowledges that more in-depth analysis using these time series in terms of change point detection, t-tests of seasonal tau values, application of Fourier and wavelet transformation to understand time and frequency domains can help de-tangle the effect of precipitation and human induced changes more profoundly.

An improvement in the ability to monitor and interpret GW systems becomes parallely vital to unlock the potential of RS products to correctly quantify deeper aquifer abstractions. Hence, as Srinivasan et.al, (2017) suggests, a comprehensive approach in coupling significant research questions and asserting field methodologies - rather than applying computer simulations alone - is crucial for investigating the water cycle as a whole and thus, for providing apt information for decision makers in order to ensure sustainability at catchment scale. At a regional water management scale increasing ET of the irrigated agriculture would keep decreasing soil moisture. Further, when coupled with the lowering of water tables and the seepage dynamics of the aquifer, clearly demonstrates rampant over exploitation. Unless some counter actions are taken, the anthropogenic induced aridification in the catchment would worsen. Such being the case, community level adaptation pathways can help replenish the aquifer and achieve more sustainable water management systems (Sivapalan et al., 2014). Instruments like water pricing, abstraction regulations, water harvesting policies, waterbody and aquifer restorations and implementation of drip and micro irrigation can abate the dependency on expensive and environmentally detrimental inter-basin projects (Lele et al., 2013).

Chapter. 6 Conclusions

The assessments of socio-hydro inter-linkages through the analysis of remotely sensed data have proven to be effective in this research. Firstly, an assessment of the important parameters contributing to the dynamics in the water balances using remote sensing products is examined. Drought was estimated through long term precipitation and temperature assessments and water scarcity examined from dynamics of the water balance fluxes adhering to anthropogenic water usage. RS results could conclusively ascertain the lack of long term drought in the catchment.

This study also demonstrated the benefits and pitfalls of remote sensing approaches in quantifying groundwater variability. A quantification of the human influences through the assimilation of GRACE and GLDAS datasets were correctly formulated to understand the spatial and temporal dynamics of aquifer systems and their interactions to anthropogenic drivers of extraction and irrigation. Unfortunately, the absence of stable GW data and the short span of the available coarse GRACE data did yield positive results to match the evidently over-extraction paradigms. Thereafter, the vegetation dynamics were assessed through a multi-spectral analysis. The developed methodologies to minimize the errors generated through cloud cover and Landsat-7 SCL corrections in NDVI derivations can be effectively applied for other studies. The long-term vegetation dynamics indicated a shift towards irrigated agriculture which rationalized water stress in the catchment. Comprehensively, the attitudes of competitive agriculture and over-extractive GW use cognitively hints towards the process of human induced aridification in the catchment. Looking at the brighter side, it becomes imperative that successive studies should review such approaches for the validations of the newer satellites along with field data as and when they become more available. Overall, with the use of RS products, the study could properly disassociate the role of humans in modifying hydro-geologic fluxes or patterns in the UAC, even if not accurately. All together the study concedes that although the results are restricted to theoretical stances, there is an advancement in understanding socio-hydrological linkages through this approach and can be used in other catchments.

Publication bibliography

Ballukraya, P N; Srinivasan, Veena (2019): Sharp variations in groundwater levels at the same location: a case study from heavily exploited, fractured rock aquifer system near Bangalore, South India. In *Current Science* 117 (1), pp. 130–138.

Banerjee, C.; Kumar, D. Nagesh (2014): Identification of prominent spatio-temporal signals in GRACE derived terrestrial water storage for India. In *Int. Arch. Photogramm. Remote Sens. Spatial Inf. Sci.* XL-8, pp. 333–338. DOI: 10.5194/isprsarchives-XL-8-333-2014.

Banerjee, Chandan; Kumar, D. Nagesh (2018): Assessment of Surface Water Storage trends for increasing groundwater areas in India. In *Journal of Hydrology* 562, pp. 780–788. DOI: 10.1016/j.jhydrol.2018.05.052.

Bhanja, Soumendra Nath; Mukherjee, Abhijit; Rodell, Matthew (2018): Groundwater Storage Variations in India. In Abhijit Mukherjee (Ed.): Groundwater of South Asia, vol. 5. Singapore: Springer Singapore (Springer Hydrogeology), pp. 49–59.

Bhave, Ajay Gajanan; Conway, Declan; Dessai, Suraje; Stainforth, David A. (2018): Water Resource Planning Under Future Climate and Socioeconomic Uncertainty in the Cauvery River Basin in Karnataka, India. In *Water resources research* 54 (2), pp. 708–728. DOI: 10.1002/2017WR020970.

Bierkens, Marc F. P.; Reinhard, Stijn; Bruijn, Jens A.; Veninga, Willeke; Wada, Yoshihide (2019): The Shadow Price of Irrigation Water in Major Groundwater-Depleting Countries. In *Water Resour. Res.* 25 (6), p. 1565. DOI: 10.1029/2018WR023086.

Blakeslee, David; Fishman, Ram; Srinivasan, Veena (2018): Way Down in the Hole: Adaptation to Long-Term Water Loss in Rural India. In *American Economic review*.

Blewitt, Geoffrey; Hammond, William C; Kreemer, Corne (2018): Harnessing the GPS Data Explosion for Interdisciplinary Science. In *Eos* 99. Available online at https://eos.org/science-updates/harnessing-the-gps-data-explosion-for-interdisciplinary-science, checked on 9/25/2019.

Blöschl, Günter; Bierkens, Marc F.P.; Chambel, Antonio; Cudennec, Christophe; Destouni, Georgia; Fiori, Aldo et al. (2019): Twenty-three unsolved problems in hydrology (UPH) – a community perspective. In *Hydrological Sciences Journal* 64 (10), pp. 1141–1158. DOI: 10.1080/02626667.2019.1620507.

Cappellari, Michele; McDermid, Richard M.; Alatalo, Katherine; Blitz, Leo; Bois, Maxime; Bournaud, Frederic et al. (2013): The Atlas3D project - XX. Mass-size and mass-sigma distributions of early-type galaxies: bulge fraction drives kinematics, mass-to-light ratio, molecular gas fraction and stellar initial mass function. In *Monthly Notices of the Royal Astronomical Society* 432 (3), pp. 1862–1893. DOI: 10.1093/mnras/stt644.

Castellazzi, Pascal; Martel, Richard; Galloway, Devin L.; Longuevergne, Laurent; Rivera, Alfonso (2016): Assessing Groundwater Depletion and Dynamics Using GRACE and InSAR: Potential and Limitations. In *Ground water* 54 (6), pp. 768–780. DOI: 10.1111/gwat.12453.

Chen, Hao; Zhang, Wanchang; Jafari Shalamzari, Masoud (2019): Remote detection of human-induced evapotranspiration in a regional system experiencing increased anthropogenic demands and extreme climatic variability. In *International Journal of Remote Sensing* 40 (5-6), pp. 1887–1908. DOI: 10.1080/01431161.2018.1523590.

Chinnasamy, P.; Maheshwari, B.; Prathapar, S. A. (2018): Adaptation of Standardised Precipitation Index for understanding watertable fluctuations and groundwater resilience in hard-rock areas of India. In *Environ Earth Sci* 77 (15), p. 645. DOI: 10.1007/s12665-018-7734-6.

Cleveland, W S; Devlin, S J (1988): Locally Weighted Regression: An Approach to Regression Analysis by local fitting. In *American Statistical Association* 83, pp. 596–610.

Cui, Xintong; Guo, Xiaoyu; Wang, Yidi; Wang, Xuelei; Zhu, Weihong; Shi, Jianghong et al. (2019): Application of remote sensing to water environmental processes under a changing climate. In *Journal of Hydrology* 574, pp. 892–902. DOI: 10.1016/j.jhydrol.2019.04.078.

Feng, Huihui (2016): Individual contributions of climate and vegetation change to soil moisture trends across multiple spatial scales. In *Scientific Reports* 6, 32782 EP -. DOI: 10.1038/srep32782.

Ferreira, Vagner; Andam-Akorful, Samuel; Dannouf, Ramia; Adu-Afari, Emmanuel (2019): A Multi-Sourced Data Retrodiction of Remotely Sensed Terrestrial Water Storage Changes for West Africa. In *Water* 11 (2), p. 401. DOI: 10.3390/w11020401.

Frappart, Frédéric; Ramillien, Guillaume (2018): Monitoring Groundwater Storage Changes Using the Gravity Recovery and Climate Experiment (GRACE) Satellite Mission: A Review. In *Remote Sensing* 10 (6), p. 829. DOI: 10.3390/rs10060829.

Gandhi, G. Meera; Parthiban, S.; Thummalu, Nagaraj; Christy, A. (2015): Ndvi: Vegetation Change Detection Using Remote Sensing and Gis – A Case Study of Vellore District. In *Procedia Computer Science* 57, pp. 1199–1210. DOI: 10.1016/j.procs.2015.07.415.

Girotto, Manuela; Lannoy, Gabriëlle J. M. de; Reichle, Rolf H.; Rodell, Matthew; Draper, Clara; Bhanja, Soumendra N.; Mukherjee, Abhijit (2017): Benefits and Pitfalls of GRACE Data Assimilation: a Case Study of Terrestrial Water Storage Depletion in India. In *Geophysical research letters* 44 (9), pp. 4107–4115. DOI: 10.1002/2017GL072994.

Gu, Xihui; Zhang, Qiang; Li, Jianfeng; Singh, Vijay P.; Liu, Jianyu; Sun, Peng; Cheng, Changxiu (2019): Attribution of Global Soil Moisture Drying to Human Activities: A Quantitative Viewpoint. In *Geophys. Res. Lett.* 46 (5), pp. 2573–2582. DOI: 10.1029/2018GL080768.

Hao, Zhen; Zhao, Hesong; Zhang, Chi; Zhou, Huicheng; Zhao, Hongli; Wang, Hao (2019): Correlation Analysis Between Groundwater Decline Trend and Human-Induced Factors in Bashang Region. In *Water* 11 (3), p. 473. DOI: 10.3390/w11030473.

Hirsch, Robert M; Slack, James R. (1984): A Nonparametric Trend Test for Seasonal Data With Serial Dependence. In *Water Resour. Res.* 20 (6), pp. 727–732.

Hora, Tejasvi; Srinivasan, Veena; Basu, Nandita B. (2019): The Groundwater Recovery Paradox in South India. In *Geophys. Res. Lett.* DOI: 10.1029/2019GL083525.

Hosseini-Moghari, Seyed-Mohammad; Araghinejad, Shahab; Tourian, Mohammad J.; Ebrahimi, Kumars; Döll, Petra (2018): Quantifying the impacts of human water use and climate variations on recent drying of Lake Urmia basin: the value of different sets of spaceborne and in-situ data for calibrating a hydrological model. In *Hydrol. Earth Syst. Sci. Discuss.*, pp. 1–29. DOI: 10.5194/hess-2018-318.

Hutton, Christopher; Wagener, Thorsten; Freer, Jim; Han, Dawei; Duffy, Chris; Arheimer, Berit (2016): Most computational hydrology is not reproducible, so is it really science? In *Water Resour. Res.* 52 (10), pp. 7548–7555. DOI: 10.1002/2016WR019285.

Jha, Madan K.; Chowdary, V. M. (2007): Challenges of using remote sensing and GIS in developing nations. In *Hydrogeol J* 15 (1), pp. 197–200. DOI: 10.1007/s10040-006-0117-1.

Kulkarni, Himanshu; Shah, Mihir; Vijay Shankar, P. S. (2015): Shaping the contours of groundwater governance in India. In *Journal of Hydrology: Regional Studies* 4, pp. 172–192. DOI: 10.1016/j.ejrh.2014.11.004.

Kulkarni, Himanshu; Shankar, P. VijayS. (2014): Groundwater resources in India: an arena for diverse competition. In *Local Environment* 19 (9), pp. 990–1011. DOI: 10.1080/13549839.2014.964192.

Landerer, F. W.; Swenson, S. C (2012): Accuracy of scaled GRACE terrestrial water storage estimates. In *Water resources research* (48).

Lele, Sharachchandra; Srinivasan, Veena; Jamwal, Priyanka; Thomas, Bejoy K; Eswar, Meghana; Zuhail, Md T (2013): Water Management in Arkavathy Baisn. A situational Analysis. Environment and Development Discussion Paper No.1.

Lele, Sharachchandra; Srinivasan, Veena; Thomas, Bejoy K.; Jamwal, Priyanka (2018): Adapting to climate change in rapidly urbanizing river basins: insights from a multiple-concerns, multiple-stressors, and multi-level approach. In *Water International* 43 (2), pp. 281–304. DOI: 10.1080/02508060.2017.1416442.

McCandless, Sarah Elizabeth (2014): Utilizing GRACE TWS, NDVI, and Precipitation for Drought Identification and Classification in Texas. Masters. University of Texas, Austin.

Miro, Michelle; Famiglietti, James (2018): Downscaling GRACE Remote Sensing Datasets to High-Resolution Groundwater Storage Change Maps of California's Central Valley. In *Remote Sensing* 10 (1), p. 143. DOI: 10.3390/rs10010143.

Mishra, Anoop Kumar; Rafiq, Mohammad (2019): Rainfall estimation techniques over India and adjoing oceanic regions. In *Current Science* 116 (1), pp. 56–68.

Mondal, Arpita; Narasimhan, Balaji; Sekhar, Muddu; Mujumdar, P. P. (2016): Hydrologic Modelling. In *Proceedings of the Indian National Science Academy* 82 (3), pp. 817–832. DOI: 10.16943/ptinsa/2016/48487.

Mondal, Arun; Lakshmi, Venkat; Hashemi, Hossein (2018): Intercomparison of trend analysis of Multisatellite Monthly Precipitation Products and Gauge Measurements for River Basins of India. In *Journal of Hydrology* 565, pp. 779–790. DOI: 10.1016/j.jhydrol.2018.08.083.

Mukherjee, Amritendu; Ramachandran, Parthasarathy (2018): Prediction of GWL with the help of GRACE TWS for unevenly spaced time series data in India : Analysis of comparative

performances of SVR, ANN and LRM. In *Journal of Hydrology* 558, pp. 647–658. DOI: 10.1016/j.jhydrol.2018.02.005.

Müller, Hannes Schmied (2017): Evaluation, modification and applitation of a global hydrological model. In *Frankfurt Hydrology paper* 16.

Nair, A. S.; Indu, J. (2018): Utilizing GRACE and GLDAS data for estimating groundwater storage variability over the Krishna Basin. In *ISPRS Ann. Photogramm. Remote Sens. Spatial Inf. Sci.* IV-5, pp. 129–136. DOI: 10.5194/isprs-annals-IV-5-129-2018.

Nair, Akhilesh; Indu, J. (2016): Enhancing Noah Land Surface Model Prediction Skill over Indian Subcontinent by Assimilating SMOPS Blended Soil Moisture. In *Remote Sensing* 8 (12), p. 976. DOI: 10.3390/rs8120976.

Nayak, H. P.; Sinha, Palash; Satyanarayana, A. N. V.; Bhattacharya, A.; Mohanty, U. C. (2019): Performance Evaluation of High-Resolution Land Data Assimilation System (HRLDAS) Over Indian Region. In *Pure Appl. Geophys.* 176 (1), pp. 389–407. DOI: 10.1007/s00024-018-1946-2.

Ouma, Yashon O.; Aballa, D. O.; Marinda, D. O.; Tateishi, R.; Hahn, M. (2015): Use of GRACE time-variable data and GLDAS-LSM for estimating groundwater storage variability at small basin scales: a case study of the Nzoia River Basin. In *International Journal of Remote Sensing* 36 (22), pp. 5707–5736. DOI: 10.1080/01431161.2015.1104743.

Pangaluru, Kishore; Velicogna, Isabella; A, Geruo; Mohahjerani, Yara; Ciraci, Enrico; Cpepa, Sravani et al. (2019): Soil Moisture Variability in India: Relationship of Land Surface-Atmospher Fields using Maximum Covariance Analysis. In *Remote Sensing* 11 (335).

Patil, Vikram S.; Thomas, Bejoy K.; Lele, Sharachchandra; Eswar, Meghana; Srinivasan, Veena (2019): Adapting or Chasing Water? Crop Choice and Farmers' Responses to Water Stress in Peri-Urban Bangalore, India. In *Irrig. and Drain.* 68 (2), pp. 140–151. DOI: 10.1002/ird.2291.

Paul, Reba; Kenway, Steven; McIntosh, Brian; Mukheibir, Pierre (2018): Urban Metabolism of Bangalore City: A Water Mass Balance Analysis. In *Journal of Industrial Ecology* 22 (6), pp. 1413–1424. DOI: 10.1111/jiec.12705.

Pedro-Monzonís, María; Solera, Abel; Ferrer, Javier; Estrela, Teodoro; Paredes-Arquiola, Javier (2015): A review of water scarcity and drought indexes in water resources planning and management. In *Journal of Hydrology* 527, pp. 482–493. DOI: 10.1016/j.jhydrol.2015.05.003.

Penny, G. (2017a): The drying of the Arkavathy river: understanding hydrological change in a human-dominated watershed. Doctoral. University of California, Berkeley, USA. Engineering - Civil & Enviornmental Engineering.

Penny, Gopal (2017b): The drying of the Arkavathy river: understanding hydrological change in a human-dominated watershed. Doctoral. University of California, Berkeley. Engineering - Civil and Environmental Engineering.

Penny, Gopal; Srinivasan, Veena; Dronova, Iryna; Lele, Sharachchandra; Thompson, Sally (2018): Spatial characterization of long-term hydrological change in the Arkavathy watershed

adjacent to Bangalore, India. In *Hydrol. Earth Syst. Sci.* 22 (1), pp. 595–610. DOI: 10.5194/hess-22-595-2018.

Pokhrel, Yadu N.; Hanasaki, Naota; Wada, Yoshihide; Kim, Hyungjun (2016): Recent progresses in incorporating human land-water management into global land surface models toward their integration into Earth system models. In *WIREs Water* 3 (4), pp. 548–574. DOI: 10.1002/wat2.1150.

Poyil, Rohith P.; S., Dhanalakshmi; Goyal, Pramila (2016): Predicting future changes in climate and its impact on change in land use: a case study of Cauvery Basin. In Reza Khanbilvardi, Ashwagosh Ganju, A. S. Rajawat, Jing M. Chen (Eds.): Land Surface and Cryosphere Remote Sensing III. SPIE Asia-Pacific Remote Sensing. New Delhi, India, Monday 4 April 2016: SPIE (SPIE Proceedings), 98772Y.

Qi, Wei; Liu, Junguo; Chen, Deliang (2018): Evaluations and Improvements of GLDAS2.0 and GLDAS2.1 Forcing Data's Applicability for Basin Scale Hydrological Simulations in the Tibetan Plateau. In *J. Geophys. Res. Atmos.* 123 (23), D24115. DOI: 10.1029/2018JD029116.

Rodell, M; Houser, P R; Jambor, U; Gottschalck, J; Mitchell, K; Meng, C J et al. (2004): The Global Land Data Assimilation System. In *American Meterological Society* 85:3, pp. 381–394.

Rodriguez-Iturbe, I. (2000): Ecohydrology: A hydrologic perspective of climate-soil-vegetation dynamies. In *Water resources research* 36 (1), pp. 3–9.

Rowlands, D. D.; Luthcke, S. B.; McCarthy, J. J.; Klosko, S. M.; Chinn, D. S.; Lemoine, F. G. et al. (2010): Global mass flux solutions from GRACE: A comparison of parameter estimation strategies—Mass concentrations versus Stokes coefficients. In *J. Geophys. Res.* 115 (B1), p. 1275. DOI: 10.1029/2009JB006546.

Sakumura, C.; Bettadpur, S.; Bruinsma, S. (2014): Ensemble prediction and intercomparison analysis of GRACE time-variable gravity field models. In *Geophys. Res. Lett.* 41 (5), pp. 1389–1397. DOI: 10.1002/2013GL058632.

Schmugge, Thomas J; Kustas, William P; Ritchie, Jerry C; Jackson, Thomas J; Rango, Al (2002): Remote Sensing in Hydrology. In *Advances in Water Resources* 25, pp. 1367–1385.

Sekhar, M.; Tomer, Sat; Thiyaku, S.; Giriraj, P.; Murthy, Sanjeeva; Mehta, Vishal (2018): Groundwater Level Dynamics in Bengaluru City, India. In *Sustainability* 10 (2), p. 26. DOI: 10.3390/su10010026.

Shwetha, H. R.; Nagesh Kumar, D. (2018): Performance evaluation of satellite-based approaches for the estimation of daily air temperature and reference evapotranspiration. In *Hydrological Sciences Journal* 63 (9), pp. 1347–1367. DOI: 10.1080/02626667.2018.1505046.

Sinha, Debanjan; Syed, Tajdarul H.; Reager, John T. (2019): Utilizing combined deviations of precipitation and GRACE-based terrestrial water storage as a metric for drought characterization: A case study over major Indian river basins. In *Journal of Hydrology* 572, pp. 294–307. DOI: 10.1016/j.jhydrol.2019.02.053.

Sivapalan, M.; Konar, M.; Srinivasan, V.; Chhatre, A.; Wutich, A.; Scott, C. A. et al. (2014): Socio-hydrology: Use-inspired water sustainability science for the Anthropocene. In *Earth's Future* 2 (4), pp. 225–230. DOI: 10.1002/2013EF000164.

Skaskevych, Alla (2014): A comparision study of GRACE based groundwater modelling for data-rich and data-poor regions. Masters. Faculty of the University of Missouri-Kansas City, Missouri Kansas City. Department of Geosciences.

Srinivasan, V.; Sanderson, M.; Garcia, M.; Konar, M.; Blöschl, G.; Sivapalan, M. (2016): Prediction in a socio-hydrological world. In *Hydrological Sciences Journal* 2 (3), pp. 1–8. DOI: 10.1080/02626667.2016.1253844.

Srinivasan, V.; Thompson, S.; Madhyastha, K.; Penny, G.; Jeremiah, K.; Lele, S. (2015): Why is the Arkavathy River drying? A multiple-hypothesis approach in a data-scarce region. In *Hydrol. Earth Syst. Sci.* 19 (4), pp. 1905–1917. DOI: 10.5194/hess-19-1905-2015.

Srinivasan, Veena; Gorelick, Steven M.; Goulder, Lawrence (2010): Sustainable urban water supply in south India: Desalination, efficiency improvement, or rainwater harvesting? In *Water Resour. Res.* 46 (10), p. 1216. DOI: 10.1029/2009WR008698.

Srinivasan, Veena; Lele, Sharchandra (Eds.) (2017): From Groundwater Regulation to Integrated Water Management. The Biophysical Case. Economic and Political Weekly LII (31): Economic and Political Weekly.

Srinivasan, Veena; Penny, Gopal; Lele, Sharachchandra; Thomas, Bejoy K.; Thompson, Sally (2017): Proximate and underlying drivers of socio-hydrologic change in the upper Arkavathy watershed, India. In *Hydrol. Earth Syst. Sci. Discuss.*, pp. 1–28. DOI: 10.5194/hess-2017-543.

Sun, Alexander Y; Scanlon, Bridget R; Zhang, Zizhan; Walling, David; Bhanja, Soumendra N; Mukherjee, Abhijit; Zhong, Zhi (2019): Combining Physically Based Modelling and Depp learning for fusing GRACE satellite data: Can we learn from Mismatch? In *Water resources research* (55), pp. 1179–1195.

Thomas, Bejoy K; Lele, Sharachchandra; Srinivasan, Veena; Eswar, Meghana; Kenchaigol, Sanjeev D (2015): Rethinking Resilience in Urbanizing River Basins. ICARUS Fourth Global Meeting. University of Illinois at Urbana-Champaign, 2015. Available online at http://www.icarus.info/wp-content/uploads/2015/05/Thomas-et-al.-Enhancing-resilience-or-furthering-vulnerability.pdf.

Thompson, S. E.; Sivapalan, M.; Harman, C. J.; Srinivasan, V.; Hipsey, M. R.; Reed, P. et al. (2013): Developing predictive insight into changing water systems: use-inspired hydrologic science for the Anthropocene. In *Hydrol. Earth Syst. Sci.* 17 (12), pp. 5013–5039. DOI: 10.5194/hess-17-5013-2013.

Troy, T. J.; Konar, M.; Srinivasan, V.; Thompson, S. (2015): Moving sociohydrology forward: a synthesis across studies. In *Hydrol. Earth Syst. Sci.* 19 (8), pp. 3667–3679. DOI: 10.5194/hess-19-3667-2015.

van Meter, Kimberly J.; Steiff, Michael; McLaughlin, Daniel L.; Basu, Nandita B. (2016): The socioecohydrology of rainwater harvesting in India: understanding water storage and release dynamics across spatial scales. In *Hydrol. Earth Syst. Sci.* 20 (7), pp. 2629–2647. DOI: 10.5194/hess-20-2629-2016.

Verbesselt, Jan; Hyndman, Rob; Newnham, Glenn; Culvenor, Darius (2010): Detecting trend and seasonal changes in satellite image time series. In *Remote Sensing of Environment* 114 (1), pp. 106–115. DOI: 10.1016/j.rse.2009.08.014.

Vissa, Naresh Krishna; Anandh, P. C.; Behera, Mama Manjali; Mishra, Sameeksha (2019): ENSO-induced groundwater changes in India derived from GRACE and GLDAS. In *J Earth Syst Sci* 128 (5), p. 1001. DOI: 10.1007/s12040-019-1148-z.

Wagener, Thorsten; Sivapalan, Murugesu; Troch, Peter A.; McGlynn, Brian L.; Harman, Ciaran J.; Gupta, Hoshin V. et al. (2010): The future of hydrology: An evolving science for a changing world. In *Water Resour. Res.* 46 (5), p. 1080. DOI: 10.1029/2009WR008906.

Wien, T. U. (2019): GLDAS Documentation: NASA Goddard Earth Sciences Data and Information Services Center (GES DISC)., checked on 5/21/2019.

Woodcock, Curtis E; Strahler, Alan H; Franklin, Janet (1983): Remote sensing for land management and planning. In *Environmetal Management* 7 (3), pp. 223–237.

Wu, Qifan; Si, Bingcheng; He, Hailong; Wu, Pute (2019): Determining Regional-Scale Groundwater Recharge with GRACE and GLDAS. In *Remote Sensing* 11 (2), p. 154. DOI: 10.3390/rs11020154.

Xie, Zunyi; Huete, Alfredo; Ma, Xuanlong; Restrepo-Coupe, Natalia; Devadas, Rakhesh; Clarke, Kenneth; Lewis, Megan (2016): Landsat and GRACE observations of arid wetland dynamics in a dryland river system under multi-decadal hydroclimatic extremes. In *Journal of Hydrology* 543, pp. 818–831. DOI: 10.1016/j.jhydrol.2016.11.001.

Appendix

)

Appendix -1

List of Landsat Images used for NDVI analysis

LT05_L1TP_144051_20090520_20161028_01_T1
LT05_L1TP_144051_20090605_20161025_01_T1
LT05_L1TP_144051_20100216_20161016_01_T1
LT05_L1TP_144051_20100608_20161016_01_T1
LT05_L1TP_144051_20100131_20161017_01_T1
LT05_L1TP_144051_20091128_20161017_01_T1
LT05_L1TP_144051_20090909_20161021_01_T1
LT05_L1TP_144051_20111017_20161005_01_T1
LT05_L1TP_144051_20110307_20161209_01_T1
LT05_L1TP_144051_20110203_20161010_01_T1
LT05_L1TP_144051_20110118_20161010_01_T1
LT05_L1TP_144051_20100710_20161015_01_T1
LE07_L1TP_144051_20120129_20161203_01_T1
LE07_L1TP_144051_20120301_20161203_01_T1
LE07_L1TP_144051_20120317_20161202_01_T1
LE07_L1TP_144051_20120402_20161203_01_T1
LE07_L1TP_144051_20120418_20161202_01_T1
LE07_L1TP_144051_20120504_20161201_01_T1
LE07_L1TP_144051_20120520_20161202_01_T1
LE07_L1TP_144051_20120925_20161129_01_T1
LE07_L1TP_144051_20121011_20161128_01_T1
LE07_L1TP_144051_20130827_20161121_01_T1
LE07_L1TP_144051_20130928_20161120_01_T1
LE07_L1TP_144051_20070304_20170104_01_T1
LE07_L1TP_144051_20070320_20170104_01_T1
LE07_L1TP_144051_20070405_20170104_01_T1
LE07_L1TP_144051_20080306_20161230_01_T1
LE07_L1TP_144051_20080219_20161230_01_T1
LE07_L1TP_144051_20080203_20161230_01_T1
LE07_L1TP_144051_20080118_20161230_01_T1
LE07_L1TP_144051_20080102_20161231_01_T1
LE07_L1TP_144051_20071201_20170101_01_T1
LE07_L1TP_144051_20071115_20170101_01_T1
LE07_L1TP_144051_20071014_20170101_01_T1
LE07_L1TP_144051_20081117_20161224_01_T1
LE07_L1TP_144051_20081101_20161224_01_T1
LE07_L1TP_144051_20080930_20161224_01_T1
LE07_L1TP_144051_20080525_20161229_01_T1
LE07_L1TP_144051_20080423_20161229_01_T1
LE07_L1TP_144051_20080407_20161229_01_T1
LE07_L1TP_144051_20090629_20161219_01_T1
LE07_L1TP_144051_20090528_20161222_01_T1
LE07_L1TP_144051_20090512_20161222_01_T1
LE07_L1TP_144051_20090410_20161220_01_T1

LE07_L1TP_144051_20090309_20161223_01_T1
LE07_L1TP_144051_20090205_20161222_01_T1
LE07_L1TP_144051_20090120_20161222_01_T1
LE07_L1TP_144051_20081203_20161223_01_T1
LE07_L1TP_144051_20091019_20161217_01_T1
LE07_L1TP_144051_20091222_20161216_01_T1
LE07_L1TP_144051_20100107_20161216_01_T1
LE07_L1TP_144051_20100123_20161215_01_T1
LE07_L1TP_144051_20100208_20161217_01_T1
LE07_L1TP_144051_20100224_20161217_01_T1
LE07_L1TP_144051_20100515_20161215_01_T1
LE07_L1TP_144051_20111212_20161204_01_T1
LE07_L1TP_144051_20111110_20161205_01_T1
LE07_L1TP_144051_20110502_20161209_01_T1
LE07_L1TP_144051_20101209_20161211_01_T1
LE07_L1TP_144051_20121027_20161127_01_T1
LE07_L1TP_144051_20121214_20161126_01_T1
LE07_L1TP_144051_20130115_20161127_01_T1
LE07_L1TP_144051_20130131_20161126_01_T1
LE07_L1TP_144051_20140424_20161115_01_T1
LE07_L1TP_144051_20140408_20161116_01_T1
LE07_L1TP_144051_20140323_20161117_01_T1
LE07_L1TP_144051_20140307_20161117_01_T1
LE07_L1TP_144051_20140203_20161118_01_T1
LE07_L1TP_144051_20131217_20161118_01_T1
LE07_L1TP_144051_20141017_20161101_01_T1
LE07_L1TP_144051_20141001_20161101_01_T1
LE07_L1GT_144051_20140915_20161102_01_T2
LE07_L1GT_144051_20140830_20161112_01_T2
LE07_L1TP_144051_20140627_20161112_01_T1
LE07_L1TP_144051_20140510_20161115_01_T1
LE07_L1TP_144051_20141118_20161031_01_T1
LE07_L1TP_144051_20141204_20161030_01_T1
LE07_L1TP_144051_20150105_20161030_01_T1
LE07_L1TP_144051_20150121_20161029_01_T1
LE07_L1TP_144051_20141220_20161030_01_T1
LE07_L1TP_144051_20150206_20161029_01_T1
LE07_L1TP_144051_20150222_20161029_01_T1
LE07_L1TP_144051_20150310_20161028_01_T1
LE07_L1TP_144051_20150529_20161026_01_T1
LE07_L1TP_144051_20150427_20161027_01_T1
LE07_L1TP_144051_20151223_20161018_01_T1
LE07_L1TP_144051_20160108_20161016_01_T1
LE07_L1TP_144051_20160124_20161015_01_T1
LE07_L1TP_144051_20160209_20161015_01_T1
LE07_L1TP_144051_20160225_20161014_01_T1
LE07_L1TP_144051_20160328_20161013_01_T1
LE07_L1TP_144051_20160413_20161012_01_T1

LE07_L1TP_144051_20161006_20170302_01_T1
LE07_L1TP_144051_20160515_20161011_01_T1
LE07_L1TP_144051_20160429_20161012_01_T1
LE07_L1TP_144051_20170331_20170426_01_T1
LE07_L1TP_144051_20170227_20170325_01_T1
LE07_L1TP_144051_20170211_20170310_01_T1
LE07_L1TP_144051_20170110_20170320_01_T1
LE07_L1TP_144051_20161225_20170219_01_T1

LC08_L1TP_144051_20130413_20170505_01_T1
LC08_L1TP_144051_20131107_20170428_01_T1
LC08_L1TP_144051_20131225_20170427_01_T1
LC08_L1TP_144051_20140518_20170422_01_T1
LC08_L1TP_144051_20140502_20170423_01_T1
LC08_L1TP_144051_20140416_20170423_01_T1
LC08_L1TP_144051_20140315_20170425_01_T1
LC08_L1TP_144051_20140331_20170424_01_T1
LC08_L1TP_144051_20140227_20170425_01_T1
LC08_L1TP_144051_20140211_20170425_01_T1
LC08_L1TP_144051_20140126_20170426_01_T1
LC08_L1TP_144051_20140110_20170426_01_T1
LC08_L1TP_144051_20141110_20170417_01_T1
LC08_L1TP_144051_20150419_20170409_01_T1
LC08_L1TP_144051_20150403_20170411_01_T1
LC08_L1TP_144051_20150318_20170412_01_T1
LC08_L1TP_144051_20150129_20170413_01_T1
LC08_L1TP_144051_20150214_20170413_01_T1
LC08_L1TP_144051_20150113_20170414_01_T1
LC08_L1TP_144051_20141126_20170417_01_T1
LC08_L1TP_144051_20150521_20170408_01_T1
LC08_L1TP_144051_20150606_20170408_01_T1
LC08_L1TP_144051_20150825_20170405_01_T1
LC08_L1TP_144051_20151012_20170403_01_T1
LC08_L1TP_144051_20160320_20170327_01_T1
LC08_L1TP_144051_20160304_20170328_01_T1
LC08_L1TP_144051_20160201_20170330_01_T1
LC08_L1TP_144051_20160116_20170405_01_T1
LC08_L1TP_144051_20151231_20170331_01_T1
LC08_L1TP_144051_20151215_20180524_01_T1
LC08_L1TP_144051_20160405_20170327_01_T1
LC08_L1TP_144051_20160421_20170326_01_T1
LC08_L1TP_144051_20160507_20170325_01_T1
LC08_L1TP_144051_20160523_20170324_01_T1
LC08_L1TP_144051_20160811_20170322_01_T1
LC08_L1TP_144051_20170203_20170215_01_T1
LC08_L1TP_144051_20170118_20170311_01_T1
LC08_L1TP_144051_20170102_20170312_01_T1
LC08_L1TP_144051_20161217_20180524_01_T1

LC08_L1TP_144051_20161115_20170318_01_T1
LC08_L1TP_144051_20170307_20170316_01_T1
LC08_L1TP_144051_20170323_20170329_01_T1
LC08_L1TP_144051_20170408_20170414_01_T1
LC08_L1TP_144051_20170424_20170502_01_T1
LC08_L1TP_144051_20170526_20170615_01_T1
LC08_L1TP_144051_20171220_20171224_01_T1
LC08_L1TP_144051_20171102_20171109_01_T1
LC08_L1TP_144051_20180105_20180118_01_T1
LC08_L1TP_144051_20180121_20180206_01_T1
LC08_L1TP_144051_20180206_20180221_01_T1
LC08_L1TP_144051_20180222_20180308_01_T1
LC08_L1TP_144051_20180310_20180320_01_T1
LC08_L1TP_144051_20180326_20180404_01_T1
LC08_L1TP_144051_20180427_20180502_01_T1
LC08_L1TP_144051_20180513_20180517_01_T1
LC08_L1TP_144051_20180411_20180417_01_T1
LC08_L1TP_144051_20181105_20181115_01_T1
LC08_L1TP_144051_20181020_20181031_01_T1
LC08_L1TP_144051_20180902_20180912_01_T1
LC08_L1TP_144051_20181207_20181211_01_T1
LC08_L1TP_144051_20181223_20181227_01_T1
LC08_L1TP_144051_20190108_20190130_01_T1
LC08_L1TP_144051_20190124_20190205_01_T1
LC08_L1TP_144051_20190225_20190309_01_T1
LC08_L1TP_144051_20190313_20190325_01_T1
LC08_L1TP_144051_20190329_20190404_01_T1
LC08_L1TP_144051_20190414_20190422_01_T1
LC08_L1TP_144051_20190921_20190926_01_T1
LC08_L1TP_144051_20190617_20190620_01_T1
LC08_L1TP_144051_20190601_20190605_01_T1
LC08_L1TP_144051_20190516_20190521_01_T1
LC08_L1TP_144051_20190430_20190508_01_T1

LT05_L1TP_144051_20090520_20161028_01_T1
LT05_L1TP_144051_20090605_20161025_01_T1
LT05_L1TP_144051_20100216_20161016_01_T1
LT05_L1TP_144051_20100608_20161016_01_T1
LT05_L1TP_144051_20100131_20161017_01_T1
LT05_L1TP_144051_20091128_20161017_01_T1
LT05_L1TP_144051_20090909_20161021_01_T1
LT05_L1TP_144051_20111017_20161005_01_T1
LT05_L1TP_144051_20110307_20161209_01_T1
LT05_L1TP_144051_20110203_20161010_01_T1
LT05_L1TP_144051_20110118_20161010_01_T1
LT05_L1TP_144051_20100710_20161015_01_T1
LE07_L1TP_144051_20120129_20161203_01_T1
LE07_L1TP_144051_20120301_20161203_01_T1

LE07_L1TP_144051_20120317_20161202_01_T1
LE07_L1TP_144051_20120402_20161203_01_T1
LE07_L1TP_144051_20120418_20161202_01_T1
LE07_L1TP_144051_20120504_20161201_01_T1
LE07_L1TP_144051_20120520_20161202_01_T1
LE07_L1TP_144051_20120925_20161129_01_T1
LE07_L1TP_144051_20121011_20161128_01_T1
LE07_L1TP_144051_20130827_20161121_01_T1
LE07_L1TP_144051_20130928_20161120_01_T1
LE07_L1TP_144051_20070304_20170104_01_T1
LE07_L1TP_144051_20070320_20170104_01_T1
LE07_L1TP_144051_20070405_20170104_01_T1
LE07_L1TP_144051_20080306_20161230_01_T1
LE07_L1TP_144051_20080219_20161230_01_T1
LE07_L1TP_144051_20080203_20161230_01_T1
LE07_L1TP_144051_20080118_20161230_01_T1
LE07_L1TP_144051_20080102_20161231_01_T1
LE07_L1TP_144051_20071201_20170101_01_T1
LE07_L1TP_144051_20071115_20170101_01_T1
LE07_L1TP_144051_20071014_20170101_01_T1
LE07_L1TP_144051_20081117_20161224_01_T1
LE07_L1TP_144051_20081101_20161224_01_T1
LE07_L1TP_144051_20080930_20161224_01_T1
LE07_L1TP_144051_20080525_20161229_01_T1
LE07_L1TP_144051_20080423_20161229_01_T1
LE07_L1TP_144051_20080407_20161229_01_T1
LE07_L1TP_144051_20090629_20161219_01_T1
LE07_L1TP_144051_20090528_20161222_01_T1
LE07_L1TP_144051_20090512_20161222_01_T1
LE07_L1TP_144051_20090410_20161220_01_T1
LE07_L1TP_144051_20090309_20161223_01_T1
LE07_L1TP_144051_20090205_20161222_01_T1
LE07_L1TP_144051_20090120_20161222_01_T1
LE07_L1TP_144051_20081203_20161223_01_T1
LE07_L1TP_144051_20091019_20161217_01_T1
LE07_L1TP_144051_20091222_20161216_01_T1
LE07_L1TP_144051_20100107_20161216_01_T1
LE07_L1TP_144051_20100123_20161215_01_T1
LE07_L1TP_144051_20100208_20161217_01_T1
LE07_L1TP_144051_20100224_20161217_01_T1
LE07_L1TP_144051_20100515_20161215_01_T1
LE07_L1TP_144051_20111212_20161204_01_T1
LE07_L1TP_144051_20111110_20161205_01_T1
LE07_L1TP_144051_20110502_20161209_01_T1
LE07_L1TP_144051_20101209_20161211_01_T1
LE07_L1TP_144051_20121027_20161127_01_T1
LE07_L1TP_144051_20121214_20161126_01_T1
LE07_L1TP_144051_20130115_20161127_01_T1

LE07_L1TP_144051_20130131_20161126_01_T1
LE07_L1TP_144051_20140424_20161115_01_T1
LE07_L1TP_144051_20140408_20161116_01_T1
LE07_L1TP_144051_20140323_20161117_01_T1
LE07_L1TP_144051_20140307_20161117_01_T1
LE07_L1TP_144051_20140203_20161118_01_T1
LE07_L1TP_144051_20131217_20161118_01_T1
LE07_L1TP_144051_20141017_20161101_01_T1
LE07_L1TP_144051_20141001_20161101_01_T1
LE07_L1GT_144051_20140915_20161102_01_T2
LE07_L1GT_144051_20140830_20161112_01_T2
LE07_L1TP_144051_20140627_20161112_01_T1
LE07_L1TP_144051_20140510_20161115_01_T1
LE07_L1TP_144051_20141118_20161031_01_T1
LE07_L1TP_144051_20141204_20161030_01_T1
LE07_L1TP_144051_20150105_20161030_01_T1
LE07_L1TP_144051_20150121_20161029_01_T1
LE07_L1TP_144051_20141220_20161030_01_T1
LE07_L1TP_144051_20150206_20161029_01_T1
LE07_L1TP_144051_20150222_20161029_01_T1
LE07_L1TP_144051_20150310_20161028_01_T1
LE07_L1TP_144051_20150529_20161026_01_T1
LE07_L1TP_144051_20150427_20161027_01_T1
LE07_L1TP_144051_20151223_20161018_01_T1
LE07_L1TP_144051_20160108_20161016_01_T1
LE07_L1TP_144051_20160124_20161015_01_T1
LE07_L1TP_144051_20160209_20161015_01_T1
LE07_L1TP_144051_20160225_20161014_01_T1
LE07_L1TP_144051_20160328_20161013_01_T1
LE07_L1TP_144051_20160413_20161012_01_T1
LE07_L1TP_144051_20161006_20170302_01_T1
LE07_L1TP_144051_20160515_20161011_01_T1
LE07_L1TP_144051_20160429_20161012_01_T1
LE07_L1TP_144051_20170331_20170426_01_T1
LE07_L1TP_144051_20170227_20170325_01_T1
LE07_L1TP_144051_20170211_20170310_01_T1
LE07_L1TP_144051_20170110_20170320_01_T1
LE07_L1TP_144051_20161225_20170219_01_T1

Appendix 2 – Script for GRACE extraction

```
wdir0='E:\vajedian\Tejas\Grace\CSR'

region=[77.1 77.8 12.9 13.5];

lon_UL=region(1); lat_UL=region(4); % Upper Left coordinates
```

```
lon_LR=region(2); lat_LR=region(3);;% Lower Right coordinate
boundary=[       77.24401760605072,12.95902276667219,0 77.2439065677009)
Lon_a=Arkavathy_total(1:2:end); Lat_a=Arkavathy_total(2:2:end);
lon_b=boundary(1:3:end); lat_b=boundary(2:3:end);
date_origin=datenum(2002,01,01);
% extract LW from the available dataset
cd(wdir0)
list_nc=ls('*.nc');
for i=1:size(list_nc)
   if i==1
      ncdisp(list_nc(i,:));
      lon=ncread(list_nc(i,:),'lon');
      lat=ncread(list_nc(i,:),'lat');
      [Lon,Lat]=meshgrid(lon,lat);
   end
 LW(:,:,i)=ncread(list_nc(i,:),'lwe_thickness');
 time_bounds(i,:)=ncread(list_nc(i,:),'time_bounds')+date_origin;
%   str_date(i,1)=
%   end_date(i,1)=
%
 i
end
ind_lon=find(lon>lon_UL & lon<lon_LR);
ind_lat=find(lat>lat_LR-0.5 & lat<lat_UL);
% figure; imagesc(LW(:,:,2)); colormap  jet;
cropped_region=[ind_lon(1)-1 ind_lat(1)-1;
 ind_lon(end)+1 ind_lat(1)-1;
 ind_lon(end)+1 ind_lat(end)+1;
 ind_lon(1)-1    ind_lat(end)+1;
 ind_lon(1)-1 ind_lat(1)-1];
hold on; line(cropped_region(:,1),cropped_region(:,2),'color','k')
close all
```

```
filename='grace_CSR.gif';
for i=1: size(LW,3)
   step=1;
   tmp_LW=LW(:,:,i)';
   crop_lw=tmp_LW(ind_lat(1)-step*0:ind_lat(end)+step,ind_lon(1)-step*0:ind_lon(end)+step*0);
   crop_lon=Lon(ind_lat(1)-step*0:ind_lat(end)+step,ind_lon(1)-step*0:ind_lon(end)+step*0);
   crop_lat=Lat(ind_lat(1)-step*0:ind_lat(end)+step,ind_lon(1)-step*0:ind_lon(end)+step*0);


  h0= figure(1);
cmap0=colormap(gray);
dem(crop_lon(1,:),crop_lat(:,1),crop_lw,'Contrast',0,'AxisEqual','auto','ColorMap',cmap0);
step=0;  crop_lw0=tmp_LW(ind_lat(1)-step:ind_lat(end)+step,ind_lon(1)-step:ind_lon(end)+step);
hold on;
% plot(lon(ind_lon(1)),lat(ind_lat(1)),'*r')
   lw_m(i)=mean(crop_lw0);
   lw_t(i)=tmp_LW(ind_lat(1)-1,ind_lon(1));
%
   line(lon_b,lat_b,'color','r','linewidth',1.5);% colorbar;
   line(Lon_a,Lat_a,'color','r','linewidth',1.5);
 cbh=colorbar('h');cy=get(cbh,'XTick'); caxis([min(crop_lw) max(crop_lw)])
 set(cbh,'Limits',[min(crop_lw) max(crop_lw)])
% set(cbh,'XTick',[min(crop_lw) max(crop_lw)])
% set(cbh,'XTickLabel',{num2str(min(crop_lw)),num2str(max(crop_lw))})
            title(strcat('Starting:',datestr(time_bounds(i,1)),'- Ending:', datestr(time_bounds(i,2)))  )
%    colorbar;
       frame = getframe(h0);
         im = frame2im(frame);
    [imind,cm] = rgb2ind(im,256);
    if i == 1
       imwrite(imind,cm,filename,'gif', 'Loopcount',inf);
    else
       imwrite(imind,cm,filename,'gif','WriteMode','append');
```

```
    end
i
end
figure; plot(mean(time_bounds,2),lw_t./(time_bounds(:,2)-time_bounds(:,1))','--.'); title('CSR')
% -0.0003757 *(date_grace(end)-date_grace(1))
[datestr(time_bounds(:,1)) repmat(',',[size(time_bounds,1) 1]) datestr(time_bounds(:,2))
repmat(',',[size(time_bounds,1) 1]) num2str((lw_t./(time_bounds(:,2)-time_bounds(:,1))'*30)') ]
final_data_grace_CSR=[time_bounds (lw_t./(time_bounds(:,2)-time_bounds(:,1))')']
save final_data_grace_CSR final_data_grace_CSR% line[]
% line[]
% Red_img=Red_img(ind_y(1):ind_y(end),ind_x(1):ind_x(end));
%     NIR_img=NIR_img(ind_y(1):ind_y(end),ind_x(1):ind_x(end));
 grace_intp = interp1(final_data_grace(:,1),final_data_grace(:,2),final_data_GLDAS(:,1));
figure; plot(final_data_GLDAS(:,1),final_data_GLDAS(:,2),'.-r')
hold on; plot(final_data_GLDAS(:,1),grace_intp*10-final_data_GLDAS(:,2),'.-b')
```

Appendix 3 – Script for GLDAS extraction

```
%read NC grace file
clear; close all
addpath(genpath('E:\vajedian\softwares\GBIS_V1.0'))
addpath('E:\vajedian\Tejas\fLOESS')
cd E:\vajedian\Tejas\Gldas\nc_files
region=[77.1 77.8 12.9 13.5];
boundary=[0 77.2447947131061,12.95839599320932,0 ];
lon_b=boundary(1:3:end); lat_b=boundary(2:3:end);
lon_UL=min(lon_b); lat_UL=max(lat_b); % Upper Left coordinates
lon_LR=max(lon_b); lat_LR=min(lat_b);;% Lower Right coordinate

input_data='g4.subsetted.GLDAS_NOAH025_M_2_1_Qs_acc.200808010000.77E_12N_77E_13N.nc';
ncdisp(input_data);
lon=ncread(input_data,'lon');
```

```
lat=ncread(input_data,'lat');
[Lon,Lat]=meshgrid(lon,lat);
ind_lon=find(lon>=lon_UL & lon<=lon_LR);
ind_lat=find(lat<=lat_UL & lat>=lat_LR);
cropped_region=[ind_lon(1)-1 ind_lat(1)-1;
 ind_lon(end)+1 ind_lat(1)-1;
 ind_lon(end)+1 ind_lat(end)+1;
 ind_lon(1)-1    ind_lat(end)+1;
 ind_lon(1)-1 ind_lat(1)-1];
step0=0;
 crop_lon=Lon(ind_lat(1)-1-step0:ind_lat(end)+step0,ind_lon(1)-1-step0:ind_lon(end)+step0);
 crop_lat=Lat(ind_lat(1)-1-step0:ind_lat(end)+step0,ind_lon(1)-1-step0:ind_lon(end)+step0);
CanopInt_inst=zeros(size(Lon,1),size(Lon,2),205);
Storm_SSR=zeros(size(Lon,1),size(Lon,2),205);
SM0_10=zeros(size(Lon,1),size(Lon,2),205);
SM10_40=zeros(size(Lon,1),size(Lon,2),205);
SM40_100=zeros(size(Lon,1),size(Lon,2),205);
SM100_200=zeros(size(Lon,1),size(Lon,2),205);
date_num=zeros(205,1);
ls0=ls; cnt1=1; cnt2=1;cnt3=1;cnt4=1;cnt5=1;cnt6=1;
for i=3:length(ls0)
     if ~isempty(strfind(ls0(i,:),'CanopInt_inst'))
       input_data=ls0(i,:);

CanopInt_inst(:,:,cnt1)=transpose(ncread(input_data,'GLDAS_NOAH025_M_2_1_CanopInt_inst'));
       tmp=ls0(i,34+14:34+14+7);
       date_num(cnt1)=datenum(str2num(tmp(1:4)),str2num(tmp(5:6)),str2num(tmp(7:8)));
            cnt1=cnt1+1;
     elseif ~isempty(strfind(ls0(i,:),'Qs_acc'))
       input_data=ls0(i,:);
       Storm_SSR(:,:,cnt2)=transpose(ncread(input_data,'GLDAS_NOAH025_M_2_1_Qs_acc'));
        cnt2=cnt2+1;
```

```
      elseif ~isempty(strfind(ls0(i,:),'SoilMoi0_10cm'))
       input_data=ls0(i,:);

SM0_10(:,:,cnt3)=transpose(ncread(input_data,'GLDAS_NOAH025_M_2_1_SoilMoi0_10cm_inst'));
        cnt3=cnt3+1;
       elseif ~isempty(strfind(ls0(i,:),'SoilMoi10_40cm'))
       input_data=ls0(i,:);

SM10_40(:,:,cnt4)=transpose(ncread(input_data,'GLDAS_NOAH025_M_2_1_SoilMoi10_40cm_inst'));
        cnt4=cnt4+1;
       elseif ~isempty(strfind(ls0(i,:),'SoilMoi40_100cm'))
       input_data=ls0(i,:);

SM40_100(:,:,cnt5)=transpose(ncread(input_data,'GLDAS_NOAH025_M_2_1_SoilMoi40_100cm_inst'
));
        cnt5=cnt5+1;
      elseif ~isempty(strfind(ls0(i,:),'SoilMoi100_200cm'))
       input_data=ls0(i,:);

SM100_200(:,:,cnt6)=transpose(ncread(input_data,'GLDAS_NOAH025_M_2_1_SoilMoi100_200cm_i
nst'));
        cnt6=cnt6+1;
     end
end
% reading time averaged products
% Canopy Water storage
input_data='../g4.timeAvgOverlayMap.GLDAS_NOAH025_M_2_1_CanopInt_inst.20011201-
20190630.77E_12N_77E_13N.nc';
CanopInt_inst_avg=transpose(ncread(input_data,'GLDAS_NOAH025_M_2_1_CanopInt_inst'));
figure(1);
dem(Lon(1,:),Lat(:,1),CanopInt_inst_avg(:,:,1),'Contrast',0,'AxisEqual','auto');%colormap(flipud(jet));
hold on; line(lon_b,lat_b,'color','k','linewidth',2); title('Canopy Water storage')
%%%%%%%%%%%%%%%%%%%%%
% Surface water
```

```
% % input_data='../g4.timeAvgOverlayMap.GLDAS_NOAH025_M_2_1_Qs_acc.20011201-20190630.77E_12N_77E_13N.nc';

% % SSR_avg=transpose( ncread(input_data,'GLDAS_NOAH025_M_2_1_Qs_acc'));

% % figure(2);
dem(Lon(1,:),Lat(:,1),SSR_avg(:,:,1),'Contrast',0,'AxisEqual','auto');%colormap(flipud(jet));

% % hold on; line(lon_b,lat_b,'color','k','linewidth',2); title('Surface water')

%%%%%%%%%%%%%%%%%%%%%

% Soil moisture 0 10cm

input_data='../g4.timeAvgOverlayMap.GLDAS_NOAH025_M_2_1_SoilMoi0_10cm_inst.20011201-20190630.77E_12N_77E_13N.nc';

SM0_10_avg=transpose(ncread(input_data,'GLDAS_NOAH025_M_2_1_SoilMoi0_10cm_inst'));

%%%%%%%%%%%%%%%%%%%%%

% Soil moisture 10 40cm

input_data='../g4.timeAvgOverlayMap.GLDAS_NOAH025_M_2_1_SoilMoi10_40cm_inst.20011201-20190630.77E_12N_77E_13N.nc';

SM10_40_avg=transpose( ncread(input_data,'GLDAS_NOAH025_M_2_1_SoilMoi10_40cm_inst'));

%%%%%%%%%%%%%%%%%%%%%

% Soil moisture 40cm - 100 cm

input_data='../g4.timeAvgOverlayMap.GLDAS_NOAH025_M_2_1_SoilMoi40_100cm_inst.20011201-20190630.77E_12N_77E_13N.nc';

SM40_100_avg=transpose(ncread(input_data,'GLDAS_NOAH025_M_2_1_SoilMoi40_100cm_inst'));

%%%%%%%%%%%%%%%%%%%%%

% Soil moisture 100cm - 200 cm

input_data='../g4.timeAvgOverlayMap.GLDAS_NOAH025_M_2_1_SoilMoi100_200cm_inst.20011201-20190630.77E_12N_77E_13N.nc';

SM100_200_avg=transpose(ncread(input_data,'GLDAS_NOAH025_M_2_1_SoilMoi100_200cm_inst'));

T_SM0_200=SM0_10_avg+SM10_40_avg+SM40_100_avg+SM100_200_avg;

figure(3);
dem(Lon(1,:),Lat(:,1),T_SM0_200(:,:,1),'Contrast',0,'AxisEqual','auto');%colormap(flipud(jet));

hold on; line(lon_b,lat_b,'color','k','linewidth',2); title('Soil moisture 0 200cm')

% Calculate Delta , Total Water Storage from GLDAS

% Calculate monthly Avg

T_SM=SM0_10+ SM10_40+ SM40_100+ SM100_200;

clear D_T_SM D_CanopInt_inst
```

```
D_CanopInt_inst=CanopInt_inst*0;

D_T_SM=CanopInt_inst*0;

for k=1:12

Canopy_avg(:,:,k)=mean(CanopInt_inst(:,:,k:12:end),3);

T_SM_avg(:,:,k)=mean(T_SM(:,:,k:12:end),3);

D_CanopInt_inst(:,:,k:12:end)=CanopInt_inst(:,:,k:12:end)-repmat(Canopy_avg(:,:,k),[1 1
length([k:12:size(CanopInt_inst,3)])]);

D_T_SM(:,:,k:12:end)=T_SM(:,:,k:12:end)-repmat(T_SM_avg(:,:,k),[1 1 length([k:12:size(T_SM,3)])]);

end

% D_Storm_SSR= Storm_SSR-SSR_avg(1,1);

% T_SM_avg=SM0_10_avg+SM10_40_avg+SM40_100_avg+SM100_200_avg;

delta_TWS_GLDAS= D_CanopInt_inst+D_T_SM;

dtws0(:)=delta_TWS_GLDAS(2,2,:)

D_T_SM0(:)=D_T_SM(2,2,:);

T_SM0(:)=T_SM(2,2,:);

 [date_num_s,I] = sort(date_num,1,'ascend')

[datestr(date_num(I)) repmat(',',[size(date_num,1) size(date_num,2)]) num2str(dtws0(I)') ]

final_data_GLDAS=[date_num(I) dtws0(I)']

save final_data_GLDAS final_data_GLDAS

% Plot T-series data

figure; plot(final_data_GLDAS(:,1),final_data_GLDAS(:,2),'--r'); hold on ;

% plot(final_data_GLDAS(:,1),D_T_SM0,'--b');

%% read grace time series

load('E:\vajedian\Tejas\Grace\CSR\final_data_grace_CSR.mat')

load('E:\vajedian\Tejas\Grace\GFZ\final_data_grace_GFZ.mat')

load('E:\vajedian\Tejas\Grace\jpl_nc\final_data_grace_jpl.mat')

load('E:\vajedian\Tejas\rainfall\final_rainfall')

load('E:\vajedian\Tejas\final_gps.mat')

final_gps(:,2)=(final_gps(:,2)-final_gps(1,2))*1000;

%%%% Change in GPS

final_gps=[final_gps final_gps(:,1)*0];

for i=1:size(final_gps,1)
```

```
  tmp=datevec(final_gps(i,1));
final_gps(i,3)=tmp(2);
end
for i=1:12
  ind_tmp=find(final_gps(:,3)==i);
  avg_gps_month(i)=mean(final_gps(ind_tmp,2));
  d_gps(ind_tmp)=final_gps(ind_tmp,2)-mean(final_gps(ind_tmp,2));
end
mid_time_gfz=mean(final_data_grace_GFZ(:,1:2),2);
mid_time_csr=mean(final_data_grace_CSR(:,1:2),2);
mid_time_jpl=mean(final_data_grace_jpl(:,1:2),2);
date_gldas=final_data_GLDAS(:,1);
rate_gfz=interp1(mid_time_gfz(2:end),final_data_grace_GFZ(2:end,end),date_gldas,'linear');
rate_csr=interp1(mid_time_csr(2:end),final_data_grace_CSR(2:end,end),date_gldas,'linear');
rate_jpl=interp1(mid_time_jpl(2:end),final_data_grace_jpl(2:end,end),date_gldas,'linear');
total_rate=(rate_gfz+rate_jpl+rate_csr)/3;
% converting from rate to monthly average
cnt=1
n_day(1)=30;
cnt=cnt+1;
for i=2:length(date_gldas)
n_day(cnt)=date_gldas(i)-date_gldas(i-1);
cnt=cnt+1;
end
avg_grace_monthly=total_rate.*n_day'*10;
figure; plot(final_data_GLDAS(:,1),final_data_GLDAS(:,2),'.--b')
hold on; plot(date_gldas,avg_grace_monthly,'.--r'
Input1=avg_grace_monthly-final_data_GLDAS(:,2);
smoothed1 = fLOESS(Input1,0.99);
Input2=final_rainfall(:,2);
smoothed2 = fLOESS(Input2,0.99);
figure(1);yyaxis left;
```

```
 h=bar(final_rainfall(2:end,1),final_rainfall(2:end,2),'EdgeColor','k'); axis tight; hold on

%  plot(final_rainfall(:,1),smoothed2,'-g')

 plot(final_data_GLDAS(:,1),avg_grace_monthly-final_data_GLDAS(:,2),'.--m','LineWidth',1)

hold on; plot(final_data_GLDAS(:,1),smoothed1,'-m','LineWidth',2)


 plot(final_data_GLDAS(:,1),final_data_GLDAS(:,2),'.--c','LineWidth',1)

  smoothed_f = fLOESS(final_data_GLDAS(:,2),0.99);

hold on; plot(final_data_GLDAS(:,1),smoothed_f,'-c','LineWidth',2)

yyaxis right;

plot(final_data_GLDAS(:,1),avg_grace_monthly*10,'.--','LineWidth',1,'color',[0.5 0.5 0.5])

smoothed_g = fLOESS(avg_grace_monthly*10,0.99);

hold on; plot(final_data_GLDAS(:,1),smoothed_g,'-','LineWidth',2,'color',[0.5 0.5 0.5]) ; ylabel('LWE
grace (mm)');

set(gca,'XTick',final_data_GLDAS(1:9:end,1),'XTickLabel',datestr(final_data_GLDAS(1:9:end,1)),'XTickL
abelRotation',90)

Input3=final_gps(:,2);

smoothed3 = fLOESS(Input3,0.99);

Input4=d_gps;

smoothed4 = fLOESS(Input4',0.99);

j=find(~isnan(Input1)); date0=date_gldas(j(1)); Input1=Input1-Input1(j(1));

smoothed1=smoothed1-smoothed1(j(1));

j=find(abs(final_gps-date0)<2); final_gps(:,2)=final_gps(:,2)-final_gps(j,2);

d_gps(:)=d_gps(:)-d_gps(j);smoothed3(:)=smoothed3(:)-smoothed3(j);

smoothed4(:)=smoothed4(:)-smoothed4(j);

figure; yyaxis right;

plot(final_gps(:,1),d_gps,'--','color',[0.5 0.5 .5])

hold on;plot(final_gps(:,1),smoothed4','-k','LineWidth',2);  ylabel('mm')

yyaxis left;

plot(date_gldas,Input1,'--b','LineWidth',1.5); ind_nan=find(isnan(Input1));
smoothed1(ind_nan)=NaN;

plot(date_gldas,smoothed1,'-b','LineWidth',2); ylabel('mm')

set(gca,'XTick',final_data_GLDAS(1:9:end,1),'XTickLabel',datestr(final_data_GLDAS(1:9:end,1)),'XTickL
abelRotation',90)
```

```
% soil moisture
fid=fopen('E:\vajedian\Tejas\Gldas\SM.csv');
% fclose(fid)
l=fgetl(fid);
l=fgetl(fid);
sm=[]; sm_date=[];
while l~=-1
   j=strfind(l,',');
   sm_date=[sm_date;datenum(str2num(l(j-4:j-1)),str2num(l(4:5)),str2num(l(1:2)))];
   sm=[sm;str2num(l(j+1:end))];
   l=fgetl(fid);
end
figure; plot(sm_date,sm,'.-r')
final_sm=[sm_date sm];
save final_sm final_sm
% root soil moisture
fid=fopen('E:\vajedian\Tejas\Gldas\RZSM.csv');
% fclose(fid)
l=fgetl(fid);
l=fgetl(fid);
rsm=[]; rsm_date=[];
while l~=-1
   j=strfind(l,',');
   rsm_date=[rsm_date;datenum(str2num(l(j-4:j-1)),str2num(l(4:5)),str2num(l(1:2)))];
   rsm=[rsm;str2num(l(j+1:end))];
   l=fgetl(fid);
end
figure; plot(rsm_date,rsm,'.-r')
final_rsm=[rsm_date rsm];
save final_rsm final_rsm
% comparing NDVI , Soil moisture , Precipitation
NDVI=load('E:\vajedian\Tejas\NDVI\final_ndvi_std');
```

```
PRC=load('E:\vajedian\Tejas\NDVI\final_prc');
figure; yyaxis right;
errorbar(NDVI.final_ndvi_std(:,1),NDVI.final_ndvi_std(:,2),NDVI.final_ndvi_std(:,3),'.r');
smoothed_ndvi = fLOESS(NDVI.final_ndvi_std(:,2),0.99);
hold on;plot(NDVI.final_ndvi_std(:,1),smoothed_ndvi','-r','LineWidth',2);
yyaxis left;
h=bar(PRC.final_prc(:,1),PRC.final_prc(:,2),'EdgeColor','k'); axis tight; hold on
smoothed_prc = fLOESS(PRC.final_prc(:,2),0.99);
plot(PRC.final_prc(:,1),smoothed_prc,'-k','LineWidth',2);  ylabel('mm')
plot(rsm_date,rsm,'-g')
smoothed_rsm = fLOESS(rsm,0.99);
hold on;plot(rsm_date,smoothed_rsm,'-g','LineWidth',2);  ylabel('mm')
date4axes=[NDVI.final_ndvi_std(1,1):10*30:NDVI.final_ndvi_std(end,1)]
set(gca,'XTick',date4axes,'XTickLabel',datestr(date4axes),'XTickLabelRotation',90)
```

Appendix 4 – Script for NDVI extraction

```
lon_b=boundary(1:3:end); lat_b=boundary(2:3:end);
[X_b,Y_b]=deg2utm(lat_b,lon_b);% Lower Right coordinate
X_b=[X_b; X_b(1)]; Y_b=[Y_b; Y_b(1)];
cnt=1; std_NDVI=[]; mean_NDVI=[];
for i=3:length(dir0)
  if isdir(dir0(i).name) %& ~isempty(strfind(dir0(i).name,'LT05'))
     cd(dir0(i).name)
     display(dir0(i).name)
    % find Near-Infrared and Red bands
    ls0=ls;
    cloud_filename=''; NIR_filename=''; RED_filename='';
    for j=1:size(ls0,1)
    if ~isempty(strfind(ls0(j,:),'4.tif')) |  ~isempty(strfind(ls0(j,:),'4.TIF'))
       NIR_filename=ls0(j,:);
```

```
    elseif  ~isempty(strfind(ls0(j,:),'3.tif')) |  ~isempty(strfind(ls0(j,:),'3.TIF'))
      RED_filename=ls0(j,:);
    elseif ~isempty(strfind(ls0(j,:),'cloud_qa.tif'))
      cloud_filename= ls0(j,:);
    end
    end
  % read geotiff
  Red_img=geotiffread(RED_filename);
  NIR_img=geotiffread(NIR_filename);
  if ~isempty(cloud_filename)
  cloud=geotiffread(cloud_filename);
  end
  Info=geotiffinfo(RED_filename);

x=Info.RefMatrix(3,1):Info.RefMatrix(2,1):Info.RefMatrix(3,1)+Info.RefMatrix(2,1)*(size(Red_img,2)-
1);

y=Info.RefMatrix(3,2):Info.RefMatrix(1,2):Info.RefMatrix(3,2)+Info.RefMatrix(1,2)*(size(Red_img,1)-
1);
  [X,Y]=meshgrid(x,y);
  ind_x=find(x>X_UL & x<X_LR);
  ind_y=find(y>Y_LR & y<Y_UL);
    Red_img=Red_img(ind_y(1):ind_y(end),ind_x(1):ind_x(end));
    NIR_img=NIR_img(ind_y(1):ind_y(end),ind_x(1):ind_x(end));
    X=X(ind_y(1):ind_y(end),ind_x(1):ind_x(end));
    Y=Y(ind_y(1):ind_y(end),ind_x(1):ind_x(end));
%    save ind0 ind0
%    ind0=inpolygon(X(:),Y(:),X_b,Y_b);
  load ind0
%     Red_img=Red_img(ind0);
%     NIR_img=NIR_img(ind0);
  if ~isempty(cloud_filename)
    cloud=cloud(ind_y(1):ind_y(end),ind_x(1):ind_x(end));
```

```
%      cloud=cloud(ind0);
   else
     cloud=Red_img*0;
   end
   cnt
   if cnt==3
   cnt
   end
%    figure(1); imagesc(NIR_img); colormap gray; title('Near-InfraRed');
   NIR_img=double(NIR_img); NIR_img(NIR_img<0)=NaN;
   Red_img=double(Red_img); Red_img(Red_img<0)=NaN;
   NDVI=(NIR_img-Red_img)./(NIR_img+Red_img).*(cloud<10);
   NDVI=NDVI.*(NDVI>0.15);
        figure(1); hold off;scatter(X(ind0),Y(ind0),10,NDVI(ind0),'.'); colormap jet; title('Near-InfraRed');
caxis([0.2 0.7])
%       figure(1);imagesc(NDVI); colormap gray; title('NDVI'); colorbar
   Avg_NDVI(cnt)=mean(NDVI(NDVI>0 & NDVI<0.7));
   std_NDVI(cnt)=std(NDVI(NDVI>0 & NDVI<0.7));

   % extracts date from image name
   if ~isempty(strfind(dir0(i).name,'_144051_'))
    tmp=strfind(dir0(i).name,'_144051_');
   tmp2=dir0(i).name(tmp(1)+8:tmp(1)+15) ;
   Date_value(cnt)=datenum(str2num(tmp2(1:4)),str2num(tmp2(5:6)),str2num(tmp2(7:8)));
   elseif  ~isempty(strfind(dir0(i).name,'144051'))
   tmp=strfind(dir0(i).name,'144051');
   tmp2=dir0(i).name(tmp(1)+6:tmp(1)+13);
   Date_value(cnt)=datenum(str2num(tmp2(1:4)),str2num(tmp2(5:6)),str2num(tmp2(7:8)));
   end
     cd ..
title(datestr(Date_value(cnt)))
print(gcf,strcat('E:\vajedian\Tejas\NDVI\ndvi',num2str(cnt),'.png'),'-dpng','-r300');
```

```
cnt=cnt+1;
  end
end
 [Date_value_s,I] = sort(Date_value,2,'ascend')
figure; h=errorbar(Date_value(I),Avg_NDVI(I),std_NDVI(I),'.R')
final_ndvi_std=[Date_value(I)' Avg_NDVI(I)' std_NDVI(I)'];
save final_ndvi_std final_ndvi_std
[datestr(Date_value(I)) repmat(',',[size(Date_value,2) size(Date_value,1)]) num2str(Avg_NDVI(I)') ]
% xticks(Date_value(I))
% xticklabels(datestr(Date_value(I)))
% LT05_L1TP_144051_19940425_20170114_01_T1_B4.TIF
% LT05_L1TP_144051_19940425_20170114_01_T1
cd('E:\vajedian\Tejas\NDVI')
fid=fopen('NDVI2.csv');
% fclose(fid)
l=fgetl(fid);
l=fgetl(fid);
ndvi=[]; ndvi_date=[];
while l~=-1
   j=strfind(l,',');
   ndvi_date=[ndvi_date;datenum(str2num(l(j-4:j-1)),str2num(l(4:5)),str2num(l(1:2)))];
   ndvi=[ndvi;str2num(l(j+1:end))];
   l=fgetl(fid);
end
figure; plot(ndvi_date,ndvi,'.-r')
final_ndvi=[ndvi_date ndvi];
save final_ndvi final_ndvi
cd('E:\vajedian\Tejas\NDVI')
fid=fopen('P_for_NDVI.csv');
% fclose(fid)
l=fgetl(fid);
l=fgetl(fid);
```

```
prc=[]; prc_date=[];
while l~=-1
   j=strfind(l,',');
   prc_date=[prc_date;datenum(str2num(l(j-4:j-1)),str2num(l(4:5)),str2num(l(1:2)))];
   prc=[prc;str2num(l(j+1:end))];
   l=fgetl(fid);
end
figure; plot(prc_date,prc,'.-r')
final_prc=[prc_date prc];
save final_prc final_prc
```